EVALUATION OF ENVIRONMENTAL DURABILITY AND BOND CHARACTERISTICS OF CARBON FIBRE REINFORCED POLYMER (CFRP) STRENGTHENED STEEL STRUCTURES

Chamila Rajeev Jayanath Batuwitage

B.Sc. Eng. (Hons), M.Phil.

Submitted in fulfilment of the requirements for the degree of Doctor of Philosophy

School of Civil Engineering and Built Environment

Science and Engineering Faculty

Queensland University of Technology

2017

Keywords

accelerated corrosion, adhesive joint, CFRP, CFRP-strengthened beams, composites, corrosion, deterioration, double-strap joints, durability, experimental testing, failure modes, finite element modelling, parametric study

Abstract

Structures can undergo deterioration with age due to the loss of material properties, exposure to severe environmental conditions or increases in service loads. CFRP is a smart material, which has been popular in the fields of strengthening and rehabilitation of structures because of its excellent material properties, such as high strength-to-weight ratio, high stiffness-to-weight ratio and ease of application. The literature confirms that CFRP can be effectively used to enhance the structural performance of steel structures. However, knowledge on the durability of CFRP strengthening systems is very limited and it is crucial to evaluate the durability aspects of CFRP-steel composite systems. This thesis presents the results of an experimental program, aimed to determine the bond properties, durability performance and associated failure modes of CFRP-steel composite systems. The experimental results were used to validate the developed finite element models, which were extended to evaluate the effects of different important parameters.

In this research, extensive experimental tests and numerical simulations were conducted on the CFRP-steel bonded double strap joints to investigate the bond properties and durability performances of CFRP-steel composite systems. In addition, the structural behaviour of degraded CFRP strengthened steel beams was studied. The deterioration process of CFRP-steel composite systems was accelerated using an accelerated corrosion cell where the specimens were submerged in an aqueous solution of 5% sodium chloride. Different bond-related parameters were studied to evaluate the durability performance of CFRP-steel composite systems and the effects of surface preparation method, primer coat, number of CFRP layers, bond length and embedded GFRP layer under accelerated environmental conditions are

evaluated. Durability performance of CFRP-steel bonded joints was evaluated using the load vs. deflection behaviour, joint strength and fracture energy along with an investigation of the associated failure modes as the response parameters. In addition, shear stress-slip responses of degraded CFRP-steel bonded joints were evaluated and compared with those at ambient conditions.

The results of the experimental program revealed that the CFRP material can undergo deterioration in accelerated environmental conditions. Failure modes are significantly different from those at ambient conditions. Bond-slip behaviour of adhesively bonded CFRP-steel double strap joint is significantly affected by the environmental conditioning. The numerical study showed that the degradation levels of CFRP and adhesive are critical parameters in a strengthening system. Tested beams revealed that the load carrying capacity of CFRP strengthened beams is affected by accelerated environmental conditions. Direct exposure of CFRP material to the aggressive environments can cause CFRP material degradation, and can be identified through visual observations.

The findings of this research provide a significant contribution to the knowledge of CFRP-steel strengthening systems subjected to accelerated environmental conditions which can be used to evaluate the durability performance of CFRP-steel strengthening systems effectively.

Table of Contents

List of Figures

List of Tables

Statement of Original Authorship

The work contained in this thesis has not been previously submitted to meet requirements for an award at this or any other higher education institution. To the best of my knowledge and belief, the thesis contains no material previously published or written by another person except where due reference is made.

Signature:

Date: 12/04/2017

Acknowledgements

I would first like to thank my principal supervisor, Dr Sabrina Fawzia, for all her patience, encouragement, understanding and guidance during my PhD journey. This was not limited to her insightful comments and encouragement, but also the probing questions she posed, which provided an incentive to me to widen my research from various perspectives. I feel privileged to have studied under her supervision. She has provided me many opportunities, for which I am very grateful.

My sincere thank goes to Professor David Thambiratnam, my associate supervisor for his valuable guidance throughout my candidature. I am very grateful to him for his involvement and contribution during my study period. Thanks are also due to Dr Xuemei Liu, my associate supervisor for helping me in many ways during my PhD study.

I am extremely grateful to my external supervisors, Professor Riadh Al-Mahaidi and Professor Moataz Badawi, for providing feedback and guidance during my candidature. Meeting Professor Riadh was a turning point in my PhD study, and he has provided immense support throughout my candidature.

I would like to thank Mr Iftekharul Alam and Dr Humayun Kabir for their help and support in my laboratory experiments as well as being good friends and offering me help in many ways.

My heartfelt gratitude goes to Mr Barry Hume for his assistance during the laboratory experiments. Also, I humbly thank Mr Glen Atlee, Mr Ian Routcliffe, Mr Neil McKenzie and former technician, Mr Christophe Bonavia, for offering help and

support at QUT Banyo laboratory. I would like to thank Mr Eca Calva and Mr Frank De Bruyne, who coordinated the laboratory work at Banyo.

Professional editor, Diane Kolomeitz, provided copyediting and proofreading services, according to the guidelines laid out in the university-endorsed national 'Guidelines for editing research theses'.

I am deeply indebted to my parents for the endless love, and encouragement provided to me throughout my life. Special thanks go to my loving wife, Bhashi, for her understanding and patience over the years. Last, but certainly not least, I would like to thank my friends who helped me in many ways throughout my stay in Brisbane, making this city a second home.

List of Publications

Peer reviewed journal papers

1. **Batuwitage**, **C.**, Fawzia, S., Thambiratnam, D. and Al-Mahaidi, R. (2016). "Durability of CFRP strengthened steel plate double-strap joints in accelerated corrosion environments." *Composite Structures*, 160 (2016), pp 1287-1298 SJR: 2.408 [Q1], IF: 3.853.

2. **Batuwitage**, **C.**, Fawzia, S., Thambiratnam, D. and Al-Mahaidi, R. (2016). "Evaluation of bond properties of degraded CFRP-strengthened double strap joints." *Composite Structures*, (Revised and resubmitted).

Peer reviewed conference papers

3. **Batuwitage, C.**, Fawzia, S., Liu, x., Thambiratnam, D., and Alam, I., "Bond characteristics of retrofitted corroded steel by smart CFRP technique". *Second International Conference on Performance-based and Life-cycle Structural Engineering (PLSE 2015)*, Brisbane, Australia 9-11 December 2015.

4. **Batuwitage, C.**, Fawzia, S., Liu, x., and Alam, I., "Finite element modelling of carbon fibre reinforced polymer (CFRP) Strengthened steel tubes under axial impact". *23rd Australasian Conference on the Mechanics of Structures and Materials (ACMSM23)*, Byron Bay, Australia 9-12 December 2014.

Manuscripts under preparation

5. **Batuwitage**, **C.**, Fawzia, S., Thambiratnam, D. and Al-Mahaidi, R. "Finite element modelling of degraded CFRP-strengthened double strap joints."

6. **Batuwitage**, **C.**, Fawzia, S., Thambiratnam, D. and Al-Mahaidi, R. "Effect of material degradation on structural behaviour of CFRP-strengthened beams."

Chapter 1: Introduction

1.1 BACKGROUND

Existing civil engineering structures degrade with age, due to the loss of material properties, exposure to severe environmental conditions, or increased service loads. Figure 1.1 shows corrosion damage in steel bridges. Carbon fibre reinforced polymer (CFRP) has become very popular for the strengthening and rehabilitation of structural members in bridges and buildings because of its excellent material properties, including its high strength-to-weight ratio, high stiffness-to-weight ratio and ease of application in the field.

Majority of rehabilitation works have been carried out to retrofit old deteriorating structures, rectify damage due to seismic activities and other natural hazards. Structural strengthening is also required because of degradation problems which may arise from environmental exposure, inadequate design, poor quality construction and a need to meet current design requirement. Therefore, structural repair and strengthening has received much attention over the past two decades throughout the world. Recent experimental and analytical researches have demonstrated that the use of composite materials for retrofitting existing structural components is more cost-effective and requires less effort and time than the traditional means. Table 1.1 presents a summary of some CFRP-strengthened bridges [1]. Early research work confirmed that CFRP can be effectively used in strengthening steel sections [2-6]. In such strengthening systems durability is a main concern, because the service life depends on the durability of the system. However, despite its widespread use in strengthening and rehabilitation, [7-18] knowledge of the durability of CFRP systems remains very limited.

Figure 1.1: Deteriorated steel structural members

Under normal conditions, the strength degradation of the CFRP-steel bonded joints occurs due to the diffusion of water through the adhesive layer [19, 20]. Research to evaluate the bond properties of CFRP-steel interface [11, 19, 21] has found that CFRP material properties can be significantly affected by environmental conditions such as moisture, the marine environment and chemical attack. In addition, galvanic corrosion can result in CFRP degradation in certain applications such as marine pipe systems and offshore structures [7-9, 11].

Table 1.1: Summary of CFRP-strengthened bridges

Strengthening context	Strengthening method	Purpose
Tickford Bridge, England (1999)	Bonding of pre-impregnated CFRP laminas with polyester underlay.	Reduction of stresses in the original material.
Hythe Bridge, England (2000)	Pre-stressing of CFRP laminas.	Elimination of tensile stress in girders due to variation of loading conditions. Traffic up to 40t.
Slattocks Canal Bridge, England (2000)	Bonding of CFRP laminas.	Increased load bearing capacity. Traffic up to 40t.
King Street Bridge, England (2000)	Bonding of pre-impregnated CFRP and GFRP laminas longitudinally and transversely, respectively.	Increased load bearing capacity. Traffic up to 40t.
Acton Bridge, England (2000)	Bonding of CFRP laminas.	Reduction of strain in the original material, increase in service life and fatigue resistance.
Corona Bridge, Italy (2002)	Bonding of aramid tri-axial laminas and mono-directional strips.	Reduction of vulnerability to thermal shocks and impact loading.
Christina Creek Bridge, USA (2000)	Bonding of CFRP laminas.	A pilot project to analyse fatigue resistance and sensitivity to environmental agents.
Ashland Bridge, USA (2002)	Bonding of CFRP laminas.	Stress reduction in the original material to increase fatigue life.
7838.5S092 Bridge, USA (2003)	Bonding of CFRP laminas.	Stress reduction in original material to increase fatigue life.

Most research on the durability of CFRP-steel strengthening systems considers a maximum of 18 months of environmental exposure to marine environments, or the degradation of steel is simulated by mechanically reducing the steel thickness [13, 19, 21-30]. Such short exposure durations do not represent the complete service life of a CFRP-steel composite system. Hence, the actual time-dependent material properties of CFRP-steel strengthening systems under severe environmental conditions such as marine environments are yet to be evaluated and the related

failure modes are yet to be identified. To address these issues, accelerated tests have been used to successfully simulate the complete deterioration of CFRP-steel strengthening systems [9, 11, 31-34]. Corrosion activity is accelerated by applying direct current (DC) to specimens, which gradually degrades the specimen, depending on the exposure time and the current. For example, Kim et al. [9] used DC to artificially degrade CFRP-steel bonded joints in sodium chloride (NaCl) solution to simulate severe environmental conditions and showed that the CFRP-steel interface properties are significantly influenced by the simulated accelerated environmental conditions. Kabir et al. [11, 35] conducted experiments to study the durability performance of CFRP-strengthened beams under simulated sea-water environmental conditions and concluded that the tested environmental conditions adversely affect the durability. The above studies suggest that there may be material and/or bond degradation in CFRP-steel composite systems under simulated marine environmental conditions, and this should be investigated in detail to evaluate the failure modes, bond properties and structural performance of CFRP-steel systems.

1.2 RESEARCH GAP

Research on the durability of CFRP strengthening systems has been mainly restricted to studies on the individual performance and mechanical characteristics of CFRP, steel and adhesive materials under specific environmental conditions. Such approaches may be misleading because the actual CFRP-steel composite bond properties and material properties may be different from those influencing individual material behaviour. Most importantly, CFRP can undergo deterioration when it is in contact with metal in aggressive environments, such as in an offshore structures. There have been some studies related to the bond between the CFRP-steel interface and failure modes in ambient environmental conditions [36-40]. However, the

existing bond-slip models have restricted applicability because all were developed for non-degraded CFRP-steel systems. Furthermore, the failure modes under severe environmental conditions may differ significantly because of changes in the material and bond properties. Hence, the existing models are not capable of simulating the long-term durability performance of CFRP-strengthened steel composite systems. Therefore, the durability of CFRP-steel composite systems under different environmental conditions should therefore be studied in detail to evaluate the failure modes, bond characteristics and structural behaviour to understand the durability issues and structural performance of the CFRP-steel strengthening system.

1.3 AIM AND OBJECTIVES

The aim of this research was to evaluate the environmental durability and bond characteristics of CFRP-strengthened structural steel members. In this research, the bond properties of degraded CFRP-steel composite systems were experimentally studied using steel-CFRP double strap joints. Numerical models were then developed based on the conducted experimental study, and the models were validated using the experimental results. A wide range of parametric studies were conducted using the validated finite element (FE) models to evaluate the structural behaviour of adhesively-bonded CFRP-steel joints. In addition, CFRP-strengthened universal beam sections were tested to evaluate the structural behaviour and associated failure modes. The experimental program and the numerical study were planned to achieve the following objectives.

1. To determine the effects of the surface preparation method and application of a primer coat for steel surfaces on the structural behaviour and bond properties of CFRP-steel composite systems.

2. To examine the durability of CFRP-steel double strap joints and investigate the associated failure modes under accelerated environmental conditions.
3. To assess the durability performance of CFRP-steel composite systems with an embedded glass fibre reinforced polymer layer (GFRP).
4. To determine the effects of various parameters such as the number of CFRP layers, CFRP bond length, CFRP degradation level and adhesive degradation level on the structural behaviour of CFRP-steel double strap joints.
5. To characterise the shear stress-slip relationship of degraded CFRP-steel composite systems under accelerated environmental conditions and compare it with that under ambient conditions.
6. To evaluate the structural behaviour and associated failure modes of degraded CFRP-strengthened universal beam sections subjected to accelerated environmental conditions.

1.4 RESEARCH SIGNIFICANCE

Strengthening of structural steel members using CFRP has become a popular method to strengthen and rehabilitate buildings and bridges in recent years. Previous research work confirms that the use of CFRP is an efficient method of strengthening, which enhances the structural performance regarding load-carrying capacity under different loading conditions. However, most existing studies have evaluated the structural performance of CFRP-steel composite systems under ambient conditions. Due to the growing applications of CFRP systems in different fields, such as underwater applications, offshore buildings and bridge structures, the durability of CFRP has become a major concern. The existing experimental durability studies are

limited to a short period compared to the design life of strengthening systems. In addition, the known failure modes and structural behaviour are based on short-term studies, whereas a real structure could be exposed to aggressive environmental conditions, such as marine environments for very long periods. Various environmental exposure conditions such as moisture, temperature and chemical attacks could lead to CFRP material degradation and result in failure modes that are different from the failure modes known to occur under ambient environmental conditions. The lack of studies on degraded CFRP-steel composite systems creates a knowledge gap in the field of the durability of CFRP-steel composite systems.

This research addresses the existing knowledge gap by studying the degraded bond properties and structural performance of CFRP-steel systems subjected to accelerated environmental conditions. The bond properties and associated failure modes of degraded composite systems have been investigated using CFRP-steel double strap joints and CFRP-strengthened universal beam specimens. The proposed shear stress-slip models will help in the understanding of the structural behaviour of degraded CFRP-steel composite systems. Advanced FE models were developed to simulate the structural behaviour of degraded CFRP-steel systems and validated using experimental results with excellent correlations. A comprehensive parametric study was then carried out using the developed FE models to evaluate the effects of critical parameters on the structural behaviour of CFRP-steel composite systems. The findings of this research will add new knowledge to the durability of CFRP-steel strengthening systems.

1.5 THESIS OUTLINE

Chapter 1 details the background, research gap, aims and objectives, significance and thesis outline.

Chapter 2 presents a comprehensive literature review of topics related to the context of the thesis. Firstly, general information related to CFRP systems is provided, along with the materials and surface preparation methods. Next, the failure modes and failure behaviour are discussed. This is followed by a detailed explanation of the research literature on CFRP-steel bond behaviour and current bond slip models. Environmental factors and their effects on the CFRP systems are presented next. A summary of accelerated environmental durability studies is discussed, and the current models for predicting the durability of CFRP-steel systems are listed. After that, some of the design guidelines and their applications are discussed within the relevant contexts. Finally, a detailed summary of FE analysis studies, and the improvements made through different modelling techniques, is presented.

Chapter 3 details the experimental program conducted. The sub-sections are presented according to the three experimental series carried out. Furthermore, it describes the test specimens, specimen preparation, test scenarios and parameters involved in each series.

Chapter 4 is focused on the experimental results and discussion. The durability of CFRP-steel strengthening systems is analysed and discussed, based on each parameter evaluated. Detailed explanations of the results are presented in line with the current literature.

Chapter 5 explains the FE modelling and the results of CFRP-steel double strap joints. The developed FE models are validated with the experimental results and the validated models are used to conduct a comprehensive parametric study. The results of the evaluated parameters are then presented and their effects on the CFRP-steel double strap joint's structural behaviour are discussed.

Chapter 6 summarises the main findings and conclusions of this research, and provides recommendations for future work.

Chapter 2: Literature Review

2.1 INTRODUCTION

This chapter presents and reviews the existing research on CFRP systems, bond behaviour, bond-slip models, environmental factors, accelerated environmental tests, current durability prediction models, design guidelines and finite element (FE) studies. These critical reviews of the literature detail the current knowledge related to the research topic and identify the gaps in the field of CFRP-steel strengthening systems.

2.2 CFRP SYSTEMS

CFRP is widely used in the strengthening and rehabilitation industry. Different types of CFRP systems have been developed based on the applications (Figure 2.1 [41]). They are (i) fabrics, (ii) laminates and (iii) near-surface mounted (NSM) systems.

(a) CFRP fabrics

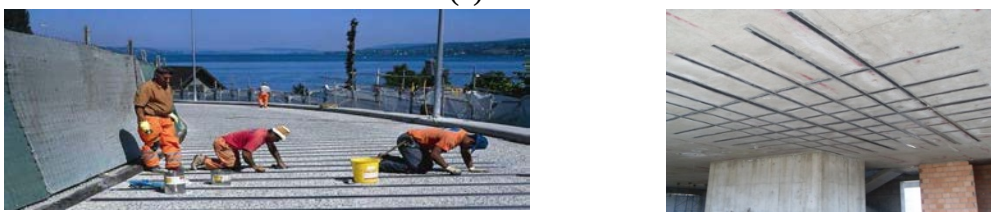

(b) CFRP laminates

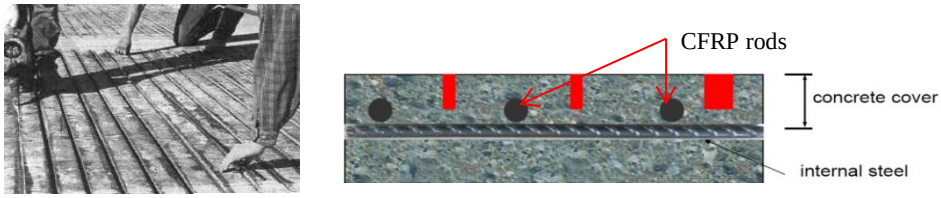

(c) Near surface mounted systems

Figure 2.1: CFRP systems

Advantages

The main advantages of CFRP materials over steel plates are their high strength and light weight, which make the installation process simple and quick. The material is easy to work with, and the flexibility of these CFRP materials also simplifies installation because:

(i) Laps and joints are not required.

(ii) The material can be used in irregularly shaped structures.

(iii) The material can be installed behind existing services.

(iv) Overlapping does not occupy a large space because of the small thickness of the material.

These factors, in combination, have led to the development of a significantly simpler strengthening technique than other strengthening methods. The application of CFRP systems does not significantly increase the weight and the final dimensions of the structural members. This is an additional advantage for bridges, tunnels and other structures with limited clearance.

Disadvantages

Despite the several advantages, limited knowledge about CFRP systems has restricted the use of CFRP materials. In particular, the lack of durability data is the main disadvantage.

2.2.1 Field applications

CFRP materials have been successfully used for strengthening and retrofitting concrete, wood and steel structures in a wide range of field applications. Some examples are shown in Figures 2.2 and 2.3 [42].

(a) Ibach bridge, Switzerland

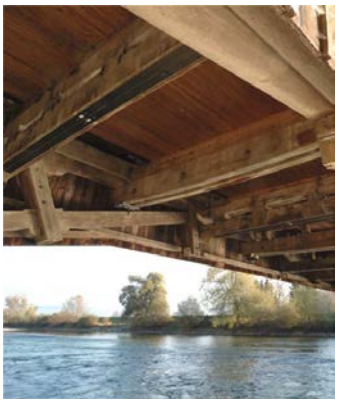

(b) A wooden bridge, Switzerland

(c) Bunbury bridge, Western Australia

Figure 2.2: CFRP strengthened bridges

(a) The old Treasury building, Western Australia

(b) Adelaide Convention Centre, South Australia

Figure 2.3: CFRP-strengthened buildings

2.2.2 Materials

CFRP

The most common fibre types used in strengthening systems are carbon, glass and aramid. These materials are known as elastic-brittle materials in the field of structural strengthening. During tensile loading, these materials follow a linear stress-strain relationship until failure. Figure 2.4 shows the stress-strain behaviour of CFRP materials under different strain rates [43]. The mechanical properties of commercially available fibres are shown in Table 2.1.

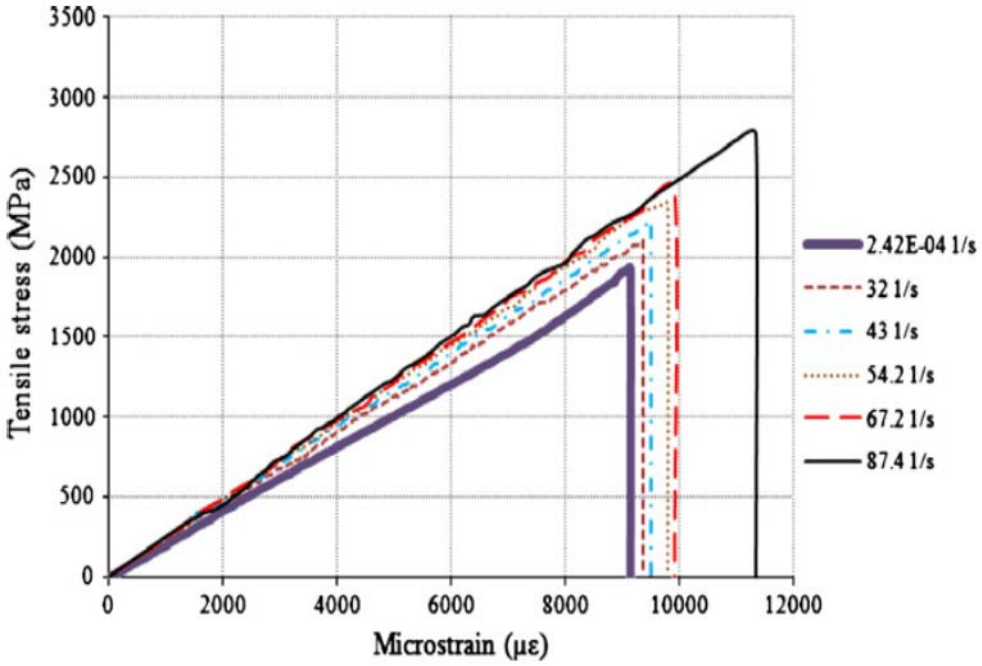

Figure 2.4: Stress-strain relationship of CFRP [41]

Table 2.1: Typical properties of FRP materials [44]

Fibre	Type	Tensile strength (MPa)	Young's modulus (GPa)	Ultimate tensile strain (%)	Density (kg/m^3)
Glass	E	3450	72.4	2.4	2500
	S	4580	85.5	3.3	2500
Carbon	High modulus	2500-4000	350-650	0.5	1950
	High strength	3500	240	1.1	1750
Aramid	High modulus	125-175	3000-4200	1.4-3.5	1400-1450
	Low modulus	60-70	2750-3000	4.4	1350-1450

Adhesives

Adhesives are recognised as both a structural and protection component in a strengthening system. Most of the commonly available adhesives are two-part epoxy resins. These two chemicals are mixed at a certain ratio to form the bonding adhesive. The selection of adhesive type is crucial when designing a composite system, because this affects both the physical and mechanical properties of the strengthening system. The epoxy resin binds the reinforcing fibre together and creates a composite layer, which transfers and distributes the load to the fibres. In addition, it acts as a barrier against external environmental attack. Different types of adhesive are used as the bonding agent of CFRP to the steel surface. Widely-used commercially available adhesives are (i) Araldite (ii) Sika and (iii) MBrace. Figure 2.5 shows the stress-strain relationship of linear and non-linear adhesives [36]. Polyester, vinyl ester and polyurethane adhesives (Table 2.2) are alternatives to epoxy adhesives and have certain drawbacks. The mechanical properties of these adhesives are listed in Table 2.3.

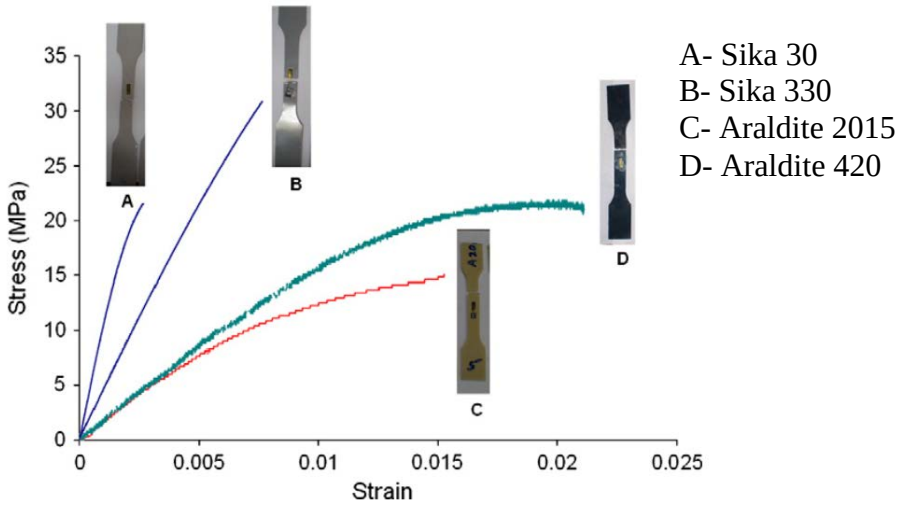

Figure 2.5: Stress-strain relationships of different types of adhesives [36]

Table 2.2: Adhesive types and their drawbacks [44]

Adhesive type	Drawbacks
Polyester	High curing shrinkage, high coefficient of thermal expansion, can be subjected to alkaline hydrolysis and difficult to bond when hardened
Vinyl ester	Curing shrinkage and badly affected by moisture
Polyurethane	High curing shrinkage, affected by moisture and difficult to bond

Table 2.3: Typical mechanical properties of adhesives [44]

Property	Matrix		
	Polyester	Epoxy	Vinyl ester
Density (kg/m^3)	1200 - 1400	1200 - 1400	1150 - 1350
Tensile strength (MPa)	34.5 - 104	55 - 130	73 -81
Longitudinal modulus(GPa)	2.1 - 3.45	2.75 - 4.10	3.0 - 3.5
Poisson's coefficient	0.35 - 0.39	0.38 - 0.40	0.36 - 0.39
Thermal expansion coefficient ($10^{-6}/^{o}C$)	55 - 100	45 - 65	50 - 75
Moisture content (%)	0.15 - 0.60	0.08 - 0.15	0.14 - 0.30

2.2.3 Surface preparation methods

Abrasive blasting

Abrasive grit blasting or sandblasting is a commonly-used industrial surface pre-treatment method. This method has been widely used by researchers for specimen preparation [11, 13, 19, 23]. The steel surface is subjected to a stream of abrasive materials under high pressure through a blasting nozzle. Sand and metal grit are the most commonly-used abrasive materials and are available in different sizes. Most of the metallic grits primarily consist of Al_2O_3. The abrasive materials are mainly divided into two categories: (1) non-metallic abrasives and (2) metallic abrasives.

Non-metallic abrasives

Naturally-occurring non-silica or heavy mineral sands such as magnetite, olivene rutile and straurolite are used to clean new steel surfaces. Flint, garnet, novaculite and zircon are used in specific cleaning applications because of their high cost. Some industrial by-products such as slag, or agricultural by-products such as corncobs, peach pits and walnut shells, are used to blast-clean new, rusted or painted surfaces. Aluminium oxide, glass beads and silicon carbide are synthetic abrasives widely used in abrasive blast-cleaning in addition to those mentioned above. These synthetic abrasives can be manufactured in various shapes varying hardness and toughness. Typically, synthetic abrasives result in non-rusting substrate.

Metallic abrasives

Iron, aluminium, copper and zinc are commonly-used metallic materials to manufacture metallic abrasives. These metallic abrasives are available in two forms: (1) shot and (2) grit. Metallic shot materials are produced by spraying or blowing molten metal into a water bath or appropriate media. These are considered to be much more durable and are typically reclaimed and re-used.

Mechanical grinding

Mechanical grinding is the simplest form of abrasive surface preparation. Sand paper, belt sanders or mechanical rotating grinders are used to remove the coating materials on the steel surface. This method has been used as a surface preparation method by different researchers [45]. For example, Fawzia [5, 38-40, 46] used abrasive grinding as the surface preparation method to fabricate double-strap joint specimens and circular hollow specimens. In a recent study, Kim et al. [9, 47] used mechanical grinding as the surface preparation method to fabricate double-strap joint specimens.

Studies of surface preparation methods

Fernando et al. [48] studied the effect of surface preparation methods using CFRP-steel single lap joint specimens. Different steel surface preparation methods were used to evaluate the bond properties. Solvent cleaning, hand grinding and grit blasting were the steel surface preparation methods used in this study. Surface energy, surface chemical composition and surface roughness and topography were the three key parameters investigated. The results showed that the grit-blasted surfaces had pore patterns that were much more densely distributed than the surfaces produced by the other two surface preparation methods. The hand-ground samples showed a scratchy finish and no pores were visible. The highest surface energy values were observed in the grit-blasted surfaces. Overall, the grit blasted surfaces were shown to have the optimum parameters for adhesive bonding and grit blasting was recommended as the steel surface preparation method before adhesive bonding. The grit size was shown to have no significant effect on the adhesion strength.

Amada and Satoh [49] conducted an experimental study followed by fractal analysis to evaluate the effect of the blasting angle of surfaces roughened by grit

blasting. Grit blasting was carried out for 6s at a distance of 150 mm at 5 kg/cm^2 pressure, varying the blasting angle from 45^0 to 90^0. It was concluded that the fractal dimension reached a maximum value at a blasting angle of 75^0, which was the same angle at which the adhesion strength of the coating reached its maximum value.

Harris and Beevers [50] conducted research to evaluate the effects of grit blasting with different alumina grits on the surface characteristics of mild steel and aluminium alloy substrates. Surface texture and surface energy were measured for each sample and the adhesion characteristics were investigated by testing single lap joints. Different sizes of grits were used to evaluate the effect of grit size on the adhesive strength. The results showed that there was no significant difference in strength between the surfaces prepared with fine and coarse grits.

Careful surface preparation is fundamental for a good adhesive bond between the CFRP materials to the steel substrate. Necessary steps mentioned in the Italian guidelines, recommended by the National Research Council committee report [1] are listed below:

1. Remove coatings, slag and other corrosion products

This operation can be carried out mechanically using wire brushing or grit blasting. Particular care should be taken in the case of brittle members (cast iron) to avoid damage to the surface of the substrate.

2. Degrease with solvent

A suitable solvent can be used to remove grease.

3. Abrasion

Dry or wet sandblasting can be used to expose a chemically active surface prior to bonding and debris should be removed using only water.

4. Drying the surface

If the surface is wet at the end of the abrasion process and the cleaning phase, it must be immediately dried to avoid the formation of oxide layers on the blasted surface.

5. Chemical etching

In the case of formation of oxide layers (galvanised steel or stainless steel), acid etching and neutralisation of etching products are required.

6. Primer application

A primer layer can be used to make the existing metallic surface compatible to bonding with CFRP material. The first layer of adhesive should be applied as soon as possible after cleaning of the substrate surface.

2.3 BOND BEHAVIOUR OF CFRP SYSTEMS

Failure modes of CFRP systems greatly depend on the bond properties and the type of materials used. A bonded joint can fail in many ways [51]. Generally, the failure modes of bonded joints are categorised into three types: cohesive, adhesive and adherend.

2.3.1 Cohesive failure

Cohesive failure takes place within the adhesive layer. In this failure mode, the presence of adhesive can be observed on both the bonded regions of the adherends. Shear loads are the main reason for cohesive failure to occur in an adhesively-bonded joint. A combination of different resultant stresses also can initiate cohesive zone failure. Poor fabrication can result in cohesive failure as a consequence of the porous adhesive layer. This failure mode normally results in very low joint capacities. A schematic representation of cohesive failure extracted from ASTM [52] is shown in Figure 2.6.

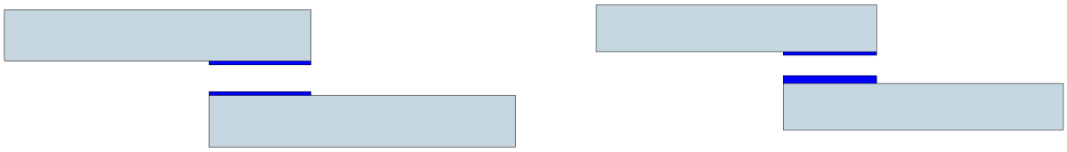

(a) Cohesive failure (b) Thin-layer cohesive failure

Figure 2.6: Cohesive failure - ASTM D5573-99

2.3.2 Adhesive failure

Adhesive failure occurs on the interface of the adhesive and the adherend. This failure mode is commonly identified as debonding failure mode. Poor surface preparation, curing and contamination can result in adhesive failure of the CFRP-steel joint. It is common that cohesive and adhesive failure occur together. This combination type of failure is classified as adhesive failure when the adherend surface is visible and a fractured adhesive layer can be observed very close to the adherend surface. A schematic representation of adhesive failure extracted from ASTM [52] is shown in Figure 2.7.

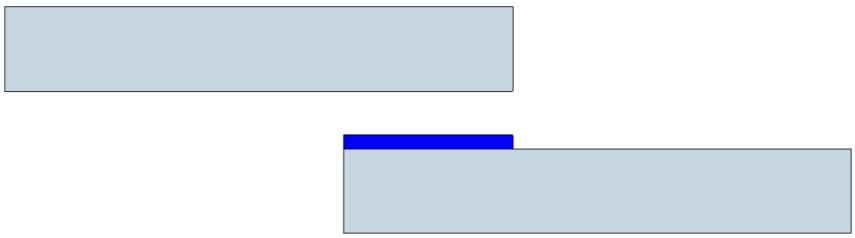

Figure 2.7: Adhesive failure - ASTM D5573-99

2.3.3 Adherend failure

Adherend failure occurs in the CFRP material on the bonded joint. Different types of failure mode can be expected as a result of the complexity involved with CFRP composite materials [36, 53]. Two types of failures are identified in the

literature: (i) interlaminar failure and (ii) fibre rupture. These failure modes can be further classified as (i) tensile fibre rupture, (ii) compressive fibre failure and (iii) matrix failure. A schematic representation of adherend failure extracted from ASTM [52] is shown in Figure 2.8.

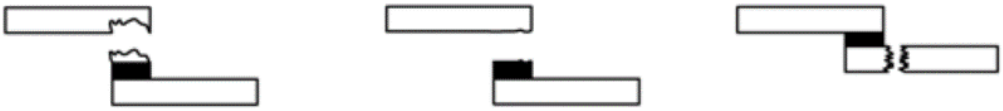

(a) Fibre-tear (b) Light-fibre-tear (c) Stock-break

Figure 2.8: Adherend failure – ASTM D5573-99

2.3.4 Enhancing the bond properties of adhesively bonded joints

The application of adhesive promoter (primer) materials has been recommended in order to produce a strong and durable adhesive joint between different substrates [54-56]. This type of surface pre-treatment can increase the bond strength by altering the substrate surface in various ways: (i) increasing surface tension, (ii) increasing surface roughness and (iii) changing surface chemistry [57]. In addition, primer material can be applied to the bonded steel surface to protect the steel surface until bonding is carried out, to increase the wettability, to prevent the occurrence of pores, as a protective layer and as a coupling agent that is capable of forming better chemical bonds with the adherend and the adhesive.

Marsh et al. [58] assessed the effects of various steel pre-treatment methods on the bond properties and resistance to corrosion on adhesively-bonded surfaces. The experimental results showed that using a silane strongly improved wet and dry adhesion, but substantially reduced resistance to corrosion.

Dawood et al. [27] studied the effects of a silane coupling agent on the durability of CFRP-steel double strap joints under marine environmental conditions. The specimens were subjected to this environmental conditioning up to six months. No strength degradation was recorded after six months of exposure in the specimens treated with primer. The results showed that the application of silane coupling agent helped to increase the durability of CFRP-steel bonded joints.

2.4 LITERATURE ON CFRP-STEEL BOND

In concrete-CFRP bonded applications, the CFRP-to-concrete surface is the weak link. In contrast, one of the interfaces between the adhesive and adherends (steel and CFRP) is the weak link in CFRP-steel composite systems. However, the existing literature shows that the failure modes and bond behaviour may vary significantly because of the implementation of different test methods and test specimens during the experiments.

Early studies carried out using CFRP as a strengthening material for bridges reported several issues [59, 60], including bond development length, peel stresses at the plate ends, durability and failure modes.

Fawzia et al. [39] conducted an experimental series using double strap CFRP-steel joints (two steel plates adhesively bonded with three CFRP layers on both sides of the plate) to study the bond properties between CFRP and steel surface. Load vs. axial displacement response, strain variation for different bond length and effective bond length were investigated using FE models validated using experimental results.

Nozaka et al. [45] conducted experiments to examine the effective bond length of CFRP laminates bonded to steel I-girders. Several types of adhesives and bond configurations were investigated, and the effective bond length was found to be 200

mm, based on the experimental results. The experimental results also indicated that an adhesive with relatively large ductility is required to redistribute the stresses successfully within the adhesive layer during increased loading. An analytical solution was proposed to estimate the effective bond length.

Xia and Teng [61] studied the direct shear effects of CFRP-steel bonded joints through a series of pull-off tests. Based on the test results a bond-slip model was developed. Yue et al. [62] studied the stress distribution along the CFRP-steel bond using CFRP adhesively-bonded onto a steel plate and found that the effective bond length for the specimens was 100 mm.

Colombi and Poggi [63] conducted experiments to study the effectiveness of CFRP-strengthened steel plates and the strain variation along the bond length of the specimens. Failure modes and failure criteria were examined and compared. They extended their studies [64] to investigate the structural characteristics of CFRP-strengthened H-shaped steel beams with different CFRP configurations bonded to a tension flange. It was found that the effect of using a single layer of CFRP at the bottom flange is negligible and two CFRP layer configurations increased the elastic stiffness by 13.8%.

Hollaway et al. [65] compared the suitability of a prepreg (a fibrous material pre-impregnated with a particular synthetic resin) composite and a compatible film adhesive in a CFRP-steel composite system. Both the methods resulted in the development of a good bond and good compaction under a vibration load. It was found that a more ductile material was needed to fully mobilise the resistance of the steel beam. Photiu et al. [51] conducted a similar type of experiment, and four types of failure mode were observed in the tested samples: (i) cohesive, (ii) interlaminar, (iii) interfacial and (iv) ultimate failure of CFRP.

Schnerch et al. [3, 4] conducted research on CFRP-steel double-strap joints and CFRP-steel I-girders to study the bond behaviour and failure modes. Based on the results design guidelines were proposed.

The effect of CFRP on strengthening I-girders was studied by Deng and Lee [66]. The effects of different types of CFRP, tapers at the plate end, and spew fillets beyond the plate were investigated. Three types of failure mode were observed: (i) beam flange buckling, (ii) CFRP plate debonded but not detached totally from the steel beam, and (iii) CFRP plate totally detached from the steel beam. The recommendation was to use longer and tapered CFRP plates to improve the efficiency of the CFRP-steel composite system.

Fawzia et al. [5] studied the structural behaviour and bond characteristics of circular tubes strengthened by CFRP subjected to axial tension. The effects of bond length and number of CFRP layers were investigated. Strain variation was found to decrease along the CFRP bond length far from the joint and the strain through the thickness of the CFRP layers decreased from top to bottom.

Linghof et al. [67] conducted experiments using CFRP-strengthened I-girders and adhesively-bonded CFRP-steel joints to study the structural performance enhancement of CFRP systems. Strengthened beams showed about 20% capacity enhancement due to the CFRP strengthening effect, and the failure mode of the strengthened beams was reported to be compression flange buckling. Based on the joints tested, it was concluded that the strength performance of a bonded joint depends to a great extent on the quality of the surface preparation and workmanship.

Yu et al. [36] experimentally studied the bond behaviour of CFRP-to-steel bonded interfaces through the testing of a series of single-lap joints. The effects of material properties, adhesive thickness and axial rigidity of CFRP were studied. The

results showed that the bond strength of the joints strongly depends on the interfacial fracture energy. It was demonstrated that non-linear adhesives with lower elastic modulus and high strain capacity possess a much higher interfacial energy than the linear adhesives. The bond-slip responses observed proved to have a triangular shape and a trapezoidal shape for the linear and non-linear adhesives, respectively.

Fernando et al. [48] conducted an experimental series to investigate the effects of different surface preparation methods and associated roughness parameters on the structural and bond behaviour of CFRP-steel double-strap joints. The test results showed that adhesion failure at the steel/adhesive interface can be avoided if the steel surface is carefully grit-blasted prior to bonding with an adhesive.

Al-Mosawe et al. [68] studied the effects of CFRP properties and sections on the bond between CFRP laminate and steel adherend under quasi-static loading. Based on the results, it was concluded that small CFRP sections are highly sensitive to bond properties and ultra-high modulus CFRP with low tensile strength has a significant effect on the bond behaviour.

The research summarised above suggests that the bond behaviour and the associated failure modes of CFRP-steel systems in ambient conditions are very complex for several reasons summarised below.

1. Usage of different types of CFRP and CFRP thicknesses
2. Different surface preparation methods
3. Usage of different types of adhesives and adhesive thicknesses
4. Installation methods
5. Types of application

2.5 BOND-SLIP MODELS

The bond behaviour of adhesively bonded materials is often studied using bond-slip models [25, 36, 40, 69].

Bond-slip model (Xia and Teng)

Xia and Teng [61] conducted an experimental test series to develop a bilinear bond-slip model (see Figure 2.9) for FRP to steel interfaces. Single lap CFRP-steel joints were used in this experimental study. Two failure modes were observed: (i) cohesive failure and (ii) a combination of plate delamination and cohesive failure. Different adhesive thicknesses were considered, ranging from 1 mm to 6 mm.

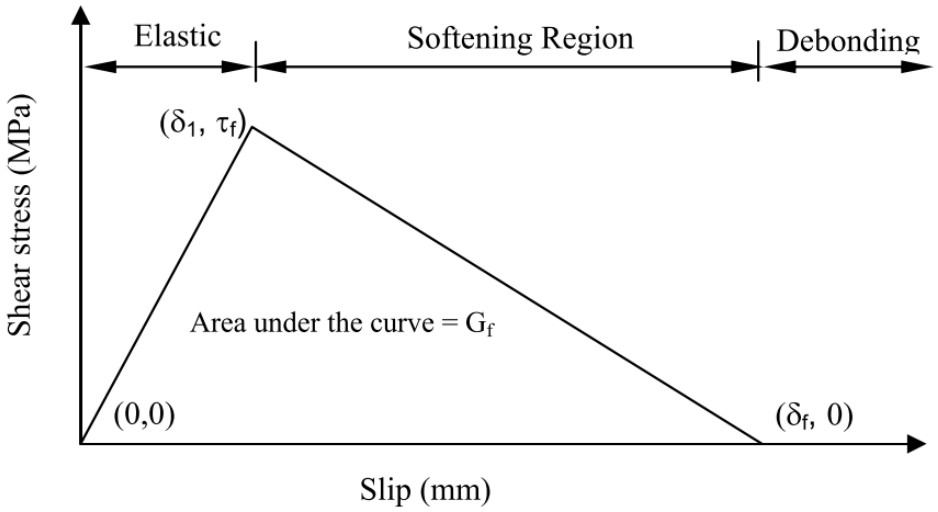

Figure 2.9: Bilinear bond-slip model [59]

The ultimate load of a bonded joint can be approximated by Equation 2.1.

$$P_{ult} = b_p\sqrt{2G_f E_p t_p} \tag{2.1}$$

Then the interfacial fracture energy for a bilinear bond-slip model is calculated using Equation 2.2.

$$G_f = 0.5\tau_f \delta_f \tag{2.2}$$

Hence, Equation 2.1 is modified as follows:

$$P_{ult} = b_p\sqrt{2E_p t_p \tau_f \delta_f} \tag{2.3}$$

In the experiments, it was observed that the value of local bond strength τ_f did not vary with the adhesive thickness and the bond strength was approximated by Equation 2.4.

$$\tau_f = 0.8 f_{t,a} \tag{2.4}$$

Then, the interfacial fracture energy was found to be related to the tensile strength $(f_{t,a})$, the shear modulus (G_a) and the thickness of the adhesive t_a. The product of $\tau_f \delta_f$ was approximated by the following expression (Equation 2.5), based on the test data:

$$\tau_f \delta_f = 62\left(\frac{f_{t,a}}{G_a}\right)^{0.56} t_a^{0.27} \tag{2.5}$$

Therefore, the slip δ_1 at the peak shear stress was defined as $\delta_f = \tau_f / k_a$ where $k_a = G_a / t_a$.

Bond-slip model (Yu et al.)

Yu et al. [36] conducted an experimental study on the behaviour of CFRP-to steel bonded surfaces by testing a series of single-lap bonded joints. Based on the experimental results, the bond-slip responses of different types of bonded joints were studied. The development of bond-slip curves was based on the equations (Equations 2.6 and 2.7) provided in a study by Pham and Al-Mahaidi [69] for CFRP-concrete interfaces:

$$\tau = \frac{E_f(\varepsilon_{f,i+1} - \varepsilon_{f,i})t_f}{\Delta L} \tag{2.6}$$

$$s_i = \frac{(\varepsilon_{f,i+1} + \varepsilon f_{,i})\Delta L}{2} + s_{i-1} \tag{2.7}$$

where, E_f and t_f are CFRP elastic modulus and thickness, $\varepsilon_{f,i+1}$ and $\varepsilon_{f,i}$ are CFRP strains, and ΔL is the distance between strain gauges. The average slip s_i is calculated as the incremental sum of the CFRP extension.

The equivalent longitudinal modulus of the fibre layer $E_{e,f}$ is determined by Equation 2.8:

$$E_{e,f} = \frac{E_a t_a + E_f t_f}{t_a + t_f} \tag{2.8}$$

where, E_a and E_f are the longitudinal tensile modulus of the adhesive and fibre, respectively, and the terms t_a and t_f represent the adhesive and fibre thickness, respectively.

2.6 ENVIRONMENTAL FACTORS

Three components can be identified within the CFRP composite system, which influence durability. They are (i) the matrix (ii) the fibres and (iii) the fibre/matrix interface. Each of the components can undergo deterioration due to various environmental conditions. The effects of different environmental conditions on durability are discussed below.

Moisture-Humidity

Moisture ingress to the CFRP/steel composite is reported as a major drawback [10], as moisture can cause swelling and softening of the bulk adhesive. Absorbed moisture can lead to structural distortions during an extended period of exposure. Once moisture has penetrated through the composite, degradation can occur within the adhesive itself or on one of the interfaces.

Tavakkolizadesh and Saadatmanesh [70] studied the effect of different environmental conditions including simulated seawater on the tensile properties of

FRP composites. They showed that the tensile properties of CFRP had very little effect after a maximum exposure of 2000 hours.

Dawood et al. [27] conducted research on the environmental durability of CFRP-bonded joints and concluded that the accelerated environmental conditions used in the study were more severe than natural environmental conditions. 60% bond strength degradation was observed after six months of exposure to severe environmental conditions. Pre-treating the bonded surface with a silane coupling agent was found to be effective against accelerated environmental conditions. The effect of a glass fibre layer on the durability of the joint was reported as similar to that of specimens bonded with adhesive only. Based on the experimental results, it was concluded that the degradation of the bond strength is primarily due to the deterioration of the interface between the steel and the adhesive.

Recent studies have found that immersion in seawater and accelerated environmental condition can significantly influence the structural behaviour of CFRP-steel composites. For example, Nguyen et al. [19] conducted research using CFRP-steel double strap joints exposed to simulated seawater environments for up to 1000 hours and found significant reductions in joint strength and stiffness.

The mechanism of the strength degradation of CFRP-steel double strap joints is similar to that of general adhesively-bonded joints. Water can penetrate to the interfaces between the adhesive and adherend by diffusion through the composite layer (adhesive and CFRP). The additional moisture due to diffusion can result in two types of degradation: the deterioration of the adhesive, and the deterioration of the interfaces (steel/adhesive and CFRP/adhesive) [71]. Long-term exposure of adhesives to water can result in a reduction in the mechanical properties of the adhesive due to the chemical and physical breakdown of the adhesive [72].

While some research suggests that CFRP can undergo significant deterioration due to accelerated environmental conditions, Other research [73] has reported that CFRP did not undergo significant deterioration during the exposure period.

Temperature

Freeze-thaw cycles can significantly influence the performance of CFRP-steel composites. Karbhari et al. [74] studied the thermal effect on the mechanical properties of CFRP composites under different temperatures and concluded that there may be a reduction in mechanical performance and increased susceptibility to moisture absorption. The following points were highlighted:

i. Exposure to sub-zero temperatures can result in matrix hardening, matrix microcracking, and fibre-matrix bond degradation.

ii. Freeze-thaw cycles in the presence of salt can cause accelerated degradation due to the formation and expansion of salt deposits. Moisture-induced swelling and drying can also cause debonding.

iii. Exposure to high temperature levels above that of processing can result in an initial post-cure, resulting in degradation of composites.

iv. The coefficients of thermal expansion of adhesives may differ from those of bulk resins and/or composites. Thermal exposure can cause premature debonding along the FRP composite-adhesive interfaces.

Based on the analysis of the available literature, Karbhari et al. [74] recommended that testing be carried out over extended (18 months) time periods. Tests conducted over short time periods (less than 18 months) can yield misleading results due to the effects of post-cure and slow interphase and fibre level degradation, and can provide erroneous results.

Kabir et al. [11] studied the environmental durability of CFRP-strengthened hollow steel tubes under accelerated environmental conditioning. Experimental results showed that there may be further degradation in stiffness in the plastic zone due to the high-temperature effect. It was concluded that increase in temperature may accelerate the degradation of the composite by softening or weakening the links of the adhesive.

The glass transition temperature (T_g) has a significant effect on durability under thermal exposure conditions [75]. Adhesives with higher T_g values can increase the long-term durability by preventing the softening of the adhesive due to moisture ingress. Durability can be further increased by applying waterproof sealant on the CFRP composite system.

Al-Shawaf et al. [76, 77] conducted a test series to study the effects of temperature on the mechanical performance and failure modes of CFRP-steel double-strap joints. The temperature was varied between 40 and 60 ^{0}C. Changes in failure modes and joint capacities were observed as a result of the temperature variation.

Chemical Attack

Carbon fibres are known to be a chemically-resistant material and epoxy resin matrix is highly vulnerable to chemicals [78]. The exposure of CFRP composite materials to different chemical solutions can result in different degradation levels. Chemical solutions can accelerate the deterioration of CFRP-steel composites due to the degradation of epoxy resin. Although CFRP itself is a good chemically inert material, exposure of the steel surface to chemical solutions can result in a significant level of steel deterioration ultimately leading to CFRP-steel composite system

failure. Degradation of the steel beneath the CFRP composite can affect the bond properties and result in premature debonding.

Ultra Violet Radiation

The degradation of polymers usually starts at the outer surface and then penetrates gradually into the bulk of the material, initiating the degradation process [79]. Therefore, UV radiation ageing is a critical environmental problem for CFRP materials. Although the degradation due to UV radiation is limited to the surface of the composite material, it can initiate the degradation process, influenced by other environmental factors such as moisture ingress and chemical attack [74, 80]. Therefore, it has been recommended to protect the composite layer from UV radiation [81, 82].

Early research work showed that the effect of UV radiation on the mechanical properties of CFRP composites was negligible [83]. However, some studies reported that UV radiation alone has a significant effect on reducing the load-carrying capacity of composite systems [80]. Nguyen [84] showed that UV radiation does not influence the tensile strength of CFRP composites after one-month exposure. In addition, the experimental results suggested that the reduction in the joint strength of the tested double-strap joints was mainly attributed to the temperature effect rather than UV rays.

Fire

The fire performance of CFRP composite is a major concern in relation to durability. When fibre composite materials are heated beyond the glass transition temperature, they may exhibit a reduction of modulus and related mechanical properties [74]. Although the carbon fibre itself can retain its strength at a very high temperature, most polymeric resins are vulnerable at a lower temperature. The

mechanical properties of epoxy resin materials decrease rapidly when the temperature exceeds glass transition temperature resulting in immature bond failure. Research conducted by Al-Shawaf et al. [76] showed that when the temperature exceeds 60 ^{0}C, adhesively-bonded CFRP-steel double-strap joints retain only about 22% of the initial joint strength measured under ambient conditions.

Nguyen et al. [23] conducted research to investigate the mechanical properties of CFRP-steel adhesively-bonded double-strap joints at elevated temperatures around the glass transition temperature (T_g 42 ^{0}C) of the adhesive. A change in failure mode from adherend failure to debonding failure was observed as the temperature approached T_g. The double strap joints showed a significant reduction in ultimate load and stiffness near T_g, while the effective bond length increased with temperature.

2.7 ACCELERATED ENVIRONMENTAL TESTS

The environmental durability of CFRP composite materials has been studied using accelerated environmental tests. Some of the tests reported in the literature are summarised below.

Dawood and Rizkalla [27] conducted a test series on the environmental durability of CFRP double-strap joints. The specimens were exposed to severe environmental conditions for different durations up to a maximum of six months. The effect of various bond configurations, the GFRP layer and the silane coupling agent were studied. The researchers found that the GFRP used did not help to improve the debility performance of the CFRP-steel double strap joints.

Nguyen et al. [19] studied the effects of harsh environmental conditions on the mechanical performance of CFRP-steel double-strap joints. The effects of simulated

seawater, temperature and relative humidity were studied for a maximum of one year exposure. Significant reductions in joint strength and stiffness were recorded for the specimens exposed to simulated sea water for one year.

Borrie [13] conducted an experimental investigation on the durability of CFRP laminate and sheeting-patched double-strap joints under elevated temperature marine submergence. CFRP-steel double-strap joints were exposed to a 5% NaCl solution for different durations up to six months at different temperatures, while under a static tensile load. The tested samples showed up to 28% strength degradation due to the exposure conditions imposed.

Carbon fibre is an electrically conductive material. Studies show that galvanic corrosion is possible in CFRP material that is in contact with metal where an electrolyte is present [85]. This phenomenon can accelerate deterioration of the composite [26]. Research suggests that the rate of galvanic corrosion can be decreased by using epoxy coating [85, 86].

Kabir et al. [11] used 5% NaCl solution and a direct current to accelerate the degradation of CFRP-strengthened hollow steel tubes under marine environmental conditions. The tubes showed a significant reduction in load-carrying capacity as a result of the accelerated environmental conditions.

Sun [87] studied the corrosion behaviour and failure mechanism of CFRP employed as an anode in a 3% NaCl solution. The experimental results showed that the tensile strength of CFRP decreases with increasing current density and the failure occurred due to the breakage of C-N bonds, which caused the depolymerisation of the epoxy.

Some research has shown that the bond properties and environmental durability of CFRP-steel composite systems are greatly influenced by electrochemical reactions [9, 11, 47]. Kim [9] conducted research to investigate the effect of galvanic current on the physical and mechanical characteristics of CFRP-steel double-strap joints. The experimental results showed that the stress-slip behaviour of the interface is influenced by the electrochemical reaction. The governing failure mode was reported to be CFRP debonding.

The physical and mechanical properties of CFRP composites are greatly influenced by the electrochemical reactions. Swelling and formation of blisters can occur during the reaction process [11]. Degradation of the mechanical properties can result in lower load carrying capacity.

A summary of some of the accelerated environmental test methods used in the research literature is presented in Table 2.4.

Table 2.4: Summary of some previous accelerated environmental tests

Study	Specimen type	Applied current (mA)	Current density ($\mu A/cm^2$)	Cathode type	Corrosion environment
Uomoto et al. (1984)	Beams	167	200-630	Copper plate	Constant immersion, 5% NaCl solution
Tachibana et al. (1990)	Beams	1000	500	Copper plate	Constant immersion, 3.3% NaCl solution
Al-Sulaimani et al. (1990)	Beams	Varies	2000	Stainless steel plate	Constant immersion, salted solution
Lee et al. (1990)	Beams	1000	2000	Copper plate	Constant immersion, 3% NaCl solution
Lee et al. (1997)	Beams	672	230	Copper plate	Constant immersion, 3% NaCl solution
Phillips(1991)	slabs	1800	600	Steel mesh	Constant immersion, 3% NaCl solution
Almusallam et al. (1996)	slabs	2000	3000	Stainless steel plate	In contact with 5% NaCl solution
Tachibana et al. (1990)	Bond- pull-out	32	500	Copper plate	Constant immersion, 3.3 % NaCl solution
Al-Sulaimani et al.(1990)	Bond- pull-out	Varies	2000	Stainless steel plate	Constant immersion, salted solution
Almusallam et al.(1996)	Bond- pull-out	400	10400	Stainless steel plate	Constant immersion, 3% NaCl solution
Bonacci et al. (1998)	Columns	150	45	Stainless steel bar	Wet and dry cycle, 3% NaCl solution
Kim et al. (2015)	Double strap joints	Varies	Varies	Steel strips	Constant immersion, 3.5% NaCl solution
Kim et al. (2016)	Beams	2000	-	Steel strips	Constant immersion, 3.5% NaCl solution
Kabir et al. (2016)	Hollow tubes	2000	482	Stainless steel bars	Constant immersion, 5% NaCl solution

2.8 MODELLING DURABILITY

Considering the number of environmental factors affecting the durability of CFRP composites, different models have been proposed by researchers based on experimental studies. Nguyen et al. [23] developed theoretical models to predict the degradation of CFRP-steel double-strap joints due to temperature effects. Joint stiffness and strength degradation were modelled using a mechanism-based model proposed by Bai et al. [88]. The Hart-Smith model [89]was modified to model variation of bond length due to temperature effects.

Kim et al. [9] conducted experiments on CFRP-steel double-strap joints subjected to accelerated corrosive environments. Complete deterioration was achieved with 72 hours exposure to accelerated environmental conditioning. The fracture energy based interface deterioration model was proposed to predict the deterioration of the CFRP-steel interface considering the long-term durability.

Knowledge is limited due to the lack of long-term experimental data related to the durability of CFRP-steel composite systems. Most of the available predictions [11, 27] and design guidelines [1, 90-92] propose a fixed reduction factor to predict long-term durability.

2.9 DESIGN GUIDELINES ON DURABILITY

Several guidelines have been published to provide design recommendations regarding the installation and maintenance of strengthening of metallic structures using CFRP [1, 44, 90]. The typical design approach is to reduce the material strength by introducing partial safety factors to account for material degradation due to environmental effects.

2.9.1 British guidelines

The British guidelines propose the use of partial safety factors to obtain design values for material properties. The guidelines [91] recommend the use of a partial safety factors based on the fibre type and manufacturing method. The partial safety factors recommended in the British guidelines are given in Tables 2.5 and 2.6.

Table 2.5: Partial safety factors for strength at the ultimate limit state (TR 55 Report)

Material	Partial safety factor (γ_{mf})
Carbon FRP	1.4
Aramid FRP	1.5
Glass FRP	3.5

Table 2.6: Additional partial safety factors (TR 55 Report)

Type of system and method of application (sheets or tapes)	Additional partial safety factor (γ_{mm})
Machine-controlled application	1.1
Vacuum infusion	1.2
Wet lay-up	1.4

Except for the two partial safety factors on the material properties, a factor of safety of 1.1 should be applied on CFRP modulus in the design process.

2.9.2 Italian guidelines

Material partial safety factors in the Italian guidelines [1] (CNR-DT 202/2005) provide an environmental reduction factor (η_a) for different exposure conditions. The values are shown in Table 2.7.

Table 2.7: Material partial safety factors (CNR-DT 202/2005)

Exposure condition	η_a
Internal	0.95
External	0.85
Aggressive environment	0.85

2.10 FINITE ELEMENT ANALYSIS

Finite element (FE) methods are widely used in civil engineering designs. Most researchers use FE models to study the behaviour of CFRP composite systems [17, 18, 93-98] under different loading conditions.

Fawzia et al. [39] developed an FE model to simulate CFRP-bonded steel plate. All the materials were modelled with eight-node brick elements. Three CFRP layers and an adhesive layer were modelled as a single layer, and the composite material properties were used in the analysis. The developed models showed good agreement with the experimental failure loads and deflection values.

Fernando et al. [96] studied debonding failure in CFRP-strengthened rectangular steel tubes subjected to end-bearing loading their proposed FE models. Steel tube was modelled using S4R shell elements with reduced integration. CFRP was considered as orthotropic material and modelled using general-purpose shell elements S4R with reduced integration. A cohesive zone modelling (CZM) approach was used to model the adhesive layer. The interaction of the contact surfaces was defined using the surface-to-surface contact. A quadratic strength criterion was used to define the damage initiation, and the damage evolution was defined using the linear fracture energy-based criterion. Traction-separation behaviour was employed to model the debonding. The proposed FE models were capable of capturing the debonding between CFRP and steel using the cohesive zone model. Overall, the FE results agreed well with the experimental results, and the traction-separation model was capable of accurately modelling debonding failure.

Al-Zubaidy et al. [94] studied the dynamic tensile properties of CFRP composites using CFRP-steel double-strap joints. The experimental results were used to develop and validate FE models. The adhesive layer was modelled using 8-

node-three-dimensional cohesive elements (COH3D8) and the steel was modelled using 8-node three-dimensional first-order reduced hourglass control elements (C3D8R). The CFRP patch was modelled using 8-node quadrilateral in-plane general purpose continuum shell elements with reduced integration with hourglass control (SC8R). An elastic-brittle material model was used to model CFRP and Hashin failure criteria were used to detect the composite damage. A mixed-mode failure criterion with a quadratic traction damage-initiation criterion was used to model the adhesive layer. Overall, the developed FE models reasonably predicted the quasi-static and dynamic behaviour of CFRP-steel-double strap joints regarding peak load, effective bond length, failure mode and strain distribution along the bond length.

Recent literature shows that the use of cohesive zone modelling (CZM) is very efficient and capable of modelling debonding failures. In a recent study, Al-Mosawe et al. [68] studied the bond properties between CFRP laminate and steel bonded by adhesive. The experimental tests were modelled and validated using FE models. The FE modelling approach used was similar to the method employed by Al-Zubaidy [94].

ABAQUS has become a FE package frequently used by researchers to model CFRP composite systems [17, 18, 34, 94, 95, 98]. Most recent FE modelling studies show a similar trend. The element types and material models used are capable of modelling the exact material behaviour. With the improvements made with cohesive zone modelling and composite damage modelling, current FE models are capable of modelling complex failure modes such as adhesive-interface debonding and CFRP failure.

2.11 CHAPTER SUMMARY

A comprehensive review of the literature relevant to the present thesis has been presented in this chapter. The review provided an extensive understanding of the CFRP systems, the bond between CFRP and steel, failure modes, material properties and environmental factors. The chapter has reviewed the literature relevant to the durability of CFRP systems. Based on the critical review presented in this chapter, several gaps were identified.

Sandblasting, metallic grit blasting and mechanical grinding are commonly-used surface preparation methods for steel-CFRP strengthening systems. The bond between steel and CFRP depends to a great extent on the surface preparation method. A comprehensive comparison of these three surface preparation methods is required to identify the most efficient surface preparation method.

The load-carrying capacity of CFRP-steel-double strap joints depends significantly on the bond behaviour between CFRP and steel. The research shows that the use of adhesion promoter (primer) can enhance the bond performance of adhesively-bonded joints. There is no existing literature that quantifies the effect of primer coat application on the durability of CFRP strengthening systems.

Studies carried out on the durability of CFRP-steel composite systems suggest that the strengthened composite can undergo deterioration for longer exposure durations under different environmental conditions. Most durability studies conducted to date have been limited to short periods compared to the expected life span of CFRP systems. Hence, the available experimental data may not reflect the actual long-term behaviour of CFRP-steel composite systems. In addition, the identified failure modes may be significantly different from those found under ambient conditions.

The literature review identified that there may be different types of failure modes in a CFRP-steel composite system, depending on the structural application. When these CFRP-steel composite systems are exposed to certain types of environmental conditions, failure may occur due to CFRP material degradation, adhesive degradation or bond degradation. The effects of the material degradation of CFRP and adhesive can lead to lower structural capacities, and material degradation can result in different failure modes compared to the failure modes identified under ambient conditions. It is necessary to identify the governing failure modes for CFRP-steel composite systems after being exposed to environmental conditioning. In addition, the bond-slip behaviour of degraded CFRP-steel interfaces may be significantly distinct from the known bond-slip behaviour under ambient conditions.

Some research has tried to evaluate the durability of an embedded GFRP layer in CFRP-steel strengthening systems. The effect of such an embedded GFRP layer in CFRP systems should be studied further to determine the structural performance, bond properties and failure modes of such strengthening system.

It is necessary to conduct a comprehensive investigation of the durability of CFRP-steel composite systems considering material degradation. The relevant bond properties and associated failure modes can be identified through a detailed experimental study. Understanding of the long-term durability and evaluation of the associated failure modes is important for the development of an efficient CFRP-steel strengthening system.

Chapter 3: Experimental program

3.1 INTRODUCTION

This chapter outlines the experimental program conducted to evaluate the bond durability and structural behaviour of CFRP-steel composite systems under accelerated environmental conditions. The experimental program was undertaken in three series to achieve the specific research objectives. Each experimental series is described in detail with the associated test scenarios and parameters in the following sections of this chapter. The electrochemical method used to impose the accelerated environmental conditions on the test specimens is illustrated. Furthermore, the material properties, the test procedures used, loading conditions and instrumentation are described in detail.

3.2 MATERIAL TESTING

3.2.1 Steel coupon tensile testing

Standard tensile tests [99] were carried out using an Instron testing machine of 100 kN capacity (Figure 3.1 (a)). Wedge grips were used at both ends of the steel coupon specimen. Displacement control loading of 1 mm/min was applied. An MTS extensometer of 50 mm gauge length was used to measure the axial elongation. Load and axial displacement were recorded at each increment. The experimentally-measured yield strength of steel was registered as 352 MPa. Refer to Appendix C for more details.

3.2.2 CFRP coupon testing

Standard tensile tests [100] were carried out using an Instron testing machine of 100 kN capacity (Figure 3.1(b)). Wedge grips were used at both ends of the CFRP coupon specimen. Displacement control loading of 1 mm/min was applied. Load and axial displacement were recorded at each increment. The experimentally-measured CFRP composite tensile strength was registered as 967 MPa. The failure modes and loads of tested CFRP coupons are presented in Appendix C.

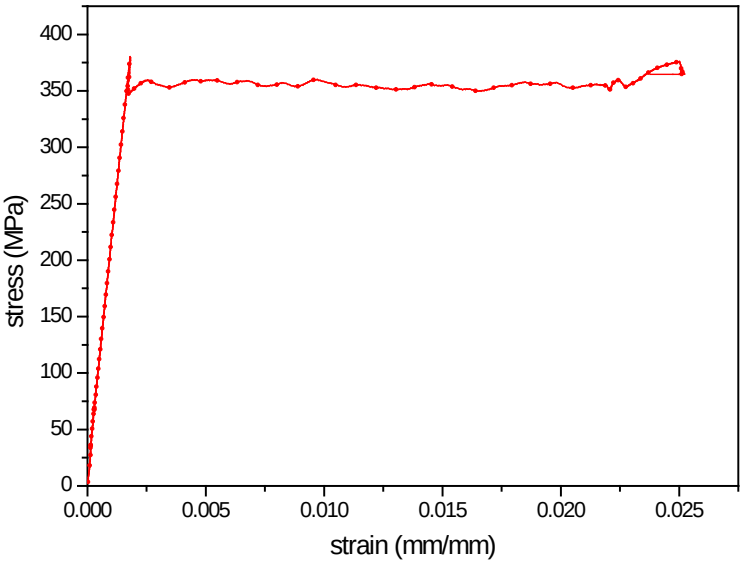

(a) Steel coupon testing

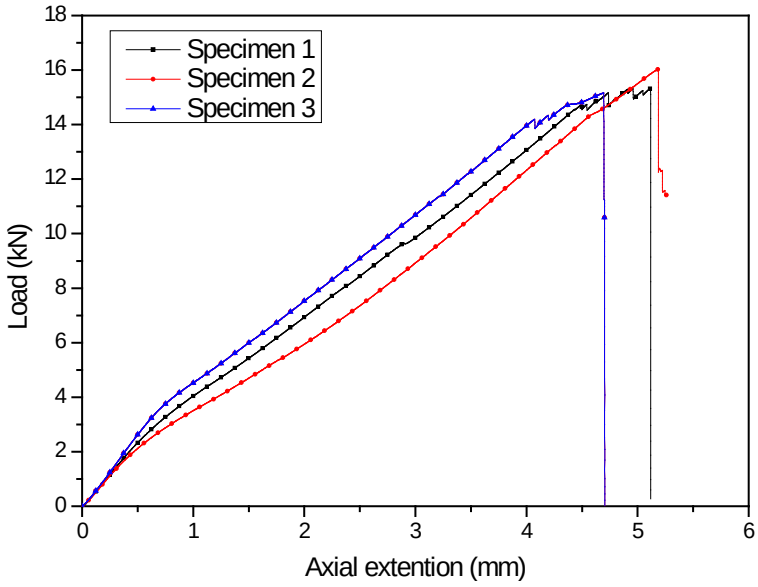

(b) CFRP coupon testing

Figure 3.1: Material testing

3.3 SERIES 1– (CFRP-STEEL DOUBLE-STRAP JOINTS)

3.3.1 Materials

Four materials were involved in this series: steel, normal modulus carbon fibre (MasterBrace FIB 300/50 CFS), two-part epoxy primer (P3500) and two-part epoxy adhesive (P4500) produced by BASF. The manufacturer-provided material properties are given in Table 3.1**.**

Table 3.1: Manufacturer-provided material properties

Engineering properties	steel	CFRP	Epoxy	Primer
Density (kg/m^3)	7850	1807	1100	1080
Elastic modulus (GPa)	210	230	-	0.7
Tensile strength (MPa)	530	4900	>17	>12
Yield stress (MPa)	350	-	-	-
Ultimate elongation (%)	36	2.1	-	3

3.3.2 Specimen preparation

The CFRP-steel double-strap joints were fabricated by joining two steel segments (25 mm in width, 6 mm thick and 200 mm in length) together with CFRP sheets, as shown in Figure 3.2. The CFRP layers on one side of the bonded joint were shorter than those on the other side of the joint to ensure that failure occurred in the shorter bond length side. The shorter bond length was selected as 75 mm, based on the effective bond length under ambient conditions [5]. The width of the CFRP sheet was maintained the same as the steel plate. The wet lay-up method was used to form the double-strap joint. The steel surface was sandblasted, grit-blasted or mechanically ground, depending on the specimen description. The prepared surface was cleaned with acetone to remove oil, grease and rust from the surface prior to bonding. The two-part epoxy primer was then applied to the cleaned, dust-free steel surface. On this primed surface, the two-part epoxy adhesive layer was applied, and pre-cut CFRP sheets were pasted on top of the adhesive layer. A flat roller and a

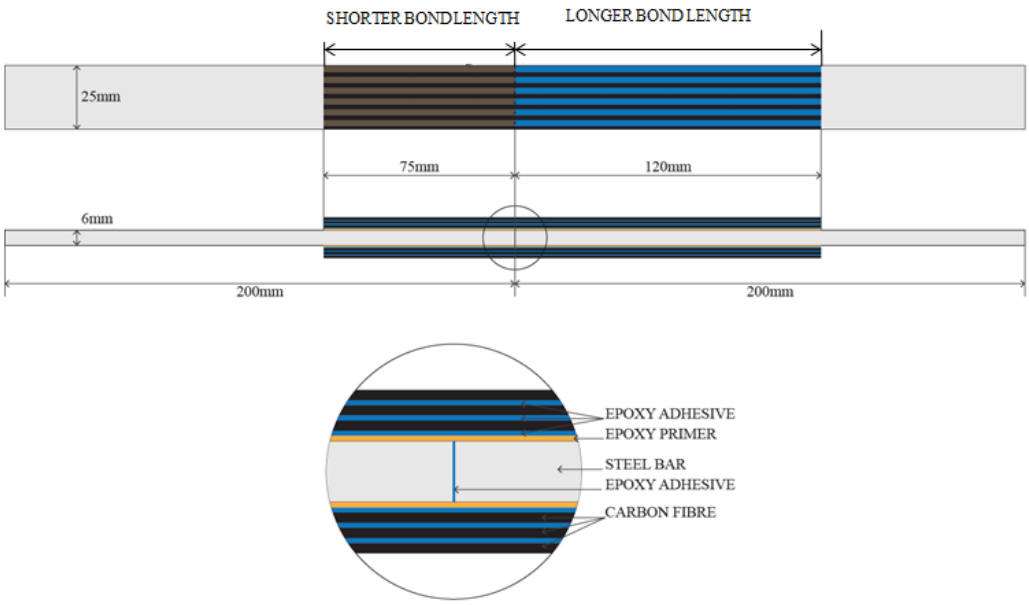

Figure 3.2: Schematic representation of a double-strap joint

ribbed roller were used to press the CFRP sheets onto the epoxy adhesive to ensure a constant adhesive thickness throughout the specimen and to remove air voids. After that, this side was cured for 24 hrs; the same procedure was followed to apply CFRP on the other side of the steel plates. The specimens were then cured for a minimum of seven days prior to subjecting them to accelerated corrosive exposure conditions.

3.3.3 Test scenarios and test specimens

This stage of the experimental program was planned to be carried out in three scenarios. The first scenario (S1) was to investigate the effect of surface preparation on CFRP-steel double-strap joints. For this purpose, three different surface preparation methods were used (i.e. sandblasting (garnet #60), aluminium grit blasting (aluminium grit #60) and mechanical grinding (80 grit abrasive belt)). Both the sandblasted and grit-blasted surfaces were shown to have rough surface profiles. In contrast to these samples, machine-ground samples had smoother and shinier surfaces. These surface profiles are shown in Figure 3.3. Specimen details and the test conditions for this scenario are given under S1 in Table 3.2. For these samples,

the first two characters represent the number of longitudinal CFRP layers used. The third and fourth letters (SB = sandblasting, AG = aluminium grit-blasting and MG = mechanical grinding) represent the surface preparation method.

(a) Sandblasted surface (b) Grit-blasted surface (c) Machine ground surface

Figure 3.3: Surface profiles

The second scenario (S2) was to investigate the effect of a primer coat on the structural behaviour and the durability of CFRP-steel double-strap joints. For this purpose, two types of specimens were fabricated, with and without a primer coat. Two exposure durations were imposed on these specimens to compare the effect of a primer coat on joint capacity. All the specimens used in S2 were sandblasted prior to strengthening and had one layer of CFRP on each side. Details of the specimens and the exposure conditions are given under S2 in Table 3.2. For these samples, the first two characters represent the number of longitudinal CFRP layers used and the third and/or fourth letter describes the application of primer (P = samples with a primer layer and NP = samples without primer layer). The next letter/s describe the exposure conditions (i.e. CS =control specimens (no exposure), A = 24 h exposure and B = 48 h exposure).

The third scenario (S3) was intended to investigate the effect of the number of CFRP layers on the bond properties of CFRP-steel double-strap joints subjected to accelerated corrosion for different exposure durations. The sandblasting surface preparation method was used for all the specimens in S3. Basically, the specimens

were divided into two types (i.e. Type F and Type SF). These two types were selected to simulate the existing structures' exposure conditions. The details of these two types are shown in Figure 3.4. In type F specimens, only the CFRP shorter bond length was subjected to accelerated corrosion. In type F specimens, the un-bonded steel was protected by applying an anti-corrosive paint followed by a silicone gel layer. In type SF specimens, the entire shorter bond length region below the joint including the steel area was subjected to accelerated corrosion. The specimens were categorised according to their CFRP layer arrangement (i.e. 1L = one longitudinal layer of CFRP, 2L = two longitudinal layers of CFRP, and 3L = three longitudinal layers of CFRP). For each category, three exposure durations were imposed. These three exposure durations, (i) Group A (24 h), (ii) Group B (48 h) and (iii) Group C (72 h), were determined based on Faraday's Law, resulting in 5%, 10% and 15% mass loss in bare steel samples. A uniform current level was maintained for all the specimens during the exposure periods. The control specimens (CS) were tested under ambient conditions without imposing any accelerated corrosion conditions. The whole testing program for S3 is given in Table 3.2, and the notations follow the system mentioned above.

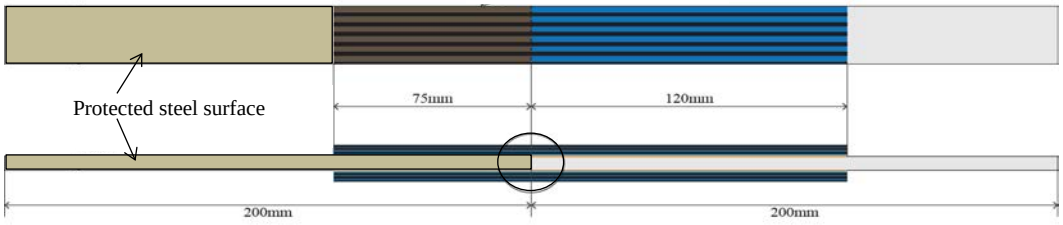

(a) Type F specimen

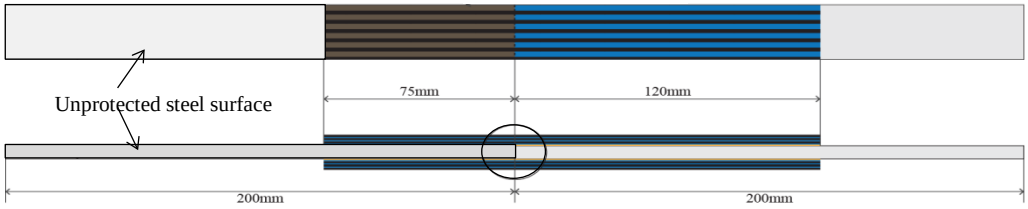

(b) Type SF specimen

Figure 3.4: Specimen details of S3 – series 1

3.3.4 Accelerated corrosion cell set-up

An electrochemical method was used to accelerate the corrosion of the CFRP-steel double-strap joint and CFRP strengthened beam specimens. A direct current of 0.18 A was applied to the specimens, using an integrated system incorporating a rectifier with a built-in ammeter to monitor the current and a potentiometer to control the current intensity. A direct current was used in this experiment, and the current density was within the range mentioned in the research [101]. The direction of the current was adjusted such that the specimen served as the anode. A stainless steel bar was positioned in the tank to act as the cathode. Each specimen's intended degradation bond length portion was fully immersed in an aqueous solution of 5% sodium chloride in a plastic tank. The salinity level used here is slightly higher than the world average salinity found in the ocean and is

used by most researchers [11, 19, 27]. A schematic representation and the laboratory test set-up of the accelerated corrosion cell are shown in Figure 3.5.

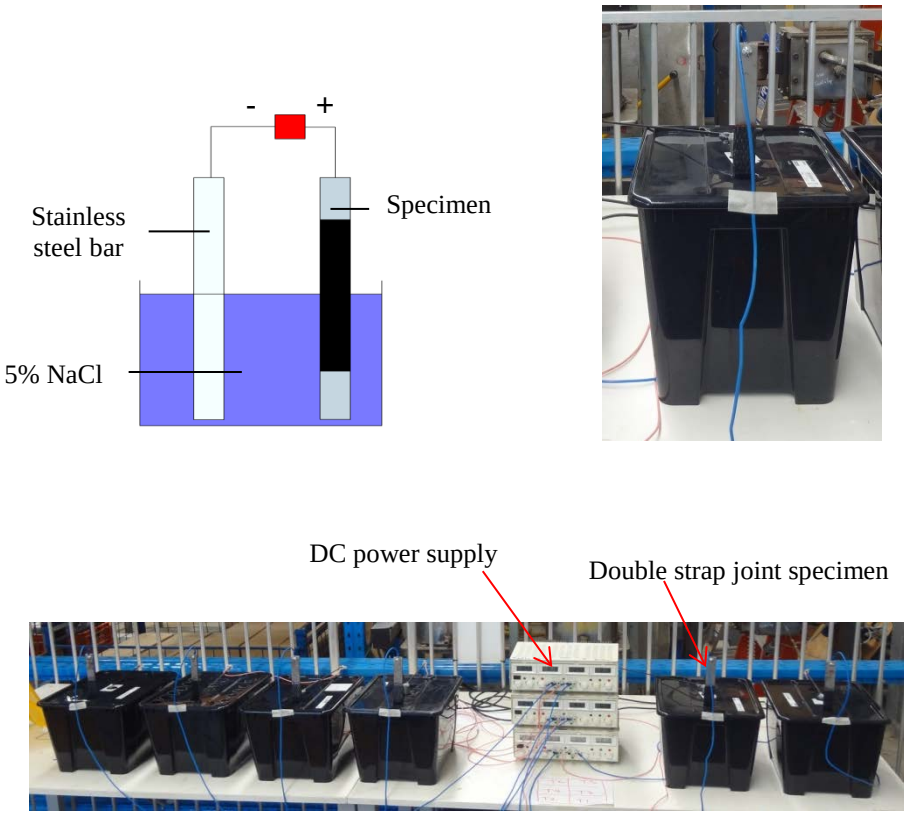

Figure 3.5: Laboratory test set-up

Table 3.2: Test specimen matrix – Series 1

Test scenario	Specimen identification	Sample description	Exposure duration (h)	Number of repetitions
S1	2L-SB	Sandblasted	0	3
	2L-AG	Grit-blasted	0	3
	2L-MG	Mechanically ground	0	3
S2	1L-P-CS	Sandblasted primed steel with one longitudinal CFRP layer	0	3
	1L-P-A		24	3
	1L-P-B		48	3
	1L-NP-CS	Sandblasted non-primed steel with one longitudinal CFRP layer	0	3
	1L-NP-A		24	6
	1L-NP-B		48	3
S3	Control specimens-Sandblasted specimens with primer coat application			
	1L-CS	One longitudinal CFRP layer	0	6
	2L-CS	Two longitudinal CFRP layers	0	3
	3L-CS	Three longitudinal CFRP layers	0	3
	Type F specimens-Sandblasted specimens with primer coat application			
	1L-F-A	One longitudinal CFRP layer	24	3
	1L-F-B		48	3
	1L-F-C		72	3
	2L-F-A	Two longitudinal CFRP layers	24	3
	2L-F-B		48	3
	2L-F-C		72	3
	3L-F-A	Three longitudinal CFRP layers	24	3
	3L-F-B		48	3
	3L-F-C		72	3
	Type SF specimens-Sandblasted specimens with primer coat application			
	1L-SF-A	One longitudinal CFRP layer	24	3
	1L-SF-B		48	3
	1L-SF-C		72	3
	2L-SF-A	Two longitudinal CFRP layers	24	3
	2L-SF-B		48	3
	2L-SF-C		72	3
	3L-SF-A	Three longitudinal CFRP layers	24	3
	3L-SF-B		48	3
	3L-SF-C		72	3

3.3.5 Instrumentation and loading procedure

Double-strap joint specimens were tested in tension to failure at a constant displacement rate of 1 mm/ min, using an Instron testing machine with a capacity of 100 kN, as shown in Figure 3.6. Self-locking grips were used at each end of the specimen to minimise the initial slip.

Figure 3.6: Tensile loading set-up

3.4 SERIES 2 – (CFRP-STEEL DOUBLE-STRAP JOINTS)

3.4.1 Materials

Five materials were involved in this series: steel, normal modulus carbon fibre (MasterBrace FIB 300/50 CFS), glass fibre, two-part epoxy primer (P3500) and two-part epoxy adhesive (P4500) produced by BASF. The manufacturer-provided material properties are given in Table 3.3**.**

Table 3.3: Manufacturer-provided material properties

Engineering properties	steel	CFRP	GFRP	Epoxy	Primer
Density (kg/m^3)	7850	1807	2540	1100	1080
Elastic modulus (GPa)	210	230	72	-	0.7
Tensile strength (MPa)	530	4900	3400	>17	>12
Yield stress (MPa)	350	-	-	-	-
Ultimate elongation (%)	36	2.1	4.8	-	3

3.4.2 Specimen preparation

The CFRP-steel double strap joints were fabricated by joining two steel segments (25 mm in width and 6 mm thick) together with CFRP sheets as shown in Figure 3.7. The width of the CFRP sheet was maintained the same as the steel plate. The bond length of the CFRP varied from 20 mm to 180 mm. The wet lay-up method was used to form the double-strap joint. The steel surface was sandblasted to remove any coating material and then cleaned with acetone to remove oil, grease and rust from the surface before bonding. The two-part epoxy primer was then applied to the cleaned, dust-free steel surface. On this primed surface, the two-part epoxy adhesive layer was applied, and pre-cut CFRP sheets were pasted on top of the adhesive layer. A flat roller and a ribbed roller were used to press the CFRP sheets onto the epoxy adhesive to ensure a constant adhesive thickness throughout the specimen and to remove air voids. Once this side had cured for 24 h, the same procedure was followed to apply CFRP on the other side of the steel plates. The specimens were

then cured for a minimum of seven days before being subjected to environmental conditioning. Foil strain gauges (FLA-6-350-1) were used to measure the strain. Figure 3.8 shows the strain gauge positions for the different series of specimens. Specimens with GFRP layers were fabricated using the same procedure.

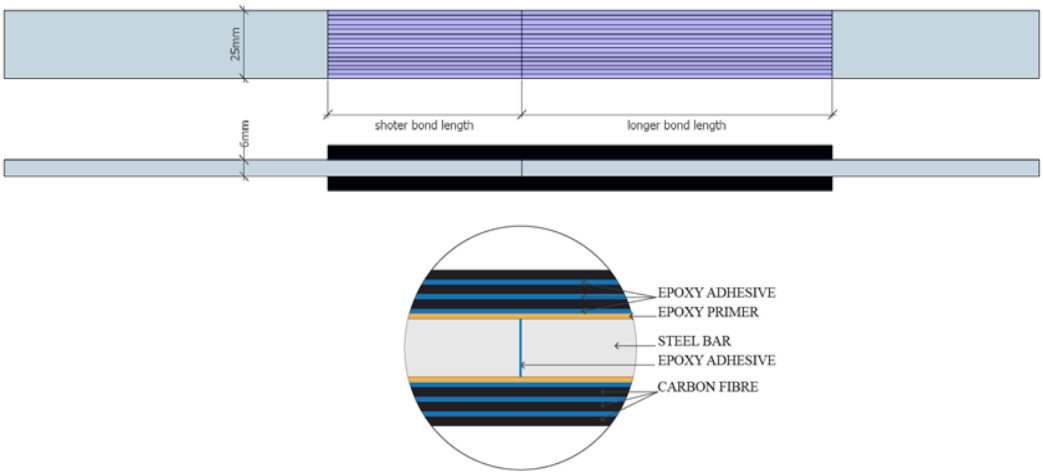

Figure 3.7: Schematic diagram of CFRP-steel double-strap joint – Series 2

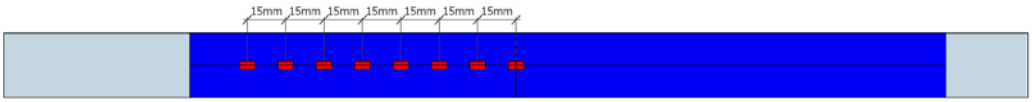

1LCF-120 and 2LCF-120

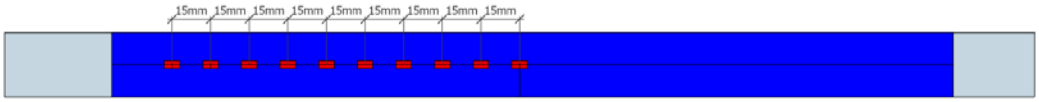

1LCF-160 and 2LCF-160

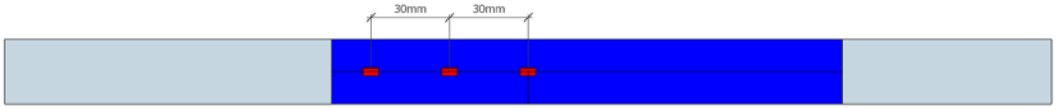

1LCF-CS, 1LGF-CS, 2LGF-CS and 3LGF-CS

Figure 3.8: Schematic diagram of strain gauge locations (not to scale)

3.4.3 Test parameters

Three parameters were used in this test series to investigate their influence on the performance of the joint capacity and the failure modes. They were (i) CFRP bond length (ii) number of CFRP layers and (iii) effect of GFRP layer. The bond configurations and the exposure durations considered in the experimental program are given in Table 3.4. Test scenarios 1 and 2 were intended to evaluate the effect of CFRP bond length and the effect of multi-layer CFRP systems, respectively. Test scenario 3 evaluated the effect of embedded GFRP layers for three different exposure durations.

In the specimen group identification in Table 3.4, the first two characters represent the number of longitudinal layers used, and the next two letters describe the type of fibre (CF = carbon fibre, GF = glass fibre, GC = both glass and carbon fibre). The last character/s represent the exposure condition (CS = control specimen, A = 24 h exposure, B = 48 h exposure and C = 72 h exposure).

Table 3.4: Test specimen matrix – Series 2

Test scenario	Specimen group	Specimen description	Exposure duration (h)	Number of specimens
S1	1LCF	One longitudinal CFRP layer both sides, bond lengths from 20 mm to 180 mm	24	9
S2	2LCF	Two longitudinal CFRP layers both sides, bond lengths from 20 mm to 180 mm	24	9
S3	1LCF-CS	One longitudinal CFRP layer both sides	0	3
	2LCF-CS	Two longitudinal CFRP layers both sides	0	3
	3LCF-CS	Three longitudinal CFRP layers both sides	0	3
	1LGF-CS	One longitudinal GFRP layer both sides	0	2
	2LGF-CS	Two longitudinal GFRP layers both sides	0	2
	3LGF-CS	Three longitudinal GFRP layers both sides	0	2
	2LGC-CS	One GFRP and one CFRP longitudinal layer both sides	0	2
	2LGC-A	One GFRP and one CFRP longitudinal layer both sides	24	2
	2LGC-B	One GFRP and one CFRP longitudinal layer both sides	48	2
	2LGC-C	One GFRP and one CFRP longitudinal layer both sides	72	2
	1LCF-A	One longitudinal CFRP layer both sides	24	3
	1LCF-B	One longitudinal CFRP layer both sides	48	3
	1LCF-C	One longitudinal CFRP layer both sides	72	3
	2LCF-A	Two longitudinal CFRP layers both sides	24	3
	2LCF-B	Two longitudinal CFRP layers both sides	48	3
	2LCF-C	Two longitudinal CFRP layers both sides	72	3

3.4.4 Accelerated corrosion cell set-up

An electrochemical method was used to accelerate the corrosion of the CFRP-steel double-strap joints and CFRP strengthened beam specimens. A direct current was applied to the specimens, using an integrated system incorporating a rectifier with a built-in ammeter to monitor the current and a potentiometer to control the current intensity. A direct current was used in this experiment, and this current density was within the range mentioned in the research [101]. The direction of the current was adjusted such that the specimen served as the anode. A stainless steel bar was positioned in the tank to act as the cathode. Each specimen's intended

degradation bond length portion was fully immersed in an aqueous solution of 5% sodium chloride in a plastic tank. The salinity level used here is slightly higher than the world average salinity found in the ocean and is used by most researchers [11, 19, 27]. A schematic representation and the laboratory test set-up of the accelerated corrosion cell are shown in Figure 3.9.

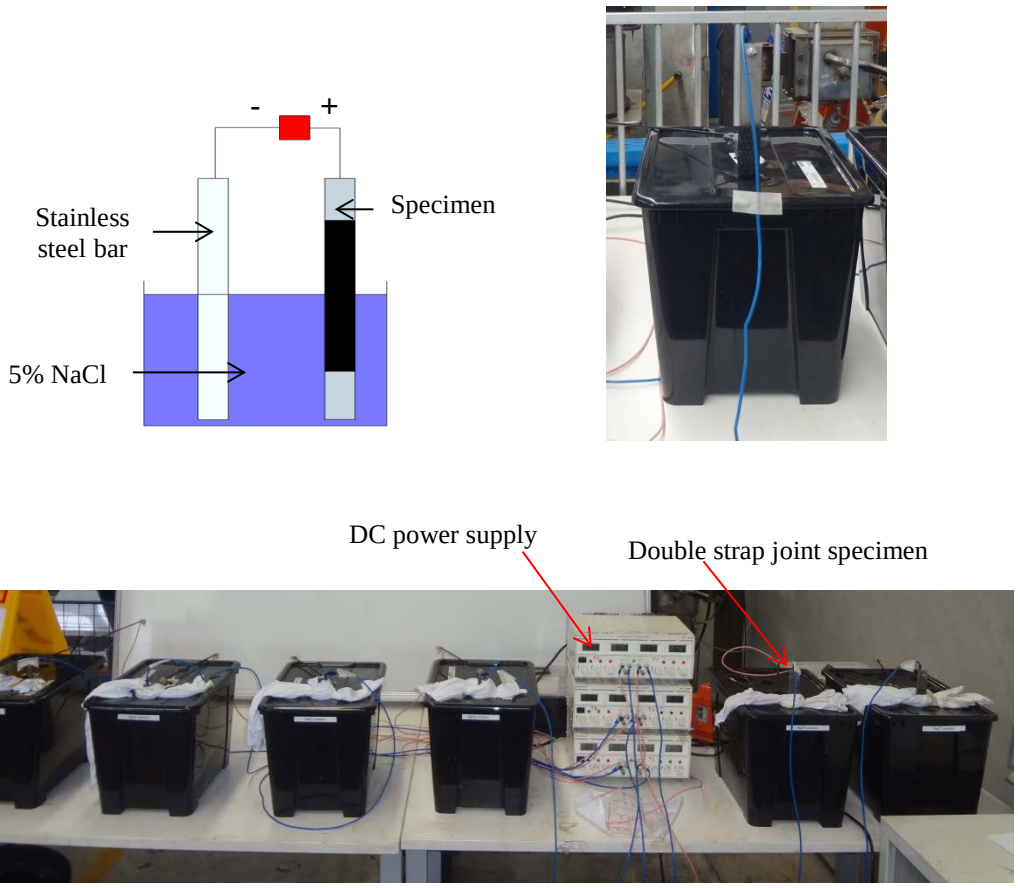

Figure 3.9: Laboratory test set-up – Series 2

3.4.5 Instrumentation and loading procedure

Double-strap joint specimens were tested in tension to failure at a constant displacement rate of 1 mm/ min using an Instron testing machine with a capacity of 100 kN (Figure 3.10). Self-locking grips were used at each end of the specimen to minimise the initial slip. Strain, load and displacement readings for each increment were recorded using a data acquisition system.

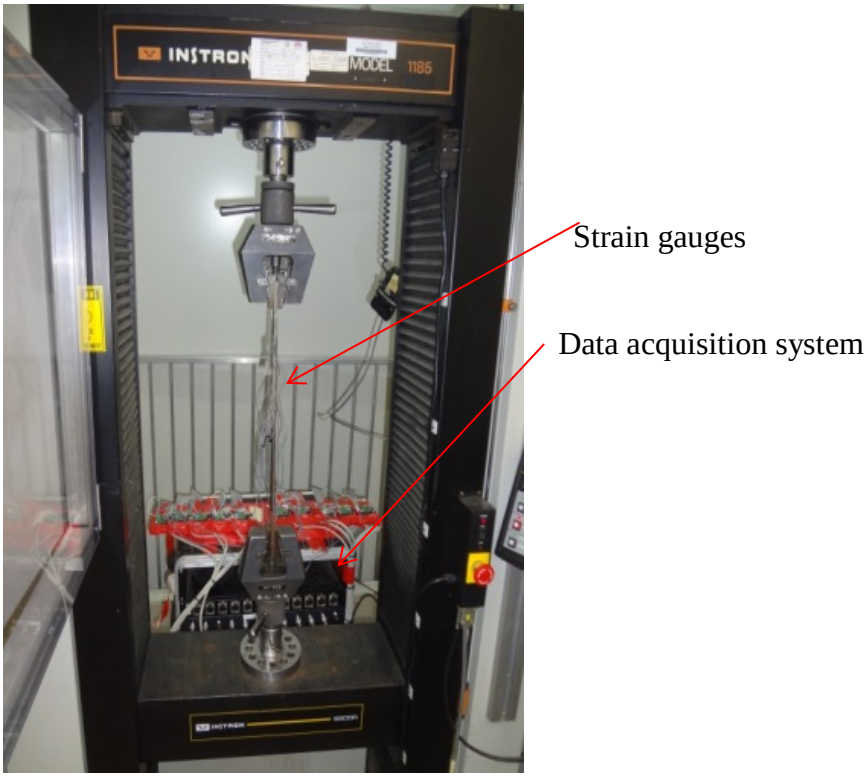

Figure 3.10: Instrumentation and loading set-up – series 2

3.5 SERIES 3 – (CFRP STRENGTHENED BEAMS)

3.5.1 Materials

Four materials were involved in this series: steel, normal modulus carbon fibre (MasterBrace FIB 300/50 CFS), two-part epoxy primer (P3500) and two-part epoxy adhesive (P4500) produced by BASF. The manufacturer-provided material properties are given in Table 3.5**.**

Table 3.5: Manufacturer-provided material properties

Engineering properties	Steel	CFRP	Epoxy	Primer
Density (kg/m^3)	7850	1807	1100	1080
Elastic modulus (GPa)	210	230	-	0.7
Tensile strength (MPa)	530	4900	>17	>12
Yield stress (MPa)	350	-	-	-
Ultimate elongation (%)	36	2.1	-	3

3.5.2 Specimen details

The steel beams used were 150 UB14 universal beam sections of 1300 mm long. A total of seven beams were cut to the required lengths before sandblasting. Figure 3.11 shows a schematic representation of a beam and its dimensions.

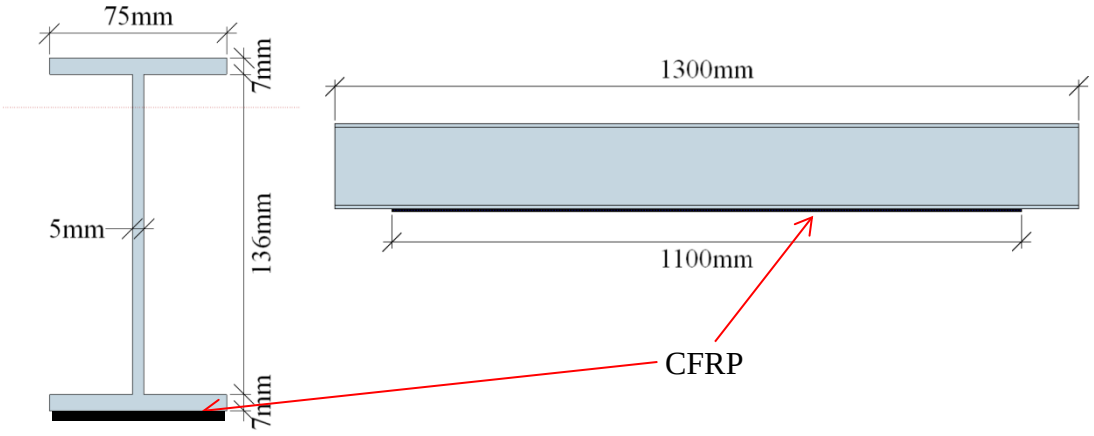

Figure 3.11: Beam details (not to scale)

3.5.3 Specimen preparation

The CFRP-strengthened beam specimens were fabricated by installing two CFRP layers on the bottom flange of the 150 UB 14 sections. The width of the CFRP sheet was maintained the same as the bottom flange width. The wet lay-up method was used. The steel surface was sandblasted before installing the CFRP. Sandblasted specimens are shown in Figure 3.12.

Figure 3.12: Sandblasted specimens

The prepared surface was cleaned with acetone to remove oil, grease and rust prior to bonding. The two-part epoxy primer was then applied to the cleaned, dust-free steel surface (Figure 3.13) On this primed surface, the two-part epoxy adhesive layer was applied, and pre-cut CFRP sheets (1100 mm) were pasted on top of the adhesive layer. A flat roller and a ribbed roller were used to press the CFRP sheets onto the epoxy adhesive to ensure a constant adhesive thickness throughout the specimen and to remove air voids. The specimens were then cured for a minimum of

seven days prior to undergoing accelerated environmental conditioning. CFRP-strengthened beams are shown in Figure 3.14.

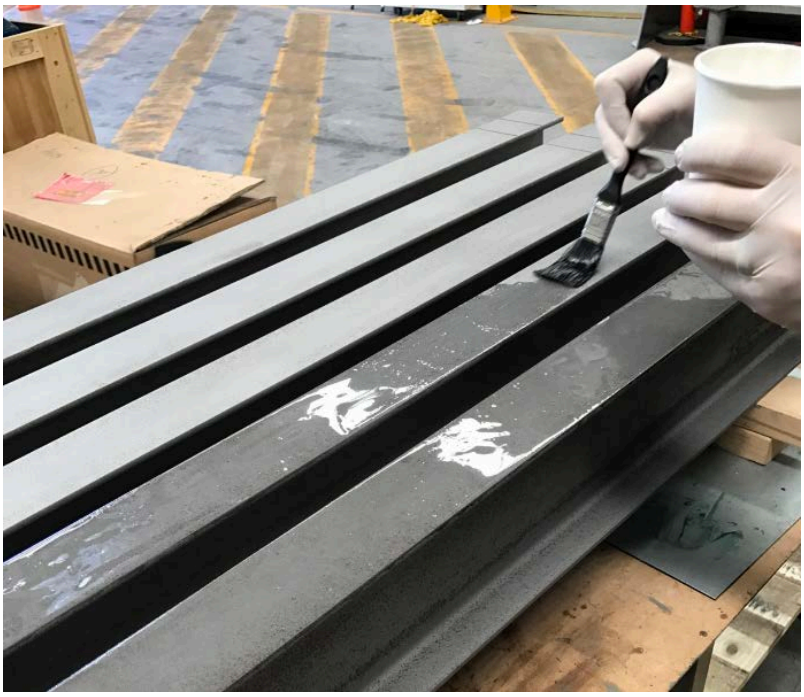

Figure 3.13: Application of primer coat on beams

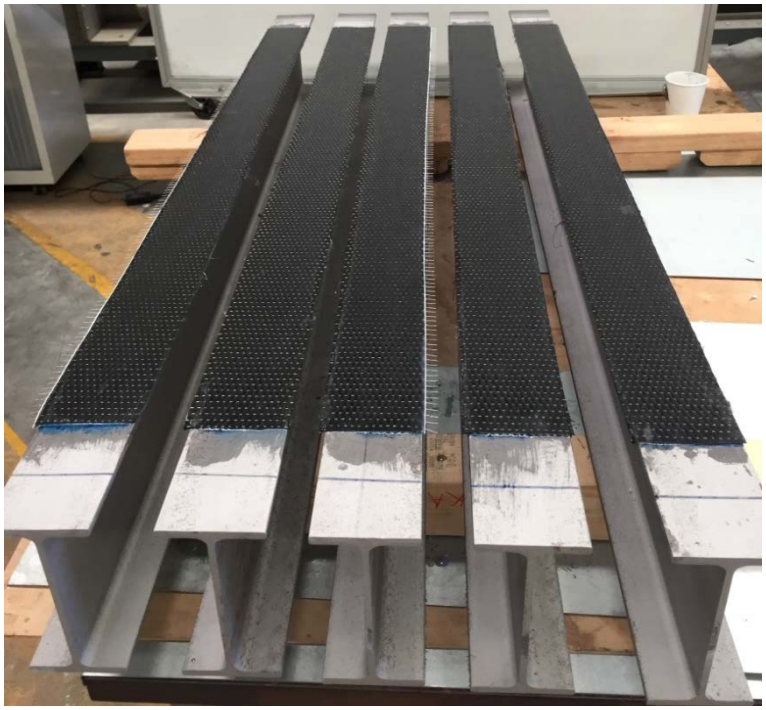

Figure 3.14: Completed CFRP-strengthened beams

3.5.4 Test parameters

Seven specimens were tested in this experimental series to study the effect of accelerated environmental conditions on structural behaviour, and the failure modes of CFRP strengthened beams. The bond configurations and the exposure durations considered in the experimental program are given in Table 3.6. The specimens were divided into four main categories: (i) control specimens without CFRP (B300-A), (ii) CFRP-strengthened steel beams without environmental exposure (B300-B), (iii) CFRP-strengthened beams where only the CFRP layer was subjected to exposure (B300-C) and (iv) CFRP strengthened beams where both the steel and CFRP layer were subjected to exposure (B300-D). Group C and D are named type F and type SF respectively. In type F specimens, precautions were taken to ensure that only the CFRP layer was in contact with the accelerated environment. Consecutive layers of corrosion-resistant paint were applied to the steel surface to protect the steel surface from corrosion, and a waterproof silicon layer was applied on top of the paint coat for additional protection. Schematic representations of type F and SF specimens are shown in Figure 3.15 and a completed type F specimen is shown in Figure 3.16.

Table 3.6: Test specimen matrix – Series 3

Beam identification	CFRP configuration	Exposure duration (h)	Number of specimens
B300-A	No CFRP layers	0	1
B300-B	Two CFRP layers on the bottom flange	0	1
B300-C (Type F)	Two CFRP layers on the bottom flange Only CFRP is exposed to environmental conditioning	120	2
B300-D (Type SF)	Two CFRP layers on the bottom flange Both CFRP and steel are exposed to environmental conditioning	120	2

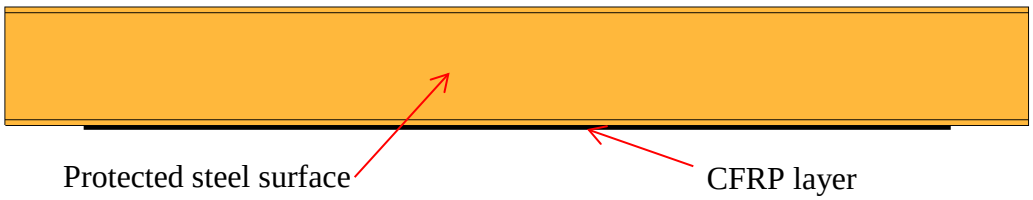

(a) Type F specimen

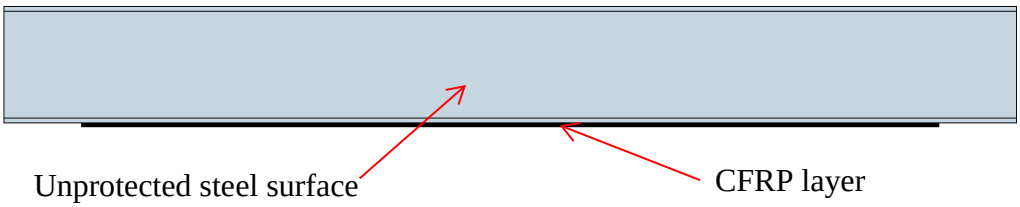

(b) Type SF specimen

Figure 3.15: Specimen details – type F and type SF

Figure 3.16: Type F specimen

3.5.5 Accelerated corrosion cell setup

An electrochemical method was used to accelerate the corrosion of the CFRP-strengthened beam specimens. A direct current was applied to the specimens, using an integrated system incorporating a rectifier with a built-in ammeter to monitor the current and a potentiometer to control the current intensity. A current density of 363 $\mu A/cm^2$ was used in this experiment, and this current density is within the range mentioned in the research [101]. The direction of the current was adjusted such that the beam specimen served as the anode. A stainless steel bar was positioned in the tank to act as the cathode. Each specimen's intended degradation bond length portion was fully immersed in an aqueous solution of 5% sodium chloride in a plastic tank. The salinity level used here is slightly higher than the world average salinity found in the ocean and is used by most researchers [11, 19, 27]. A schematic representation and the laboratory test set-up of the accelerated corrosion cell are shown in Figures 3.17 and 3.18 respectively.

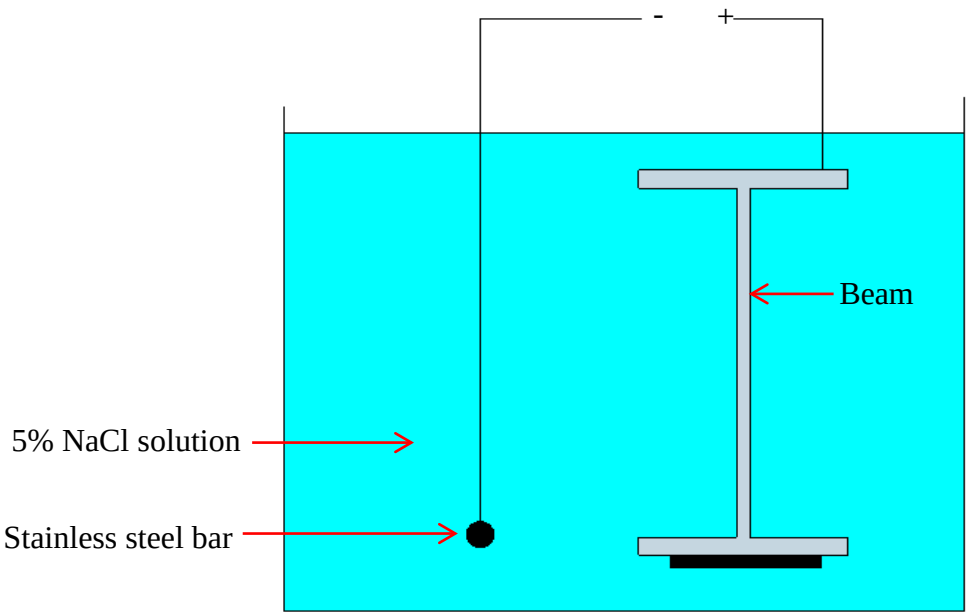

Figure 3.17: Schematic representation of the accelerated corrosion cell setup

Figure 3.18: Laboratory accelerated corrosion cell setup

3.5.6 Instrumentation and loading procedure

Beams were tested under four-point bending to failure using a hydraulic loading machine with a capacity of 400 kN. Load was applied to the loading points using a spreader beam. Rollers were used at both ends of the beams and the loading locations. Strain, load and mid-span deflection readings for each increment were recorded using a data acquisition system. Strain gauges were attached in the longitudinal direction to the centre of the bottom flange of each tested beam (Figure 3.19). Schematic representation of the loading set up and the laboratory setup are shown in Figure 3.20.

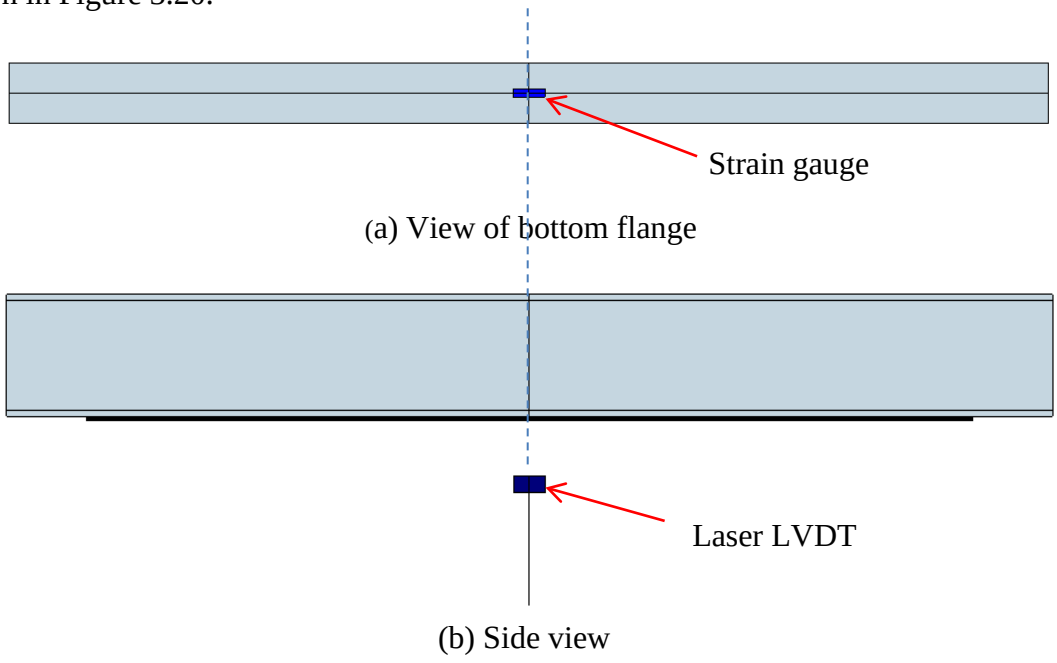

Figure 3.19: Strain gauge and LVDT location for beams

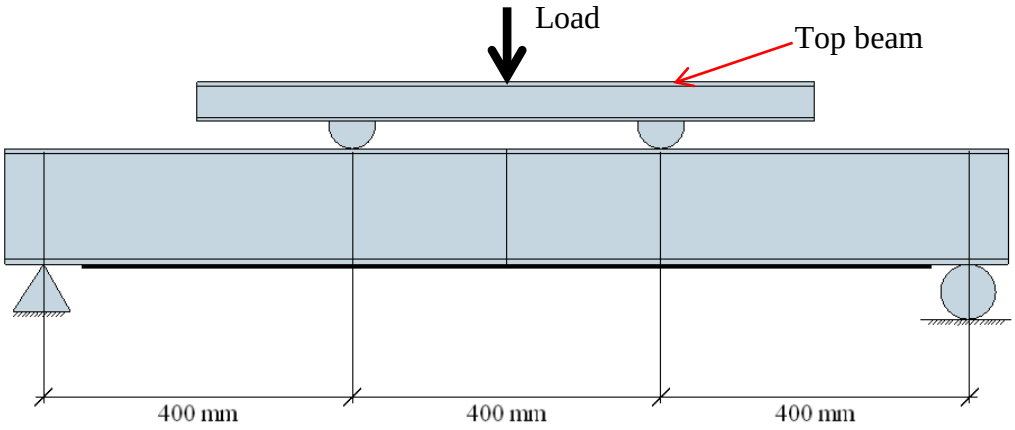

(a) Schematic diagram

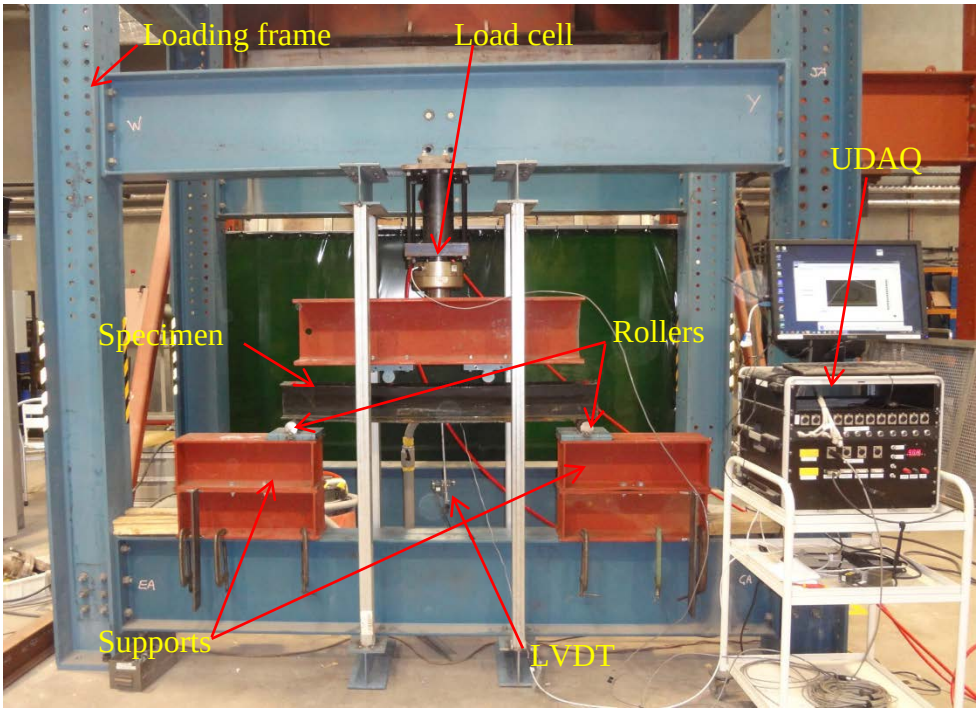

(b) Laboratory test setup

Figure 3.20 Loading setup

3.5.7 Data collection

A universal data acquisition system (UDAQ) was used to synchronise all the load, displacement and strain readings. Load cells, strain gauges, and LVDTs (Figure 3.21) were used to measure load, strain and deflection respectively. All the readings were recorded at 0.5 second intervals. Photographs were taken at each critical step during the experiments.

(a) Strain gauge

(b) Laser LVDT

Figure 3.21: Strain gauge and LVDT

3.6 CHAPTER SUMMARY

Material testing, accelerated corrosion method, specimen preparation and test procedures have been presented in detail in this chapter. The material tests provided consistent results, confirming that the specimen preparation and instrumentation were carried out accurately. Specimen dimensions, test conditions and test parameters were discussed in detail under three experimental series. The test specimen matrices contained all the details of testing conditions and the number of specimens tested for each case. Furthermore, this chapter has provided a detailed description of the testing methods used in the experiments. CFRP-steel double-strap joint specimens were tested under tension, and the beam specimens were tested under four-point bending to failure. The failure modes and test results are discussed in Chapter 4.

Chapter 4: Experimental Results and Analysis

4.1 INTRODUCTION

This chapter presents the results of the experimental program that was conducted to study the environmental durability of CFRP-strengthened steel structures exposed to accelerated environmental conditions. The experimental program consisted of three series, as presented in Chapter 3, and the results of each are analysed and presented in this chapter. The effects of the evaluated parameters under each test scenario are analysed and discussed in detail.

4.2 CFRP-STEEL DOUBLE-STRAP JOINT SPECIMENS (SERIES 1)

4.2.1 Failure loads and failure modes

The failure load and failure mode of each specimen are shown in Table 4.1. Failure modes are discussed below in detail, together with the relevant test scenario.

Table 4.1: Failure loads and failure modes of specimens – Series 1

Test scenario	Specimen identification	Average failure load (kN)	Failure mode
S1	2L-SB	19.6	Steel-adhesive interface debonding
	2L-AG	20.8	Steel-adhesive interface debonding
	2L-MG	10.9	Steel-adhesive interface debonding
S2	1L-P-CS	12.1	Steel-adhesive interface debonding
	1L-P-A	9.2	CFRP rupture and steel-adhesive interface debonding
	1L-P-B	6.0	CFRP rupture and steel-adhesive interface debonding
	1L-NP-CS	9.8	Steel-adhesive interface debonding
	1L-NP-A	5.6	CFRP rupture and steel-adhesive interface debonding
	1L-NP-B	2.5	CFRP rupture and steel-adhesive interface debonding
S3	Control specimens		
	1L-CS	12.2	Steel adhesive interface debonding
	2L-CS	18.1	Steel adhesive interface debonding
	3L-CS	21.9	Steel adhesive interface debonding
	Type F specimens		
	1L-F-A	9.2	CFRP rupture and steel-adhesive interface debonding
	1L-F-B	6.0	CFRP rupture
	1L-F-C	4.1	CFRP rupture
	2L-F-A	18.6	CFRP rupture and steel-adhesive interface debonding
	2L-F-B	14.5	CFRP rupture and steel-adhesive interface debonding
	2L-F-C	13.2	CFRP rupture and steel-adhesive interface debonding
	3L-F-A	22.6	Steel-adhesive interface debonding
	3L-F-B	20.5	Steel-adhesive interface debonding
	3L-F-C	18.2	CFRP rupture and steel-adhesive interface debonding
	Type SF specimens		
	1L-SF-A	11.6	Steel-adhesive interface debonding
	1L-SF-B	13.6	Steel-adhesive interface debonding
	1L-SF-C	13.0	Steel-adhesive interface debonding
	2L-SF-A	18.9	Steel-adhesive interface debonding
	2L-SF-B	18.3	Steel-adhesive interface debonding
	2L-SF-C	18.7	Steel-adhesive interface debonding
	3L-SF-A	22.8	Steel-adhesive interface debonding
	3L-SF-B	21.4	Steel-adhesive interface debonding
	3L-SF-C	21.2	Steel-adhesive interface debonding

Scenario 1 (S1)

All of the tested samples from S1 failed due to steel-adhesive interface debonding, as shown in Figure 4.1. No damage was observed in the CFRP layers. This type of failure is a common failure mode in double strap joints, as reported in the research literature [19, 27, 40]. The type of surface preparation did not affect the failure mode. However, the ultimate failure loads had a significant effect, depending on the surface preparation method.

Figure 4.1: Steel-adhesive interface debonding of double-strap joints

Scenario 2 (S2)

The specimens tested after exposure to the corrosive environment showed different failure modes compared to the control specimens tested under S2. Control specimens of both types 1L-P and 1L-NP showed steel-adhesive interface debonding failure. All the specimens of types 1L-P-A and 1L-NP-A showed mixed mode failure. In these samples, some of the CFRP fibres were debonded from the matrix and part of the CFRP layer showed steel-adhesive interface debonding. In addition, some CFRP fibres showed rupture. With the increment of exposure duration to 48 h, type 1L-P-B and 1L-NP-B specimens failed due to CFRP rupture at the joint location. Ruptured fibres were concentrated at the joint location and it was observed that a small number of CFRP fibres had debonded from the matrix. The failure modes of 1L-NP specimens are shown in Figure 4.2.

(a)

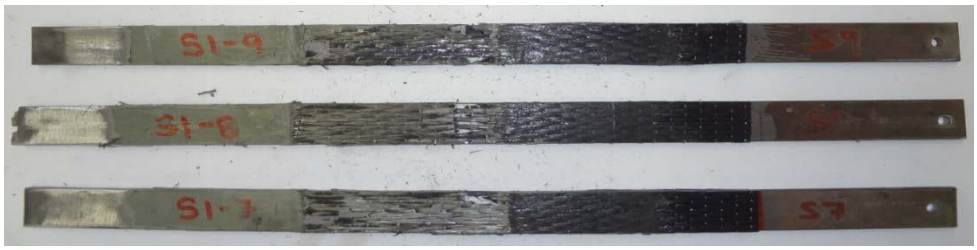

Failure mode of 1L-NP-A specimens

(b)

Failure mode of 1L-NP-B specimens

Figure 4.2: Failure mode of 1L-NP specimens

Scenario 3 (S3)

All the control specimens tested under scenario 3 failed due to steel-adhesive interface debonding, irrespective of the number of CFRP layers installed. Type 1L-F-A specimens started to show a mixed mode of failure (CFRP rupture and steel-adhesive interface debonding failure), as illustrated in Figure 4.3. In this type of failure, rupture of CFRP was not concentrated in a particular region. The specimens showed a V-shaped failure of the CFRP fibres from the joint location, and most of the outward fibres failed near the joint location, and the inner fibres failed at a distance from the joint centre. With the increment of exposure conditions, the failure region changed towards the joint location, showing full CFRP rupture at the location of the joint. This type of transformation of failure mode was also identified in type 2L-F and 3L-F samples with the increment of exposure duration. However, complete CFRP rupture was not observed after the maximum exposure duration (72 h). For 3L-F specimens with 48 h exposure, the failure mode showed some debonding of CFRP fibres from the matrix. However, the governing failure mode was identified as

steel-adhesive interface debonding failure. With further increments of exposure duration up to 72 h, the number of fibres debonded from the matrix increased. The governing failure mode remained steel-adhesive interface debonding. These results indicate that the number of CFRP layers plays a major role in accelerated corrosive environments. The failure modes of type F samples are compared in Figure 4.3.

All the type SF specimens failed due to steel-adhesive interface debonding. The failure mode of these specimens did not depend on the exposure duration. The exposed steel surface showed uniform corrosion due to the accelerated environmental conditions. The failure modes of the control specimens and type SF specimens are shown in Figure 4.4.

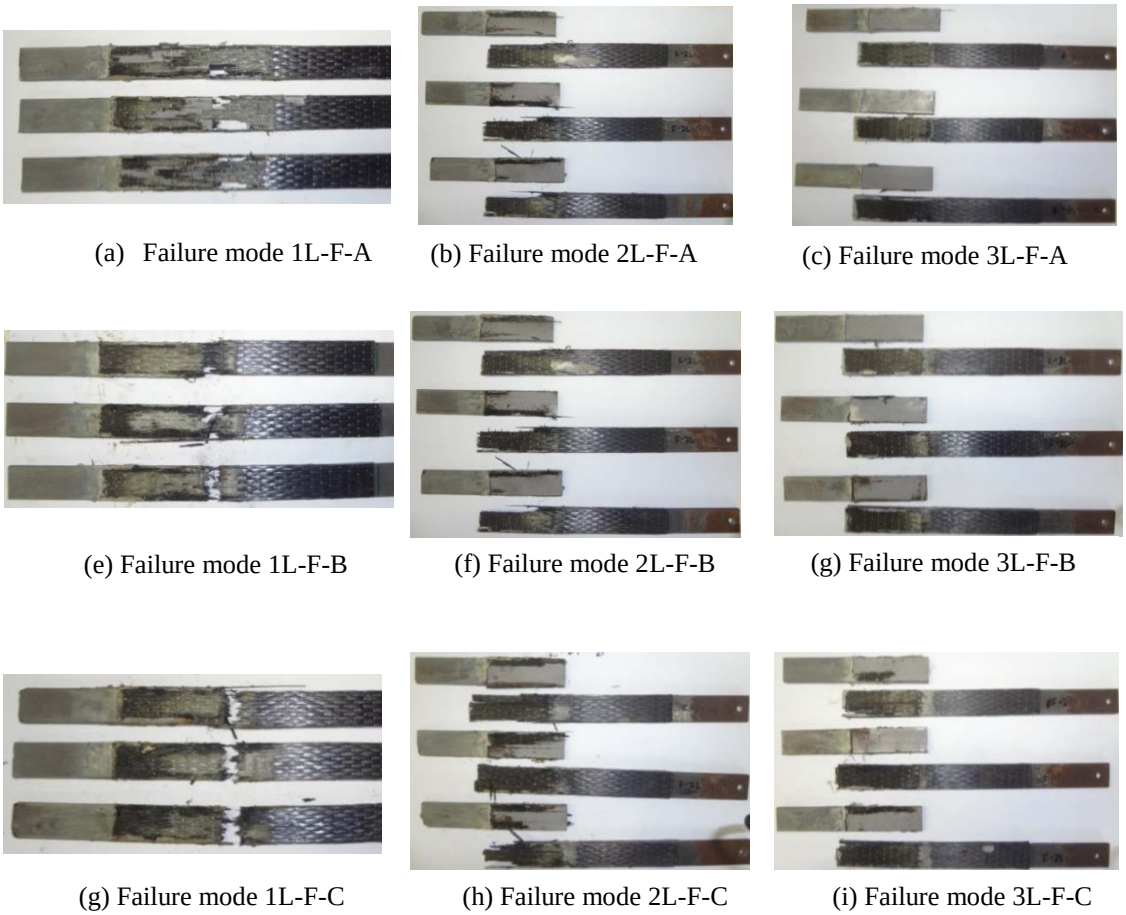

(a) Failure mode 1L-F-A (b) Failure mode 2L-F-A (c) Failure mode 3L-F-A

(e) Failure mode 1L-F-B (f) Failure mode 2L-F-B (g) Failure mode 3L-F-B

(g) Failure mode 1L-F-C (h) Failure mode 2L-F-C (i) Failure mode 3L-F-C

Figure 4.3: Failure modes of type F specimens

(a) (b)

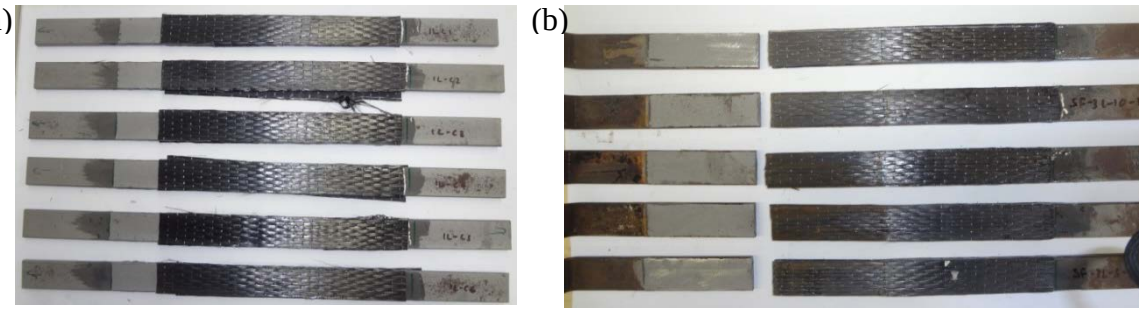

Figure 4.4: Failure modes (a) Control specimens (b) Type SF specimens

According to the research literature, unexposed specimens often undergo steel-adhesive interface failure [19, 37, 39, 102-104]. Similarly, all the control specimens (unexposed) in this experimental program showed a debonding of CFRP from the bonded steel surface, as shown in Figure 4.4. Several studies have identified a shift in the failure region after environmental ageing. Normally, after exposure to environmental ageing, the failure tends to shift to a location very close to or at the interface between the adhesive and the metal surface [19, 27]. In the present study, a significant change in failure mode was observed after exposure to accelerated corrosion. The failure mode shifted from steel-adhesive interface failure to CFRP rupture with increased exposure duration. This phenomenon is only possible if the CFRP material deteriorates. The failure mode of type 1L-F specimens shifted from steel-adhesive interface failure to CFRP rupture with increased exposure durations A, B and C, respectively. The failure mode of type 2L-F and 3L-F specimens also changed from steel-adhesive interface debonding failure to mixed mode failure (a combination of steel-adhesive interface debonding failure and CFRP rupture) with the exposure duration. This mixed mode failure indicates that the failure of type 2L-F and 3L-F specimens could be changed from steel-adhesive interface debonding failure to CFRP rupture if the specimens were exposed for longer durations.

A significant colour change was observed in the CFRP layers when exposed to accelerated corrosion. The colour variation of CFRP layers with exposure duration is shown in Figure 4.5. In particular, type F specimens showed a different colour to the control specimens and the CFRP surface became softer. Slight discoloration was observed in type SF specimens after exposure to accelerated corrosion. In both the type F and SF specimens, no corrosion was observed between the CFRP and steel-bonded surface. Analyses of failure modes indicated that CFRP material degradation is prominent rather than bond degradation due to accelerated corrosion conditions. The evolution of failure modes can be attributed to the deterioration of the CFRP composite, which was confirmed by analysing composite stress levels, as described in Section 4.2.4.

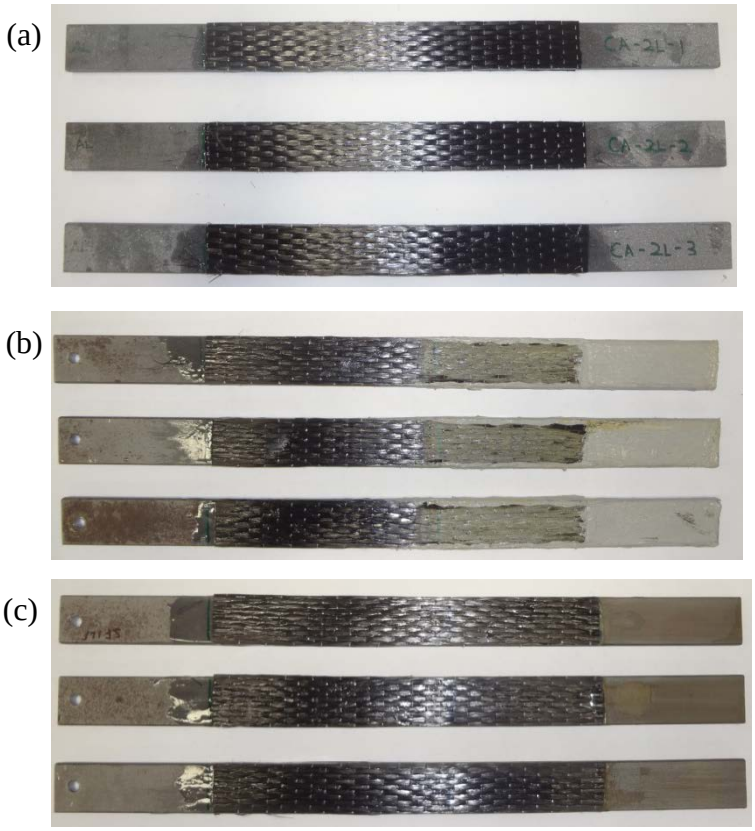

Figure 4.5: Colour transformation with exposure conditions

(a) Control specimens (b) Type F specimens (C) Type SF specimens

4.2.2 Effect of surface preparation method

Three different surface preparation methods were used, as in S1, and the load vs. joint displacement behaviour of specimens is shown in Figure 4.6. Of the three surface preparation methods, sand- and grit-blasted surfaces resulted in the same ultimate load range, while machine-ground specimens showed a significant reduction in ultimate load compared to the other two methods. This finding is consistent with that of Fernando et al. [48], who recommended that grit-blasting be used as the surface preparation technique. In addition, the results of the current research show that sandblasting led to the same ultimate load range as the grit blasted surface, thus providing an economical solution. The joint displacement of sand- and grit-blasted specimens was about 2 mm, while the machine-ground specimens showed a displacement of around 1.3 mm. This similarity in behaviour of sand- and grit-blasted surfaces can be attributed to the particle size of the sand and the aluminium grit used during the blasting process. The results indicate that #60 garnet and aluminium oxide as blasting media are capable of providing similar surface profiles and result in the same ultimate load levels.

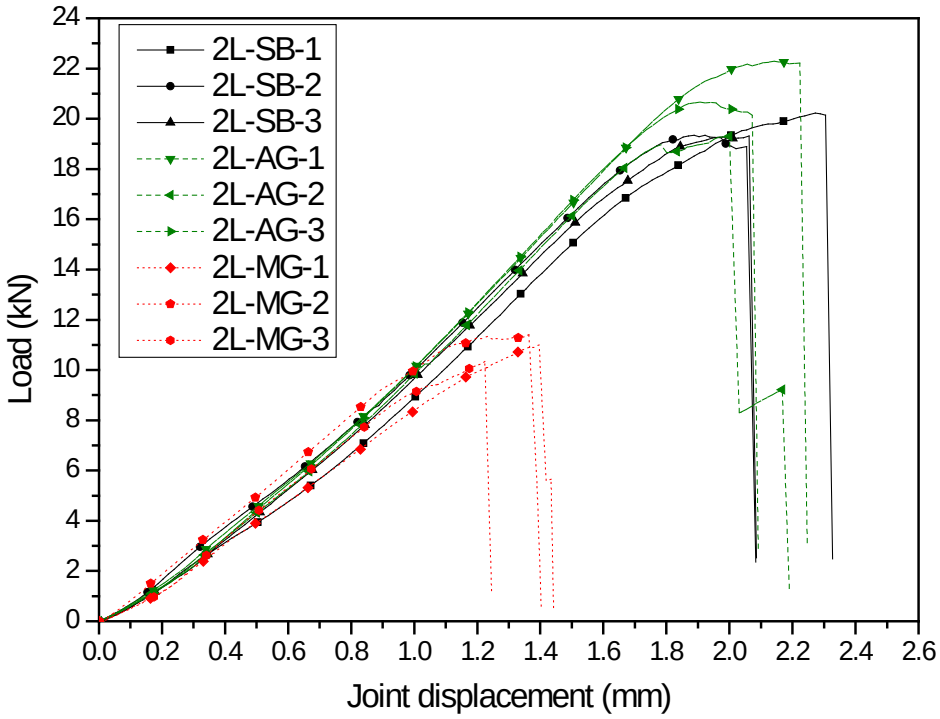

Figure 4.6: Load vs. displacement of S1 specimens

4.2.3 Effect of primer layer

The load vs. displacement results of specimens from S2 are shown in Figure 4.7. The results show that the application of primer coating prior to installing CFRP is an effective way to increase the load-carrying capacity of double-strap joints. The samples prepared with primer coat failed at an average load of 12.3 kN, and the samples without primer failed at an average load of 9.8 kN. After exposure for 24 h, type 1L-NP specimens showed a 43% decrease in load-carrying capacity. At the same level of exposure, type 1L-P specimens showed a 24% reduction in capacity. Within the next 24 h of exposure, this further reduced to 74% and 50% of full capacity for type 1L-NP and 1L-P specimens, respectively. The rate of degradation of joint capacity was higher in specimens fabricated without primer coat than the joints fabricated with a primer coat. It was also evident that the overall reduction in load-carrying capacity is lower with the application of primer. The results indicate

that the application of primer increases not only the load-carrying capacity but also the durability of CFRP strengthening systems in accelerated corrosive environments.

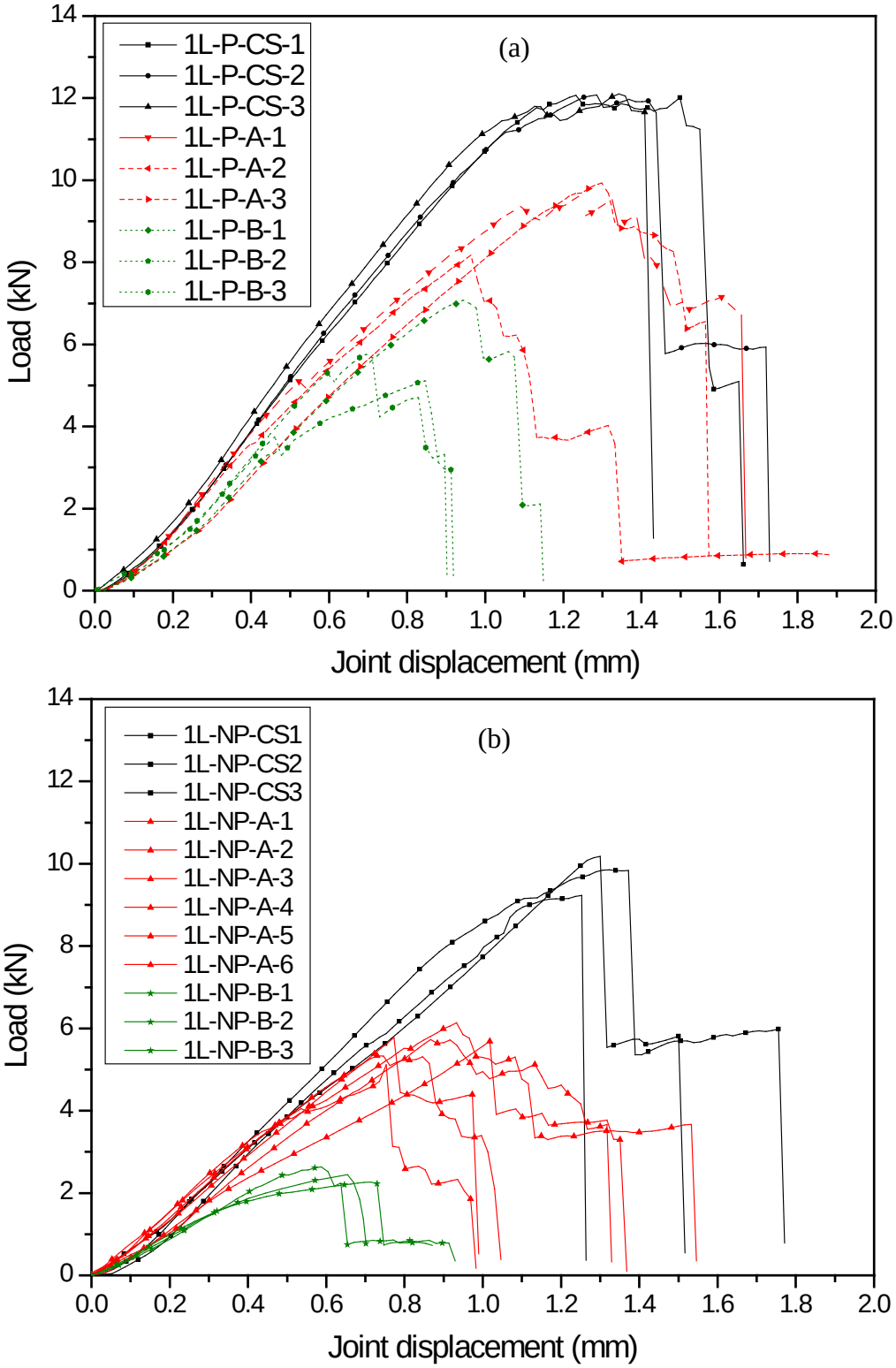

Figure 4.7: Load vs. displacement (a) 1L-P specimens (b) 1L-NP specimens

4.2.4 Effect of exposure conditions on number of CFRP layers

Joint strength

During tensile tests, linear relationships were observed for load vs. joint displacement graphs for all the types of specimens until they reached their ultimate loads. When the ultimate load was achieved, the load was suddenly reduced by a significant amount without increasing the joint displacement, indicating a sudden failure of the joint specimens.

The ultimate strength of each joint under different exposure durations was normalised to that of the unexposed one-layer CFRP joint specimens. The results for normalised strength are shown in Figure 4.8. In type 1L-F joint specimens exposed to accelerated corrosion for 24, 48 and 72 h, the strength reduced by 24%, 51% and 66% respectively. After 24 h exposure, 2L-F and 3L-F specimens did not show any strength reduction due to accelerated corrosion conditions. After that time, 20% and 6% strength reductions were observed in 2L-F and 3L-F specimens respectively, when the exposure duration increased to 48 h. Further, it reduced to 27% and 17% respectively, with 72 h exposure duration. A possible explanation for these results is the added resistance to accelerated corrosion due to the increased number of CFRP layers. The results of the 1L-F specimens show that the degradation of CFRP material occurs when it is exposed to accelerated corrosion conditions, and the severity is increased with longer exposure durations. Increasing the number of CFRP layers helps to protect the innermost CFRP layer by restricting ion penetration through the composite.

Type SF specimens did not show any strength reduction due to the application of accelerated corrosion. Compared to the control specimens, a slight increment of joint strength was observed in type SF specimens during the exposure periods.

However, no strength reduction was seen with the maximum exposure duration of 72 hours. The degradation of CFRP was delayed due to the exposed steel surface. A possible explanation for this is the difference in the rates at which corrosion takes place in steel and CFRP composite. When both CFRP and steel are exposed to accelerated corrosion, corrosion occurred at a higher rate in steel than in CFRP composite.

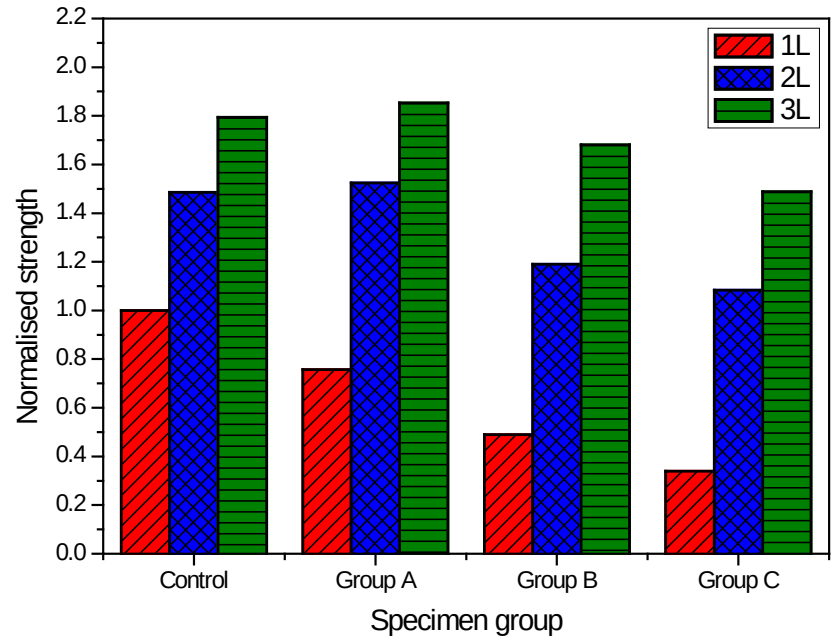

(a) Type F specimens

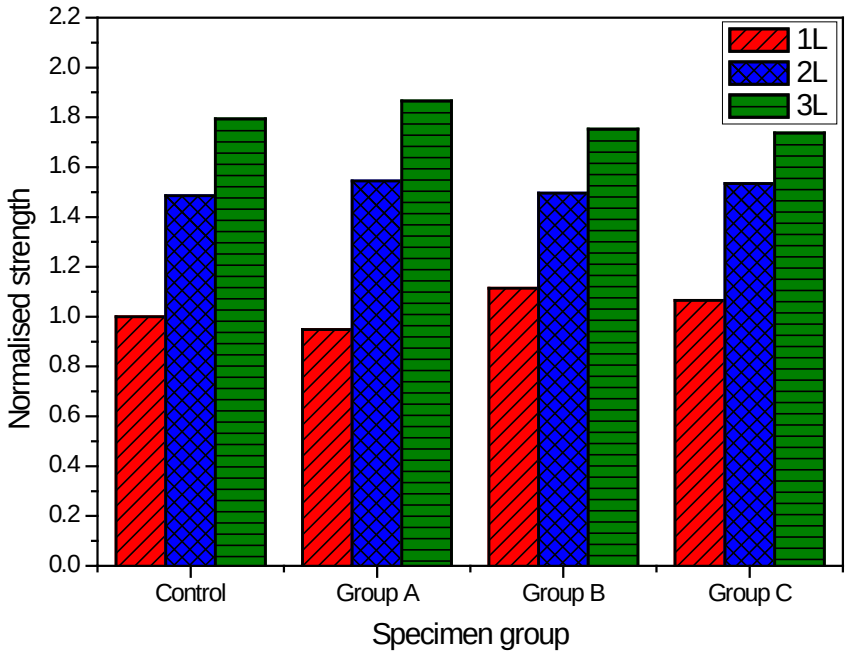

(b) Type SF specimens

Figure 4.8: Normalised joint strength

Joint stiffness

In all specimens, the load vs. joint displacement relationships showed a linear behaviour. The slope of the linear region of each graph was evaluated and normalised to that of the unexposed one-layer CFRP specimens. The resulting normalised joint stiffness values are shown in Figure 4.9.

Generally, it was observed that the joint stiffness increased gradually with the number of CFRP layers. 10% and 18% stiffness increments were achieved for 2L and 3L control specimens compared to 1L control specimens. However, with the imposition of accelerated corrosion conditions, a significant stiffness reduction was observed in all type F specimens. A 32% reduction of joint stiffness was observed in type 1L-F specimens, regardless of the exposure duration. Type 2L-F and 3L-F specimens also followed the same pattern, resulting in stiffness reductions of 32% and 20% respectively. Previous studies have reported the same observations for longer exposure times and higher salinity conditions [19]. It is concluded that the reduction in stiffness of the joint is mainly due to the stiffness reduction of the adhesive layer. With the observations made in this experimental program, supportive evidence has been found, because the joint stiffness values did not depend on the exposure duration. Regardless of the exposure duration, joint stiffness was reduced by the same amount within the same specimen category, which had the same layer arrangement. Furthermore, the CFRP composite-steel interface of the tested samples showed no corrosion activity on the steel surface, indicating that there was no ion penetration through the primer layer. The undamaged adhesive-steel interface resulted in the same stiffness value for the same specimen category.

No significant differences in stiffness were observed in type SF specimens. The stiffness remained the same as that of the control specimens, confirming that the

accelerated corrosion had no effect on CFRP composite stiffness with the exposed steel surface. A comparison of the stiffness of type F and SF specimens suggests that the reduction in stiffness may be due to the combination of adhesive degradation and CFRP material degradation. Deteriorated CFRP may lead to increased exposure of adhesive to the high salinity environment, resulting in considerable stiffness reduction of the joint.

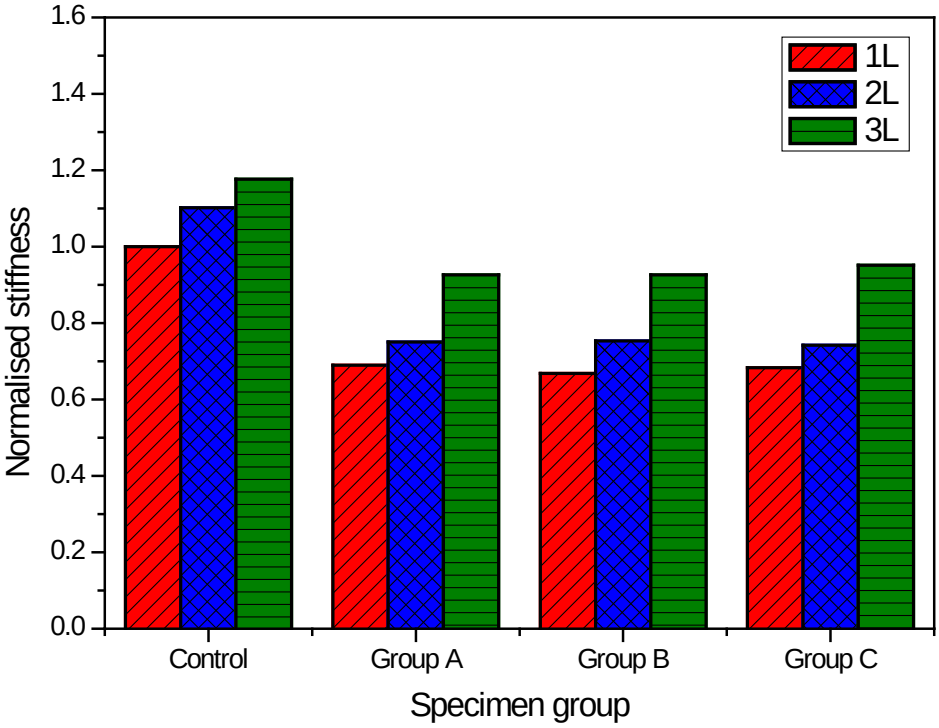

(a) Type F specimens

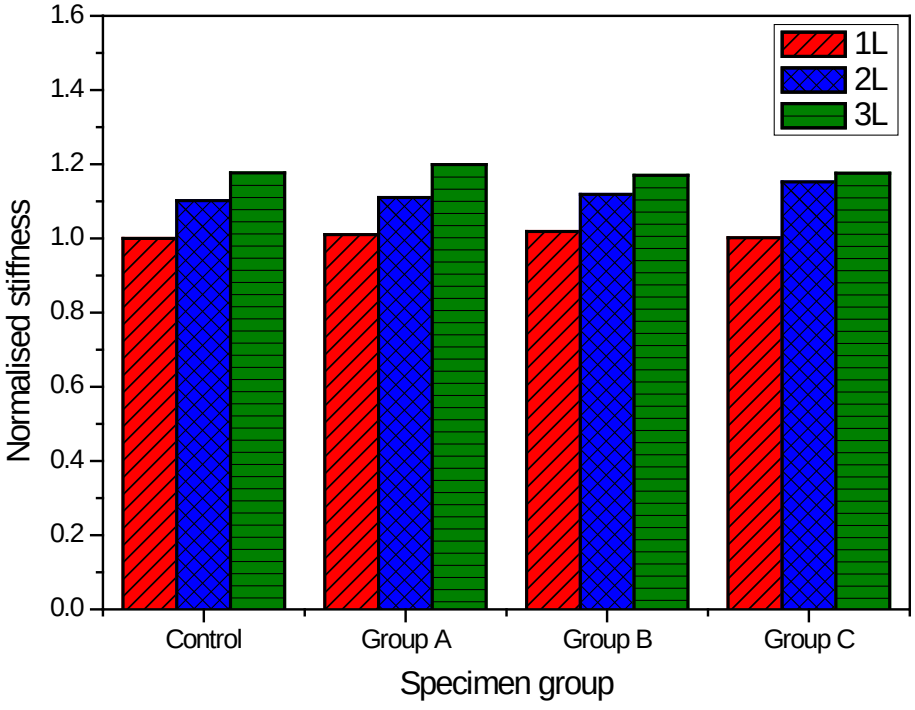

(b) Type SF specimens

Figure 4.9: Normalised joint stiffness

CFRP composite

CFRP stress levels at failure were evaluated using a cross-sectional analysis of failed joint specimens. The CFRP composite average thicknesses were 0.7 mm, 1.4 mm and 2.1 mm for 1L, 2L and 3L respectively. The width of the CFRP was 25 mm in this experiment. Stress levels at failure were calculated based on these measurements, and the results are shown in Table 4.2.

Table 4.2 shows that the calculated CFRP stress levels are well below the ultimate strengths under ambient conditions. All the control specimens tested under ambient conditions failed in steel-CFRP adhesive interface debonding. During this type of failure, CFRP cannot reach its ultimate strength level, because interface failure occurs at a lower stress level. The analysis shows that the stress levels of type F specimens decrease further with increased exposure duration. The failure mode suggests that the CFRP composite reached its maximum stress level during failure. Hence, it is clear that the calculated CFRP composite stress levels represent the ultimate strength, corresponding to the exposure duration. In type SF specimens, CFRP composite stress levels did not depend on the exposure duration. This type of stress variation can be explained considering the failure mode of the specimens. Specimens with same CFRP layer arrangement failed at a similar load level due to adhesive-interface debonding. The failure mode of type SF specimens suggests that the CFRP composite tensile capacity is higher than the joint interfacial capacity. Therefore, the governing failure mode was interfacial adhesive debonding. There may be CFRP material degradation due to accelerated corrosion. However, the intensity of material degradation was not sufficient to create CFRP rupture at failure in type SF specimens.

Table 4.2: CFRP composite stress levels at failure

Exposure conditions	CFRP composite stress level (MPa)					
	Type F			Type SF		
	1L	2L	3L	1L	2L	3L
CS	348.80	259.01	208.51	348.80	259.01	208.51
A	263.93	265.82	215.40	330.63	269.32	216.88
B	170.96	207.61	195.46	388.50	260.83	203.80
C	118.52	188.87	172.94	371.49	267.66	202.01

Fracture energy

The ultimate failure load is directly related to the fracture energy of the double-strap joint specimens. The associated fracture energy for each joint was calculated using the following equation, which is used to predict the interfacial fracture energy of a bonded plate to a substrate [9, 36, 105]:

$$P_u = b_p\sqrt{2G_f E_p t_p} \tag{4.1}$$

where, P_u is ultimate load, b_p is the width of the plate, E_p and t_p are the elastic modulus and thickness of the plate, respectively, and G_f is the fracture energy of the bonded interface.

The fracture energy of each specimen was evaluated, and the variation of fracture energy with exposure duration is shown in Figure 4.10. For type 1L-F specimens, the fracture energy was reduced from 0.741 N/mm to 0.424 N/mm at 0 to 24 h (0.0132 N/mm per hour). After that, the fracture energy was further reduced to 0.178 N/mm, between 24 h to 48 h at a rate of 0.010 N/mm per hour. Within the exposure period of 48 h to 72 h, the rate of degradation fracture energy dropped to 0.004 N/mm per hour.

For type 2L-F and 3L-F specimens, the fracture energy was constant up to 24 h, indicating that there was no degradation of the materials. The degradation initiated

after 24 h for the 2L-F specimens. The fracture energy reduced from 0.817 N/mm to 0.525 N/mm at 24 to 48 h (0.028 N/mm per hour). The fracture energy was then further reduced to 0.434 N/mm between 48 h to 72 h at a rate of 0.004 N/mm per hour. In type 3L-F specimens, the initial rate of reduction of fracture energy was 0.004 N/mm per hour and 0.006 N/mm per hour from 24 h to 48 h and 48 h to 72 h, respectively.

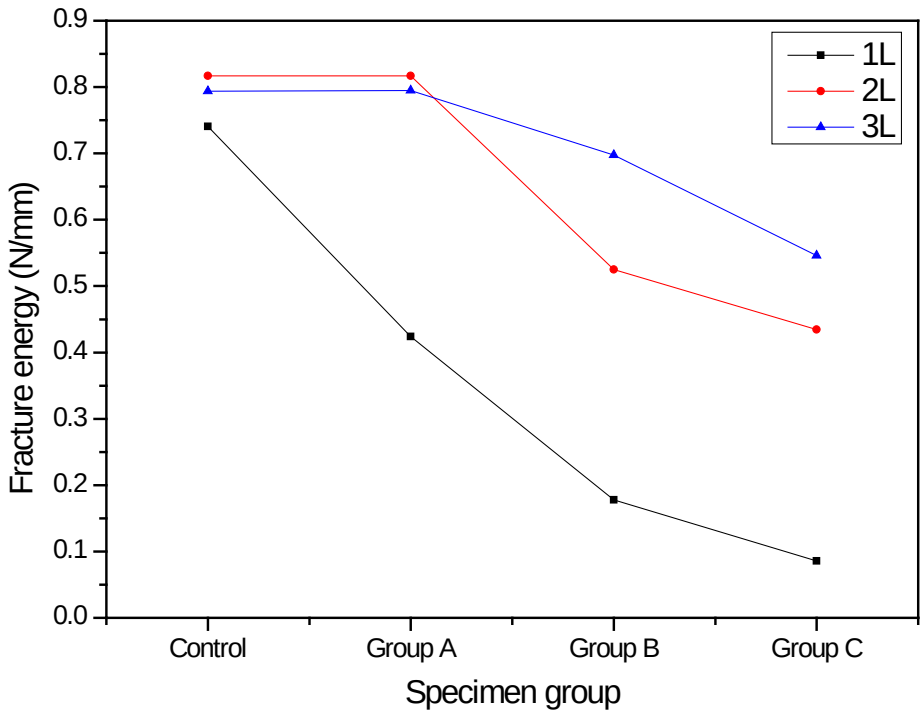

Figure 4.10: Fracture energy variation of type F specimens

Modelling deterioration

CFRP stress levels at failure were directly evaluated corresponding to the ultimate joint capacity. All type F specimens showed a capacity reduction due to accelerated corrosion. Of these, type 1L-F specimens showed gradual tensile capacity reduction with exposure duration due to accelerated corrosion. In addition,

the failure mode of these samples suggested that there is potential material degradation.

The variation of CFRP stress level of type 1L-F specimens against normalised exposure duration is shown in Figure 4.11. In addition to the specimens tested under S3, five more specimens were tested for exposure durations of 6, 15, 38, 62 and 84 h to capture the variation of CFRP degradation. The ratio *(R)* between CFRP tensile stress after arbitrary time t_i (σ_{f,t_i}) and at t_0 (σ_{f,t_0}) was calculated based on the experimental results using Equation 4.2. Then, the deterioration level *(D)* in Equation 4.3 was defined as *(1-R)*. The deterioration level associated with each exposure time was evaluated and the variation of deterioration level with exposure time is shown in Figure 4.12(a). The results were normalised over the time period and the variation of *D* with normalised time is shown in Figure 4.12(b).

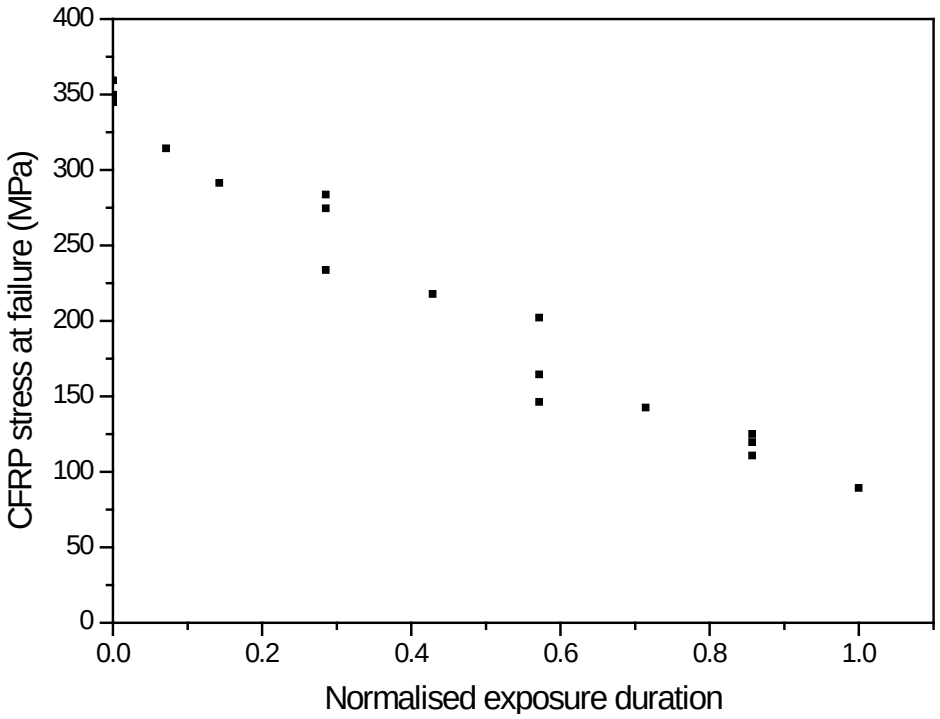

Figure 4.11: Normalised exposure duration vs. CFRP stress levels – 1L-F specimens

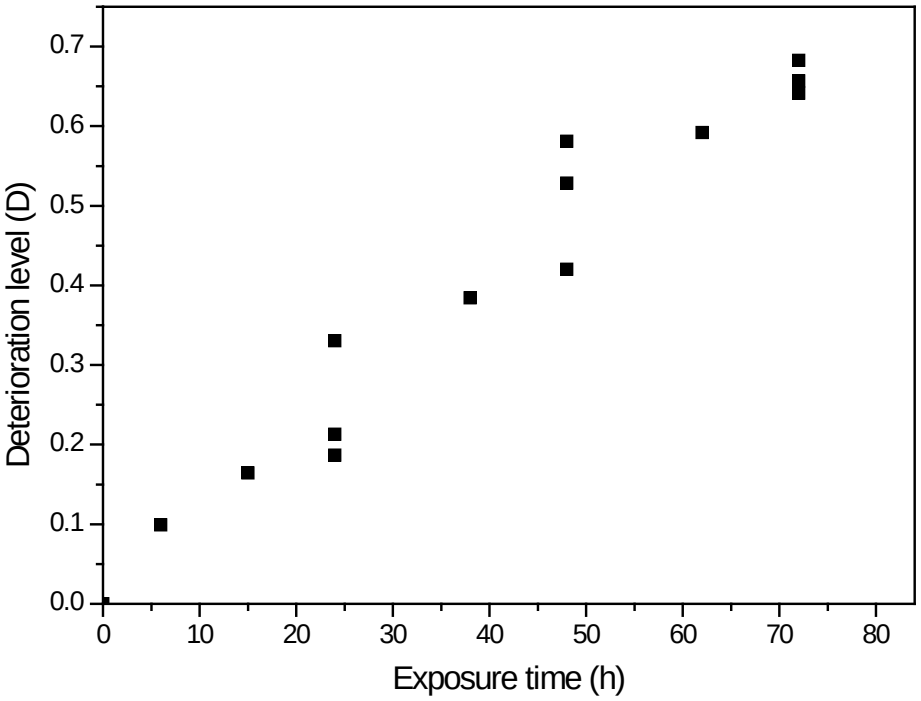

(a) With exposure time

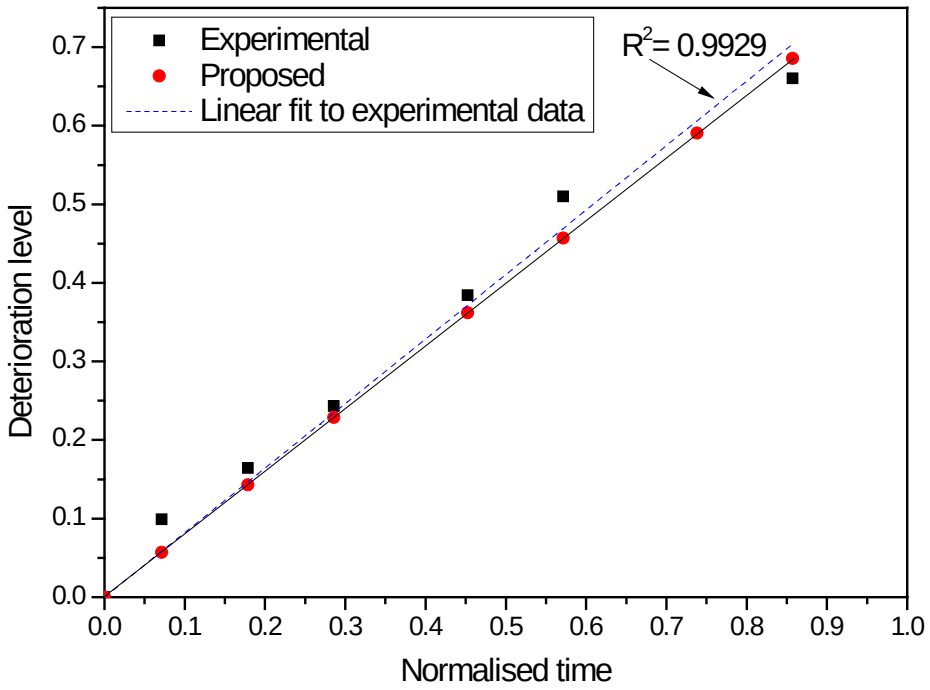

(b) With normalised exposure time

Figure 4.12: Variation of deterioration level

$$R = \frac{\sigma_{f,t_i}}{\sigma_{f,t_0}} \tag{4.2}$$

$$D = (1 - R) \tag{4.3}$$

$$D = 0.8 \times \left(\frac{T_i}{T_d}\right) \tag{4.4}$$

In order to derive the relationship between the exposure duration and the deterioration level, experimental deterioration values were plotted against normalised exposure duration, and the results are shown in Figure 4.12(b).The experimental data were approximated using the empirical relationship given in Equation 4.4, where, T_i/T_d is the ratio between an arbitrary time period and the design life of the structure. This model is capable of predicting the deterioration level of CFRP layers based on exposure duration, assuming a linear variation. Table 4.3 shows the comparison of experimental and predicted deterioration levels (D_{exp} *and* D_p) with a mean ratio of 1.16 and a coefficient of variation (COV) of 0.23. Once the deterioration level is determined, parameter *R* can be evaluated using Equation 4.3. The CFRP stress level is then calculated using Equation 4.2, provided that the CFRP stress level at zero exposure is known. This method is useful whenever CFRP material undergoes rupture failure due to CFRP degradation. In the current study, the joint capacities were evaluated at certain time intervals subjected to specific current density, and the results lie within these limited conditions.

Table 4.3: Comparison of experimental and predicted deterioration levels of 1L specimens

Normalised time	D_{exp}	D_p	D_{exp}/D_p
0.07	0.10	0.06	1.73
0.18	0.16	0.14	1.15
0.29	0.24	0.23	1.06
0.45	0.38	0.36	1.06
0.57	0.51	0.46	1.12
0.74	0.59	0.59	1.00
0.86	0.66	0.69	0.96
Mean			1.16
COV			0.23

Figure 4.13 shows the variation of deterioration levels of 1L, 2L and 3L CFRP-steel double joints with the normalised exposure duration. Experimental data are extrapolated assuming a linear variation to obtain the complete deterioration with the normalised exposure time in 2LCF and 3LCF specimens (See Appendix D for detailed explanation).

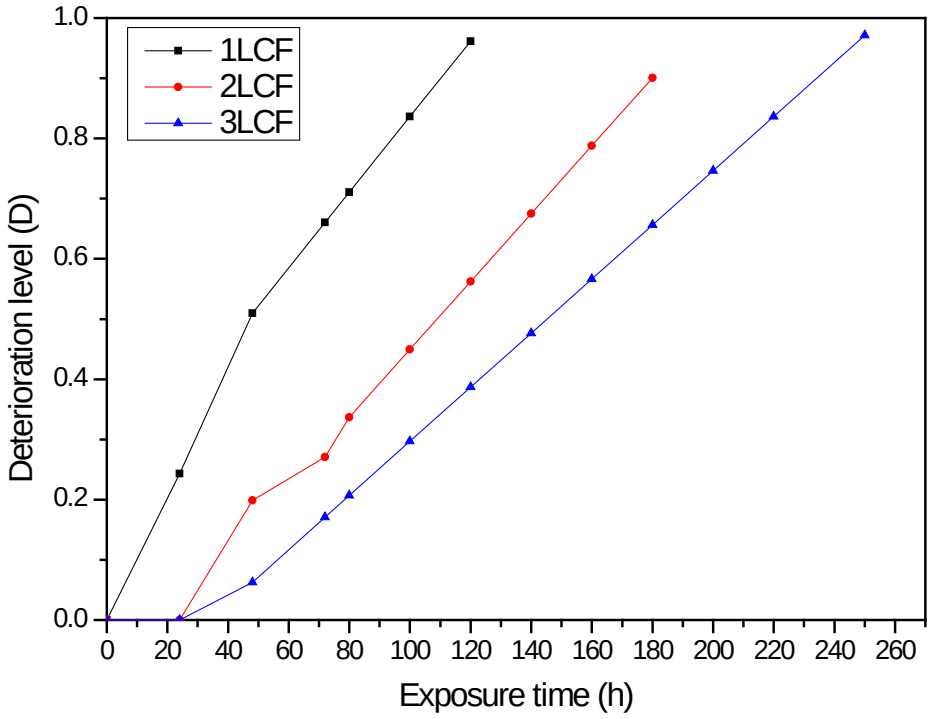

Figure 4.13: Deterioration of 1LCF, 2LCF and 3LCF specimens

The deterioration levels vs. normalised exposure time response for 2LCF and 3LCF specimens are shown in Figure 4.14 and 4.15. A linear variation of deterioration level is assumed with the normalised exposure time. Below, empirical equations are proposed to predict the deterioration level of multi-layer CFRP-steel systems.

$$D = \begin{cases} 0 \ (T \leq 0.08) \\ 1.44\ 37T - 0.1143 \ (\text{T}>0.08) \end{cases} \quad (4.5)$$

$$D = \begin{cases} 0 \ (T \leq 0.122) \\ 1.1293\ T - 0.1378 \ (\text{T}>0.122) \end{cases} \quad (4.6)$$

It is clear from Figures 4.14 and 4.15 that there is a delay in damage initiation in multi-layer CFRP-steel double strap specimens as a result of the additional CFRP layers. The proposed models for the deterioration include step functions to simulate the non-deteriorated period.

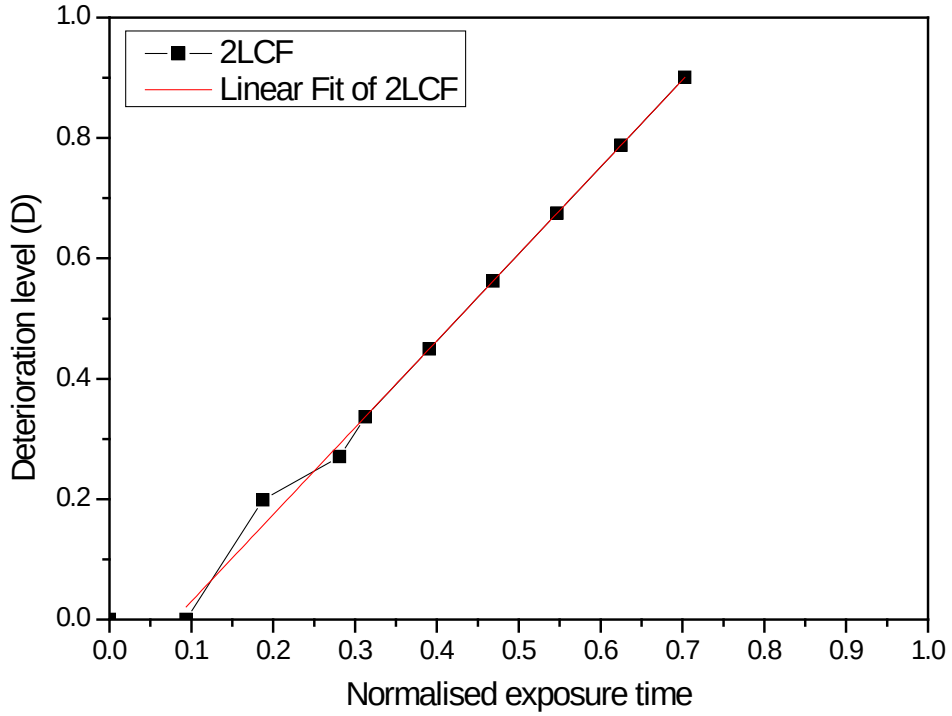

Figure 4.14: Deterioration level vs. normalised exposure time response (2LCF)

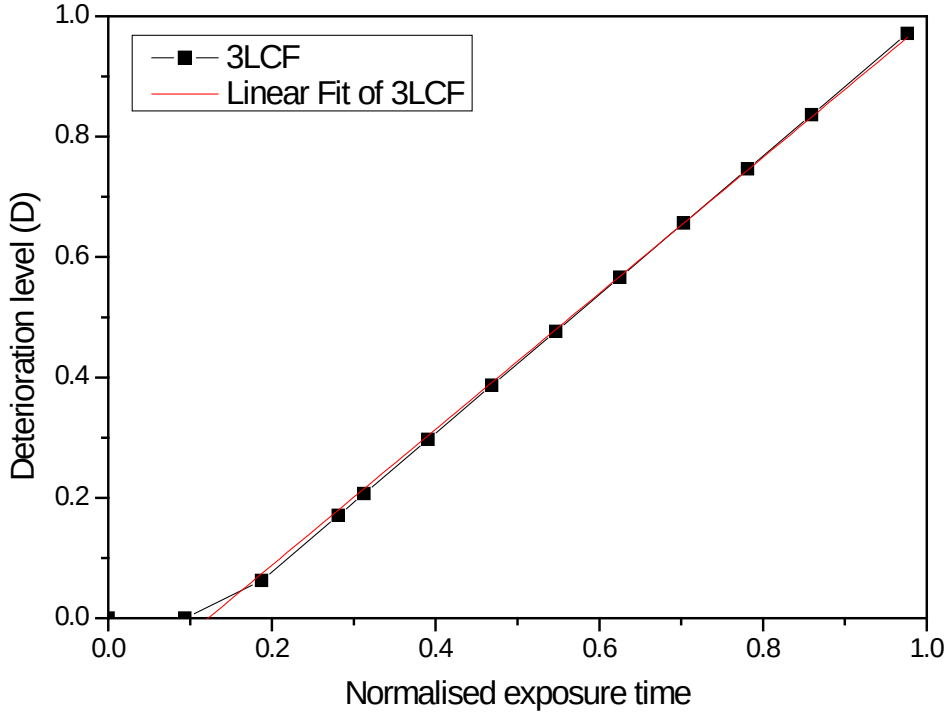

Figure 4.15: Deterioration level vs. normalised exposure time response (3LCF)

4.3 CFRP-STEEL DOUBLE SRAP JOINT SPECIMENS (SERIES 2)

4.3.1 Failure loads and failure modes

The failure mode and failure load of each specimen tested under series 2 are shown in Table 4.4. The failure modes are discussed in detail under each test scenario. The notations follow the same conventions as those described in Section 3.4.

Table 4.4: Failure loads and failure modes – Series 2

Test scenario	Specimen group identification	Average failure load (kN)	Failure mode
S1	1LCF-20	2.6	Adhesive-steel interface debonding
	1LCF-40	2.9	CFRP rupture and interface debonding
	1LCF-60	3.2	CFRP rupture and interface debonding
	1LCF-80	3.1	CFRP rupture and interface debonding
	1LCF-100	4.1	CFRP fibre rupture
	1LCF-120	3.5	CFRP fibre rupture
	1LCF-140	4.0	CFRP fibre rupture
	1LCF-160	4.2	CFRP fibre rupture
	1LCF-180	4.2	CFRP fibre rupture
S2	2LCF-20	8.3	Adhesive-steel interface debonding
	2LCF-40	11.4	Adhesive-steel interface debonding
	2LCF-60	11.5	Adhesive-steel interface debonding
	2LCF-80	12.1	Adhesive-steel interface debonding
	2LCF-100	12.4	Adhesive-steel interface debonding
	2LCF-120	11.4	Adhesive-steel interface debonding
	2LCF-140	12.6	Adhesive-steel interface debonding
	2LCF-160	12.1	Adhesive-steel interface debonding
	2LCF-180	11.4	CFRP fibre rupture
S3	1LCF-CS	12.2	Adhesive-steel interface debonding
	2LCF-CS	18.1	Adhesive-steel interface debonding
	3LCF-CS	21.9	Adhesive-steel interface debonding
	1LGF-CS	4.2	Adhesive-steel interface debonding
	2LGF-CS	5.9	Adhesive-steel interface debonding
	3LGF-CS	7.1	Adhesive-steel interface debonding
	2LGC-CS	10.1	Adhesive-steel interface debonding
	2LGC -A	11.2	Adhesive-steel interface debonding
	2LGC-B	9.0	Adhesive-steel interface debonding
	2LGC-C	7.2	Adhesive-steel interface debonding
	1LCF-A	9.2	CFRP rupture and interface debonding
	1LCF-B	6.0	CFRP fibre rupture
	1LCF-C	4.1	CFRP fibre rupture
	2LCF-A	18.6	CFRP rupture and interface debonding
	2LCF-B	14.5	CFRP rupture and interface debonding
	2LCF-C	13.2	CFRP rupture and interface debonding

Scenario 1 (S1)

Three types of failure modes could be identified in the samples tested in scenario 1: (i) steel-adhesive interface debonding (ii) mixed mode failure (interface debonding and CFRP rupture) and (iii) CFRP rupture. Specimen 1LCF-20 failed due to steel-adhesive interface debonding. With the increased bond length, the failure mode shifted to mixed mode failure (a combination of steel-adhesive interface debonding and CFRP rupture). This type of failure mode was identified in samples 1LCF-40, 1LCF-60 and 1LCF-80. CFRP rupture failure mode was observed for all the other samples with the shorter bond length of 100 mm and above. The failure modes of the 1LCF (Scenario 1) specimens are shown in Figure 4.16.

Figure 4.16: Failure modes specimens of – (Series 2-Scenario 1)

Scenario 2 (S2)

The number of CFRP layers had a significant effect on the failure mode of the double-strap joints. The governing failure mode was identified as steel-adhesive interface debonding failure in the specimens tested in scenario 2. The specimens with bond lengths from 20 mm to 160 mm showed steel-adhesive interface debonding failure. Although the specimens failed by debonding, the outer CFRP fibres showed a small amount of rupture. However, no fibre breakage was observed in the innermost CFRP layer. Specimen 2LCF-180 showed CFRP fibre rupture failure mode. The failure modes of scenario 2 specimens are shown in Figure 4.17.

Figure 4.17: Failure modes – (Series 2 - Scenario 2)

Load vs. displacement graphs for specimens 1LCF-120, 1LCF-160, 2LCF-120 and 2LCF-160 are shown in Figure 4.18. These four specimens were also used to develop shear stress-slip curves. In both 1LCF and 2LCF specimens, fibre rupture can be clearly identified at the ultimate load region in the load vs. displacement graphs. In this region, the response becomes highly non-linear, indicating CFRP composite damage. Normally, CFRP double strap joints undergo CFRP debonding failure [36, 38, 40, 43] in ambient environmental conditions. In the debonding failure mode, debonding occurs suddenly once the specimen reaches the ultimate load, without showing a plateau in load vs. displacement response. The results of the current study suggest that the load vs. displacement response is significantly different from that under ambient conditions and this response is greatly affected by the environmental conditions applied to the specimens.

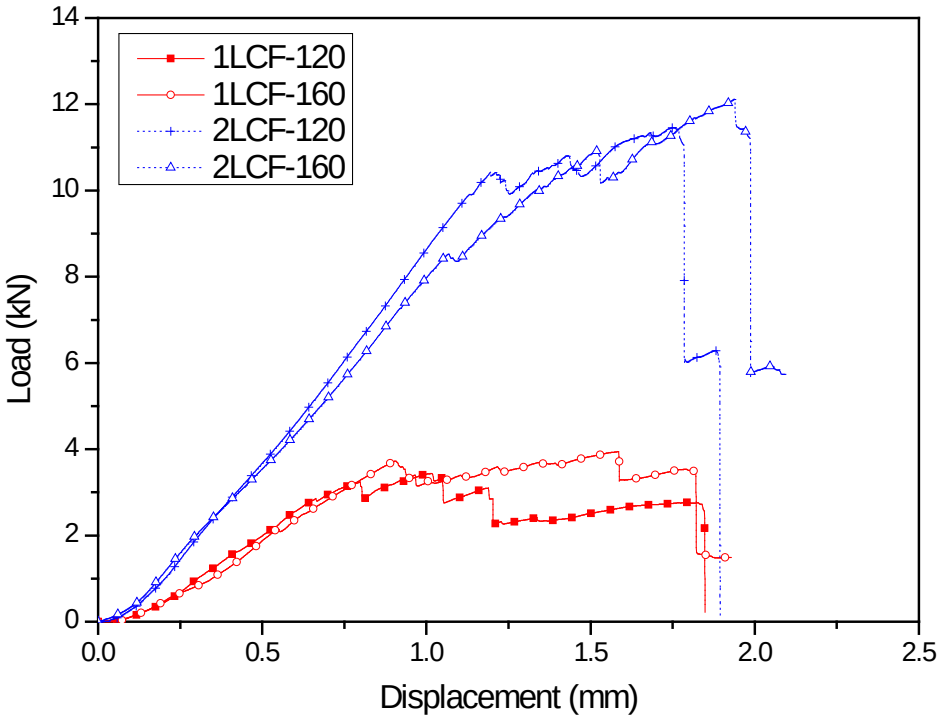

Figure 4.18: Load vs. displacement of 1LCF and 2LCF specimens

Scenario 3 (S3)

All the control specimens tested in scenario 3 failed due to steel-adhesive interface debonding, irrespective of the CFRP configuration (Figure 4.19). Debonding is the most common type of failure of FRP-strengthened steel sections under ambient conditions as reported in the research literature [36, 38, 43]. With the imposition of environmental conditioning, 1LCF specimens showed a shift in failure mode from adhesive-interface failure to CFRP rupture failure mode, while 1LCF-A specimens showed a mixed mode of failure (CFRP rupture and debonding). The failure profile showed V-shaped failure from the middle of the joint where most of the outward fibres failed near the joint location, and inner fibres failed at a distance from the joint centre. When the exposure duration increased to 48 h (1LCF-B), the failure mode became full CFRP rupture. The same failure mode was observed in 1LCF-C specimens at 72 h exposure duration. In these specimens, most of the fibres showed rupture at the joint location.

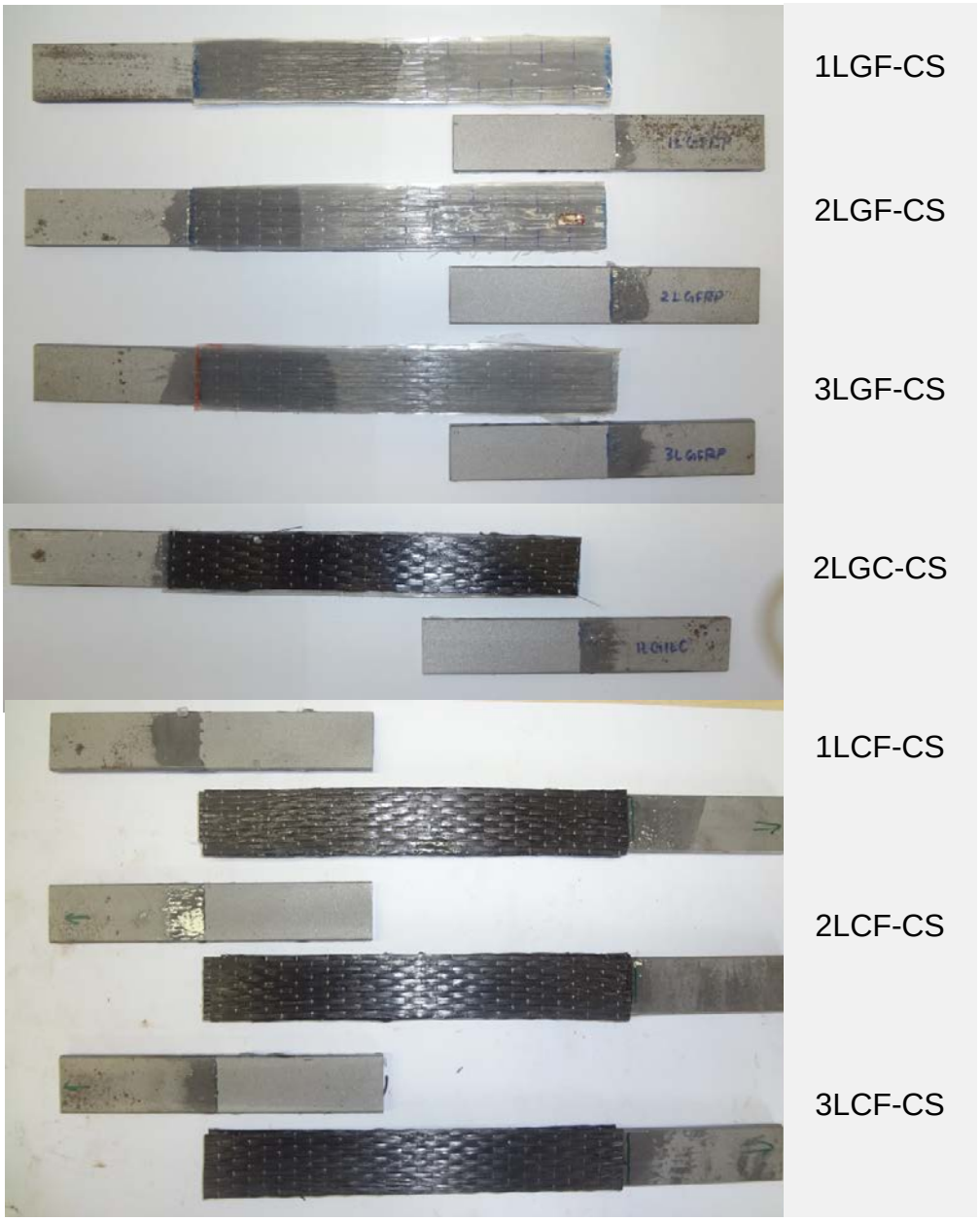

Figure 4.19: Debonding failure of control specimens – (Series 2 – Scenario 3)

All the 2LCF specimens showed the mixed mode of failure after exposure to environmental conditioning. It was observed that increased exposure duration caused the high intensity of CFRP rupture in 2LCF specimens. The specimens prepared with one GFRP and one CFRP layer on each side (2LGC) failed due to steel-adhesive interface debonding. Some of the fibres in the top layer showed rupture at a higher

exposure duration, while the steel surface did not show any deterioration. The failure modes of these specimens are shown in Figure 4.20.

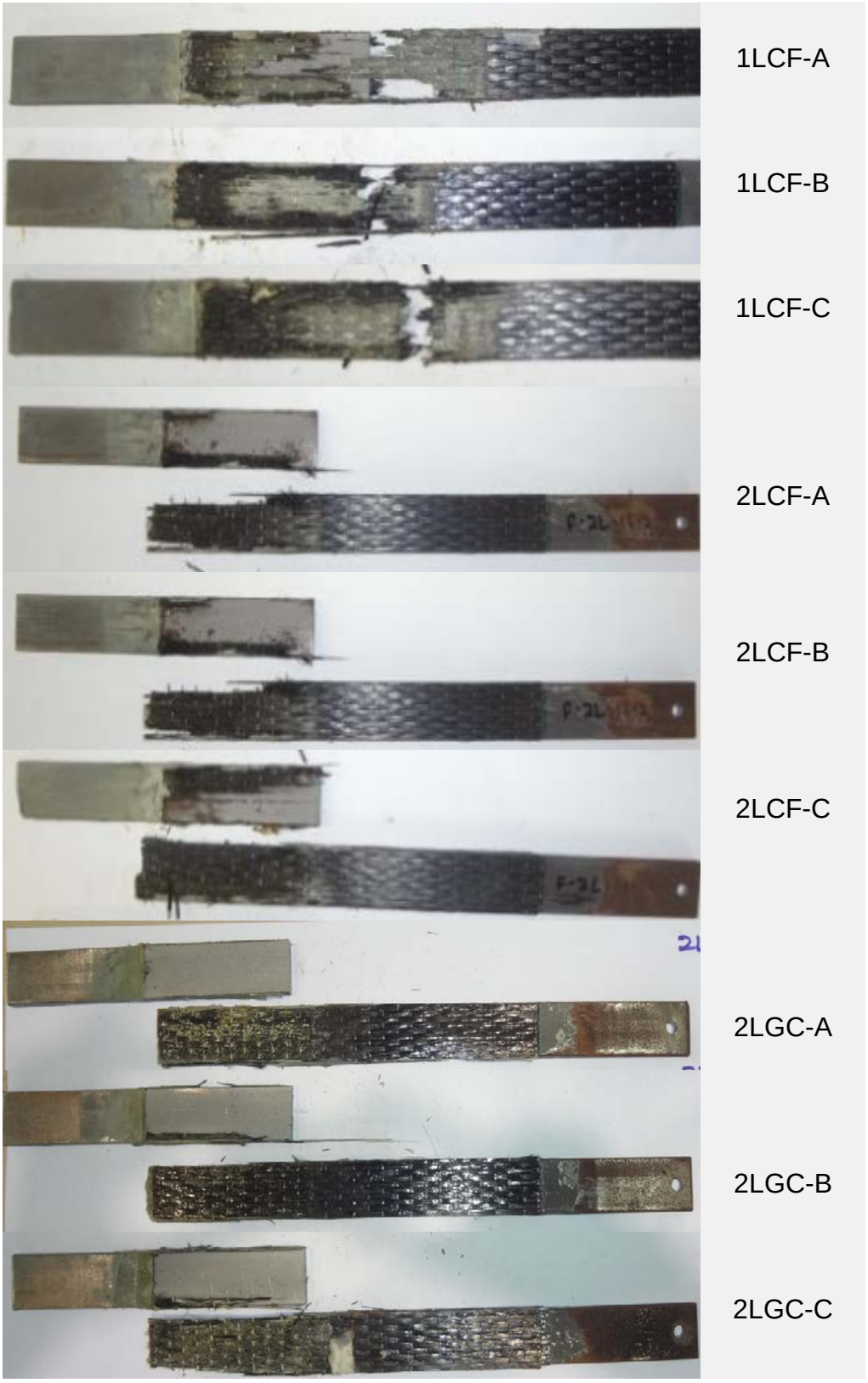

Figure 4.20: Failure modes of specimens (Series 2 – Scenario 3) after exposure

A significant colour change was observed in the CFRP layers upon exposure to environmental conditioning. The colour variation of CFRP layers with exposure duration can be seen in Figures 4.19 and 4.20. All the specimens exposed to environmental conditioning showed a different colour to that of the control specimens. The CFRP surface became softer and showed swelling compared to the control specimens. Analyses of failure modes indicated that CFRP material degradation is prominent rather than bond degradation due to the environmental conditions imposed. Some early research [19, 27] concluded that joint capacity degradation is governed by bulk adhesive degradation as a result of ion penetration into the adhesive layer. With the observations made in the present research, the joint capacity reduction can be attributed to CFRP material degradation, resulting in a transformation of failure modes from debonding to rupture.

4.3.2 Bond strength

In the context of studies of the bond between CFRP and a substrate, bond strength is defined as the ultimate load that can be resisted by the CFRP plate before debonding failure. Table 4.5 summarises the bond strengths of specimens that failed by debonding. The 1LCF specimens in scenario 1, specimen 2LCF-180, specimen 1LCF-B, and specimen 1LCF-C, were not considered for this evaluation since CFRP rupture failure occurred in these specimens. It is evident from Table 4.5 that the various layer arrangements resulted in different ultimate loads, although the same adhesive was used in all bond configurations. It was observed that the CFRP composites had higher bond strength values compared to GFRP composites with bonded steel plate.

Further, the experimental bond strengths ($P_{u,exp}$) were compared with the predictions $P_{u,predicted}$) using Equation 4.5. This equation is well-known, and has been used by different researchers [9, 36, 105] to predict the bond strength of an adhesively-bonded substrate.

$$P_u = b_p\sqrt{2E_p t_p G_f} \tag{4.5}$$

In the above equation, b_p is the plate width, E_p is the elastic modulus of the fibre type used, t_p is the thickness of the plate and G_f is the associated fracture energy. It is clear from Table 4.5 that the fracture energy values used provide accurate predictions of bond strength for each specimen. The comparison of experimental and predicted bond strengths shows good agreement, with a mean of 1.01 and a coefficient of variation (COV) of 0.03.

Table 4.5: Comparison of experimental and predicted bond strengths

Specimen type	$P_{u,exp}$ (kN)	b_p (mm)	t_p (mm)	G_f (N/mm)	$P_{u,predicted}$ (kN)	$P_{u,exp}/P_{u,predicted}$
1LCF-CS	12.21	25	0.7	0.74	12.20	1.00
2LCF-CS	18.13	25	1.4	0.81	18.06	1.00
3LCF-CS	21.89	25	2.1	0.8	21.98	1.00
1LGF-CS	4.15	25	0.5	0.4	4.24	1.02
2LGF-CS	5.98	25	0.5	0.79	5.96	1.00
3LGF-CS	7.05	25	0.5	1.1	7.04	1.00
2LGC-CS	10.80	25	0.8	0.75	10.72	0.99
1LCF-A	9.24	25	0.7	0.51	10.13	1.10
2LCF-A	18.61	25	1.4	0.86	18.61	1.00
2LCF-B	14.53	25	1.4	0.52	14.47	1.00
2LCF-C	13.22	25	1.4	0.43	13.16	1.00
2LGC -A	11.22	25	0.8	0.81	11.14	0.99
2LGC-B	9.01	25	0.8	0.53	9.01	1.00
2LGC-C	7.19	25	0.8	0.41	7.93	1.10
2LCF-20	8.33	25	1.4	0.17	8.27	0.99
2LCF-40	11.37	25	1.4	0.32	11.35	1.00
2LCF-60	11.49	25	1.4	0.33	11.52	1.00
2LCF-80	12.05	25	1.4	0.36	12.04	1.00
2LCF-100	12.43	25	1.4	0.38	12.37	1.00
2LCF-120	11.40	25	1.4	0.32	11.35	1.00
2LCF-140	12.56	25	1.4	0.39	12.53	1.00
2LCF-160	12.10	25	1.4	0.36	12.04	0.99
					Mean	1.01
					COV	0.03

4.3.3 Effect of CFRP bond length

The same environmental exposure level was imposed on CFRP double-strap joint specimens fabricated with one layer of CFRP (1LCF) and two layers of CFRP (2LCF) to determine the effect of bond length. The ultimate load variation with bond length is shown in Figure 4.21. The 1LCF specimens showed an increment in ultimate load with the increment of the CFRP bond lengths from 20 mm to 100 mm. Once the bond length exceeded 100 mm, the specimens did not show a further gain in ultimate load. This result suggests that the 1LCF specimens reached their joint capacity at 100 mm bond length. The corresponding failure mode of 100 mm bond length confirmed that CFRP material reached its tensile capacity before undergoing fibre rupture. The 2LCF specimens showed higher ultimate loads with the same corresponding bond lengths than those of the 1LCF specimens. In the 2LCF specimens, the ultimate load-carrying capacity reached a plateau at the bond length of 100 mm. However, the failure mode remained steel-adhesive interface debonding for all the specimens with bond lengths of 20 mm to 160 mm.

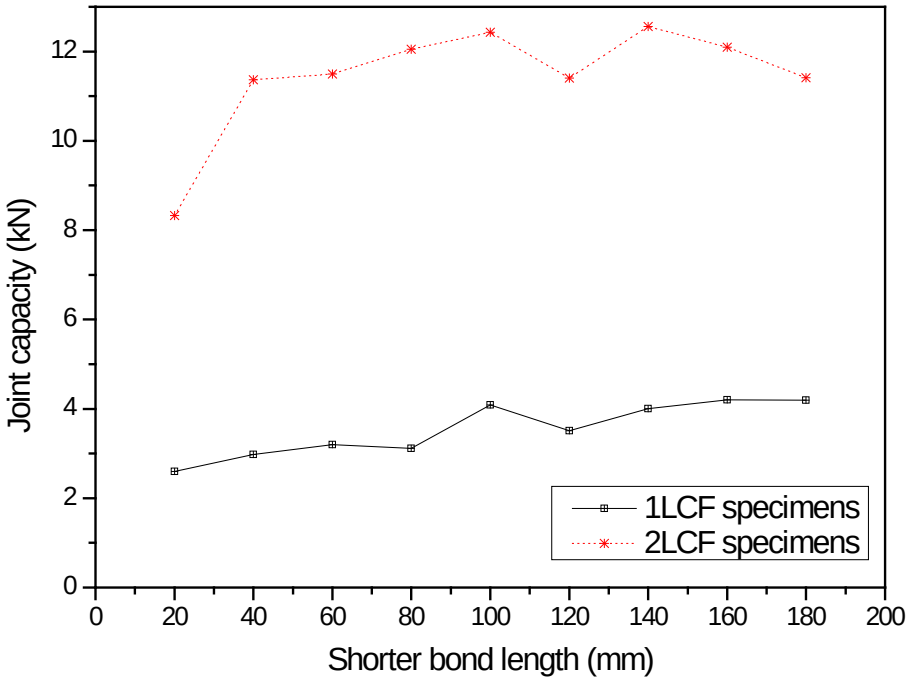

Figure 4.21: Ultimate load vs. bond length variation of 1LCF and 2LCF specimens

Studies of the bond development length of CFRP and steel [39, 46] have shown that the effective bond lengths are 100 mm and 75 mm for single- and double-strap joints, respectively. These bond lengths in ambient conditions were determined based on the debonding failure mode. The findings of the present research show that the effective bond lengths are different from the ambient values after being exposed to environmental conditioning. The effective bond length of a single-layer CFRP system is significantly affected by the exposure conditions imposed. At a particular bond length, CFRP can reach its ultimate strength by undergoing through-CFRP rupture failure. It was observed that the effective bond length of multi-layer CFRP systems is not substantially affected by the environmental conditions imposed. However, visual observations and the failure modes suggested that there is possible material degradation in the outer CFRP layers. The intensity of the material degradation may be significant for longer exposure durations.

4.3.4 Effect of number of CFRP layers

A comparison of the ultimate loads of 1LCF and 2LCF specimens showed that multi-layer CFRP systems can effectively improve the structural performance of composite systems compared to single-layer CFRP strengthening systems (Figure 4.21). The additional CFRP layers not only improve the structural performance but also enhance the durability of the strengthening system. Observations showed that the outer CFRP layer is more vulnerable to environmental conditioning. However, the ultimate capacity and the failure modes are governed by the innermost CFRP layer. In multi-layer CFRP systems, the outer layers help to protect the innermost CFRP layers from aggressive environmental conditions. All the specimens exposed to accelerated environmental conditioning showed significant softening, swelling and discolouration of the outer fibres, and the intensity of the effects was greater in the specimens fabricated with one CFRP layer. Hence, it can be concluded that multi-layer CFRP systems are more efficient than single-layer CFRP systems in aggressive environmental conditions in respect of their structural and durability performance.

4.3.5 Effect of GFRP layer

Joint strength

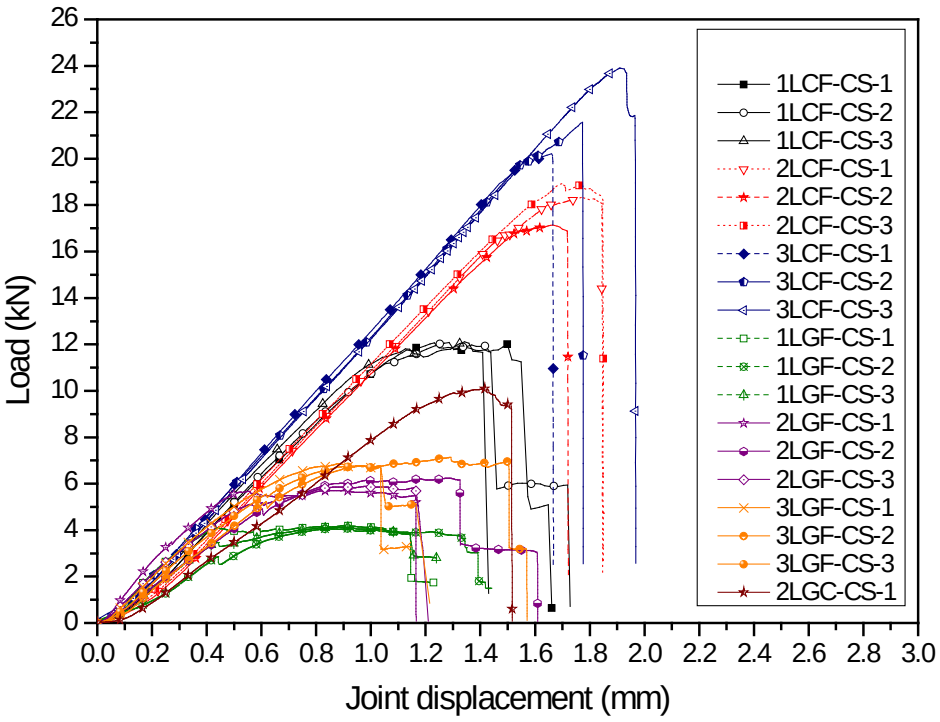

Figure 4.22: Load vs. displacement graphs – Series 3 control specimens

During tensile tests, linear relationships were observed in the load vs. joint displacement graphs for all the specimen types until they reached their ultimate loads (Figure 4.22). All the 2LCF and 3LCF control specimens showed sudden failure after they reached their ultimate loads. 1LCF specimens showed a plateau once they reached their ultimate loads and then failure occurred. This plateau continued for 0.5 mm once the specimen achieved its ultimate load. Load vs. displacement responses of GFRP-strengthened specimens showed similar behaviour to CFRP-strengthened specimens until they reached their ultimate loads. Joint displacement then increased up to 1.5 mm without showing a significant gain in load. This behaviour is directly related to the ultimate strains of the particular CFRP and GFRP used in the tests. The GFRP was capable of achieving higher strains at failure.

It was observed that the GFRP-strengthened specimens underwent significant joint capacity reduction compared to CFRP-strengthened specimens. The average joint capacities were 12.2 kN, 18.1 kN and 21.9 kN for 1LCF, 2LCF and 3LCF specimens, respectively, while the joint capacities were 4.15 kN, 5.98 kN and 7.05 kN for 1LGF, 2LGF and 3LGF specimens, respectively. This comparison shows that CFRP has better structural performance in steel-CFRP strengthening systems. Tests carried out using a combination of GFRP and CFRP layers showed that the combination of GFRP and CFRP can significantly increase the load-carrying capacity compared with GFRP-only systems. On the other hand, joints fabricated with a single layer of CFRP showed higher load-carrying capacity compared to multilayer GFRP (1LGF, 2LGF, 3LGF and 2LGC) joint specimens under ambient conditions. The variations in joint capacities according to CFRP arrangement under ambient conditions are shown in Figure 4.23.

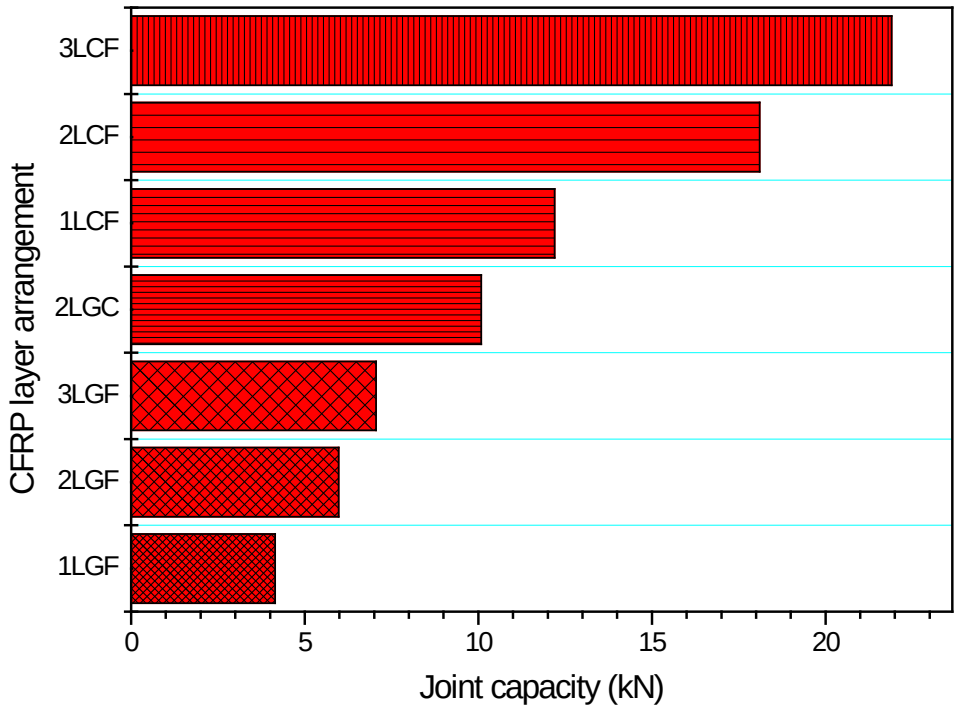

Figure 4.23: Ultimate load variation with different CFRP layer arrangements

The interfacial capacity of adhesively-bonded joints is dependent on the modulus of the bonded fibre type [37-39, 106, 107]. The CFRP and GFRP used here had longitudinal elastic moduli of 230 GPa and 72 GPa, respectively. Furthermore, the effective moduli may differ from their original values in a composite system [39, 94]. From the observations made and the results found in the current study, it can be concluded that the differences in elastic modulus led to different interfacial capacities for the control specimens.

Bond durability

The effectiveness of an embedded GFRP layer on CFRP strengthening systems was evaluated by testing the fabricated double-strap joints in three exposure durations. Load vs. displacement graphs of these specimens are shown in Figure 4.24(a). All the ultimate joint capacities were normalised to that of 1LCF control specimens for ease of comparison (Figure 4.24(b)). Double-strap joints fabricated with an embedded GFRP layer showed a similar joint capacity to that of the control specimens after 24 h exposure. Similar behaviour was observed in 2LGF specimens after 24 h exposure. However, the load-carrying capacity of 2LCF specimens was 66% higher than that of 2LGC specimens for the same exposure duration of 24 h. For the same exposure duration, 1LCF showed a 25% reduction in load-carrying capacity. With increased exposure duration up to 48 h, 2LGC specimens started showing a decrement in load-carrying capacity. Joint capacity reductions of 11% and 29% were observed in 2LGC specimens after 48 h and 72 h exposure, respectively. The 2LCF specimens showed 20% and 27% loss of joint capacity after 48 h and 72 h exposure, respectively. The 1LCF specimens showed a 51% capacity loss at 48 h, and a further 16% decrement was observed with increased exposure duration up to 72 h.

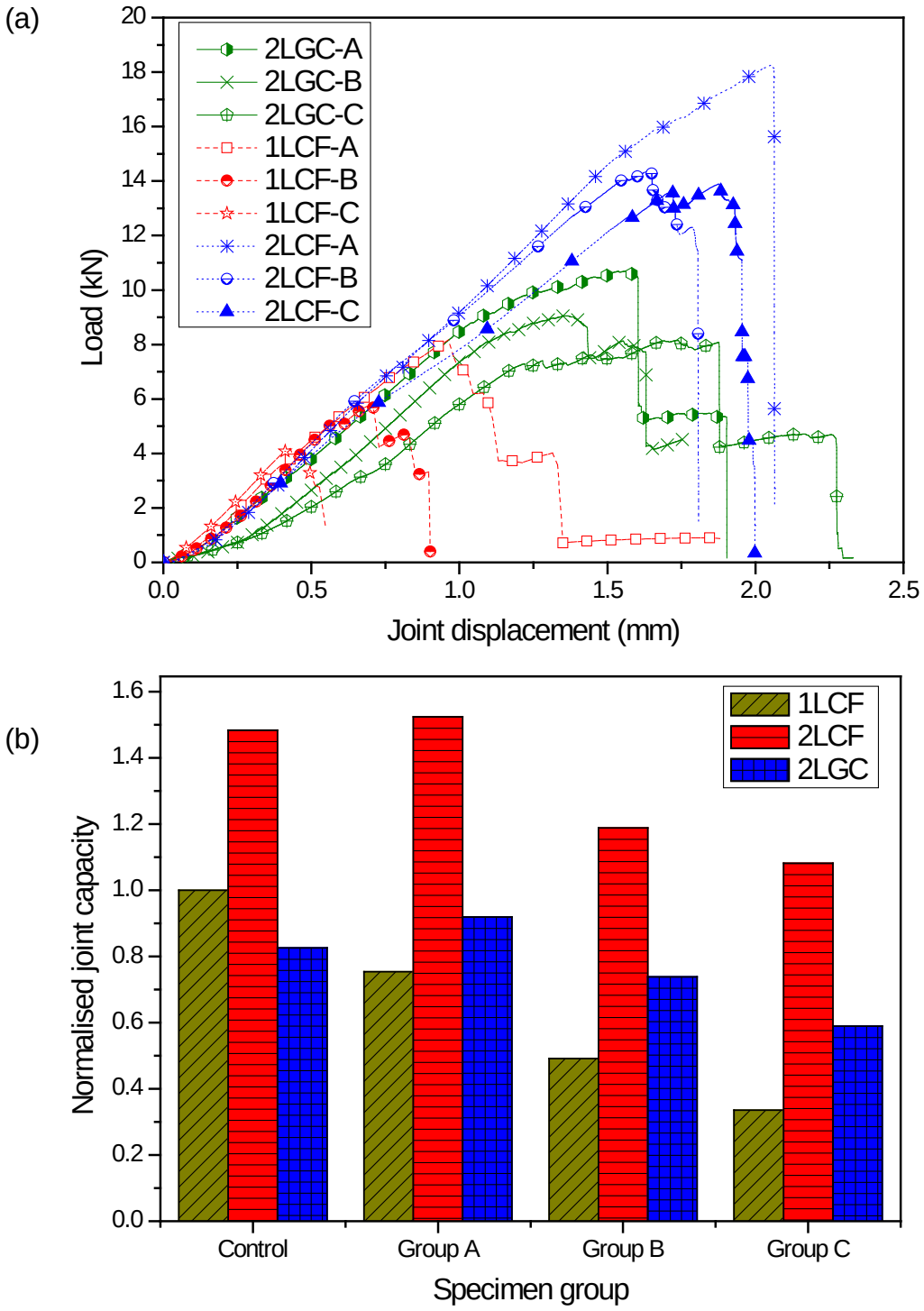

Figure 4.24: (a) Load vs. displacement graphs of 2LGC, 1LCF and 2LCF specimens (b) Normalised joint capacities of 2LGC, 1LCF and 2LCF specimens

The results indicate that the use of an embedded GFRP layer is capable of improving the durability of CFRP strengthening systems compared to single-layer CFRP systems. However, the use of GFRP as the innermost layer resulted in a lower joint capacity compared to a system with the same number of CFRP layers when exposed to environmental conditioning. This phenomenon possibly occurs due to the differences in interface bond characteristics in different materials. Higher CFRP-steel interface bond properties resulted in greater joint capacity. The findings of this experimental series show that the multi-layer CFRP system can perform efficiently under aggressive environmental conditions.

Modelling deterioration

Figure 4.25 shows the variation of deterioration levels of 2LGC steel double joints with the exposure duration. Experimental data were extrapolated assuming a liner variation to obtain the complete deterioration with the normalised exposure time in 2LGF specimens (See Appendix D for detailed explanation).

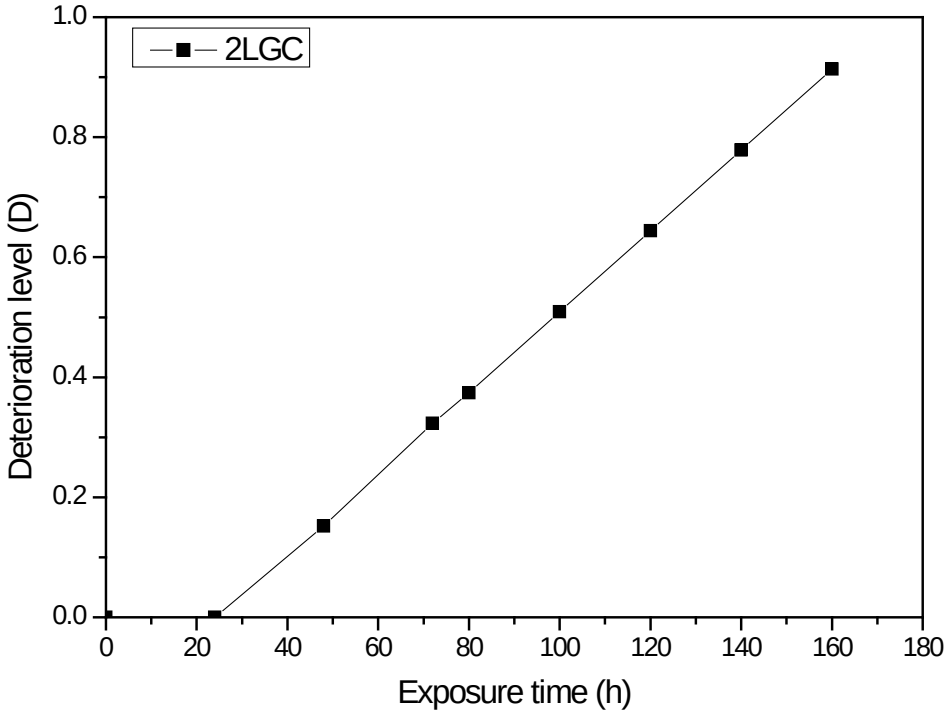

Figure 4.25: Deterioration vs. exposure time (2LGC specimens)

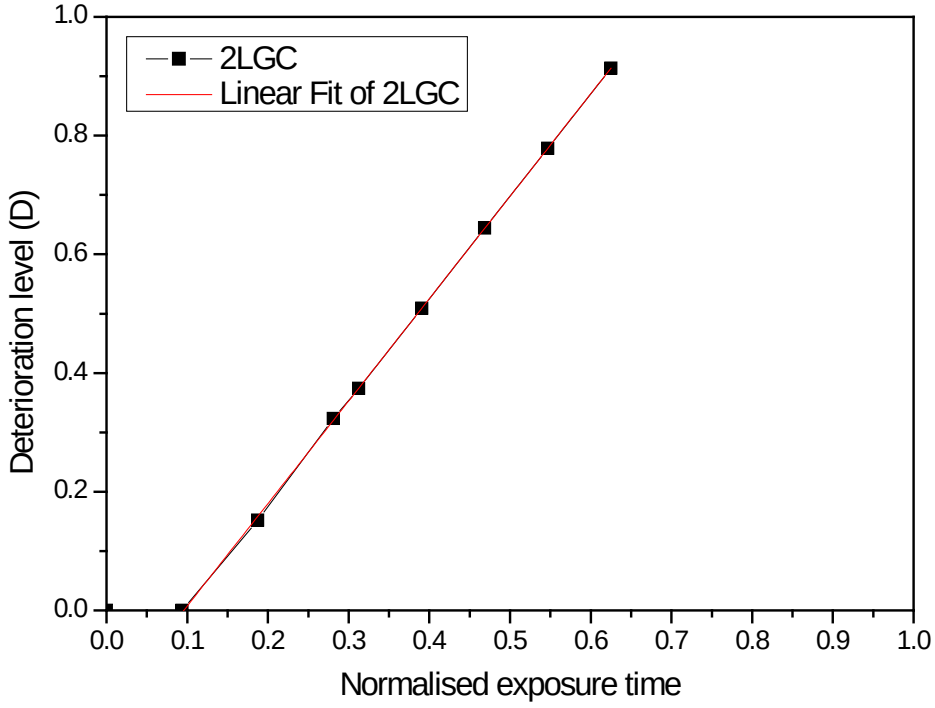

Figure 4.26: Deterioration vs. normalised exposure time (2LGC specimens)

The deterioration level vs. normalised exposure time response for 2LGC specimens is shown in Figure 4.26. A linear variation of deterioration level is assumed with the normalised exposure time. The following empirical equations are proposed to predict the deterioration of multi-layer CFRP-steel systems with an embedded GFRP layer:

$$D = \begin{cases} 0 \ (T \leq 0.096) \\ 1.7259\,T - 0.1651 \ (\text{T}>0.096) \end{cases} \tag{4.7}$$

It is clear from Figure 4.25 and 4.26 that there is a delay in damage initiation in CFRP-steel double strap specimens with embedded GFRP layer as a result of the additional GFRP layers. The proposed model of deterioration includes a step function to simulate the non-deteriorated period.

4.3.6 Axial strain distribution along CFRP composite

The strain measurements were recorded at each load increment and plotted against the bond length for different load levels. The strain distributions of specimens 1LCF-120, 1LCF-160, 2LCF-120 and 2LCF-160 are shown in Figures 4.27 to 4.29. In specimen 1LCF-160, the strain gauges failed before reaching the ultimate load. Hence, Figure 4.27(b) shows the strain variation only up to 90% of the ultimate load. It can be seen from Figures 4.29(a) and (b) that the strain gauge readings drop with the increment of joint displacement. This response is different from that reported in the research literature under ambient conditions. Under ambient conditions, maximum CFRP strain remains nearly constant in the ultimate load region, but the region where this maximum strain is reached keeps expanding with the applied loading. Hence, debonding can be identified by observing axial strain variation along the bond length [36]. With the results of axial strain responses from the current experiment, CFRP fibre damage can be identified at the ultimate load region. Non-linearity in load vs. displacement response and strain distribution can be attributed to CFRP fibre damage under tensile loading.

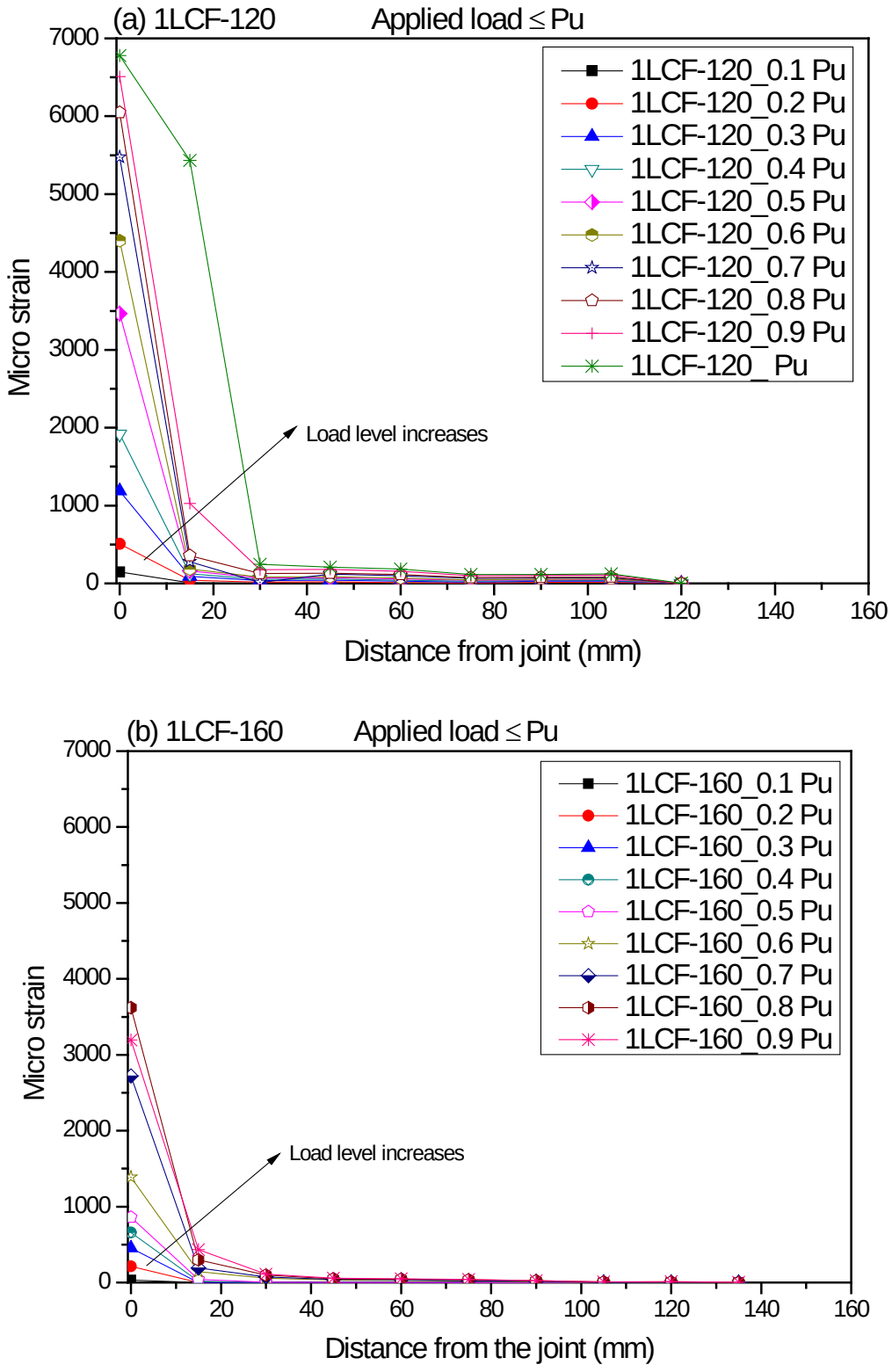

Figure 4.27: Axial strain distribution of 1LCF specimens at different load levels

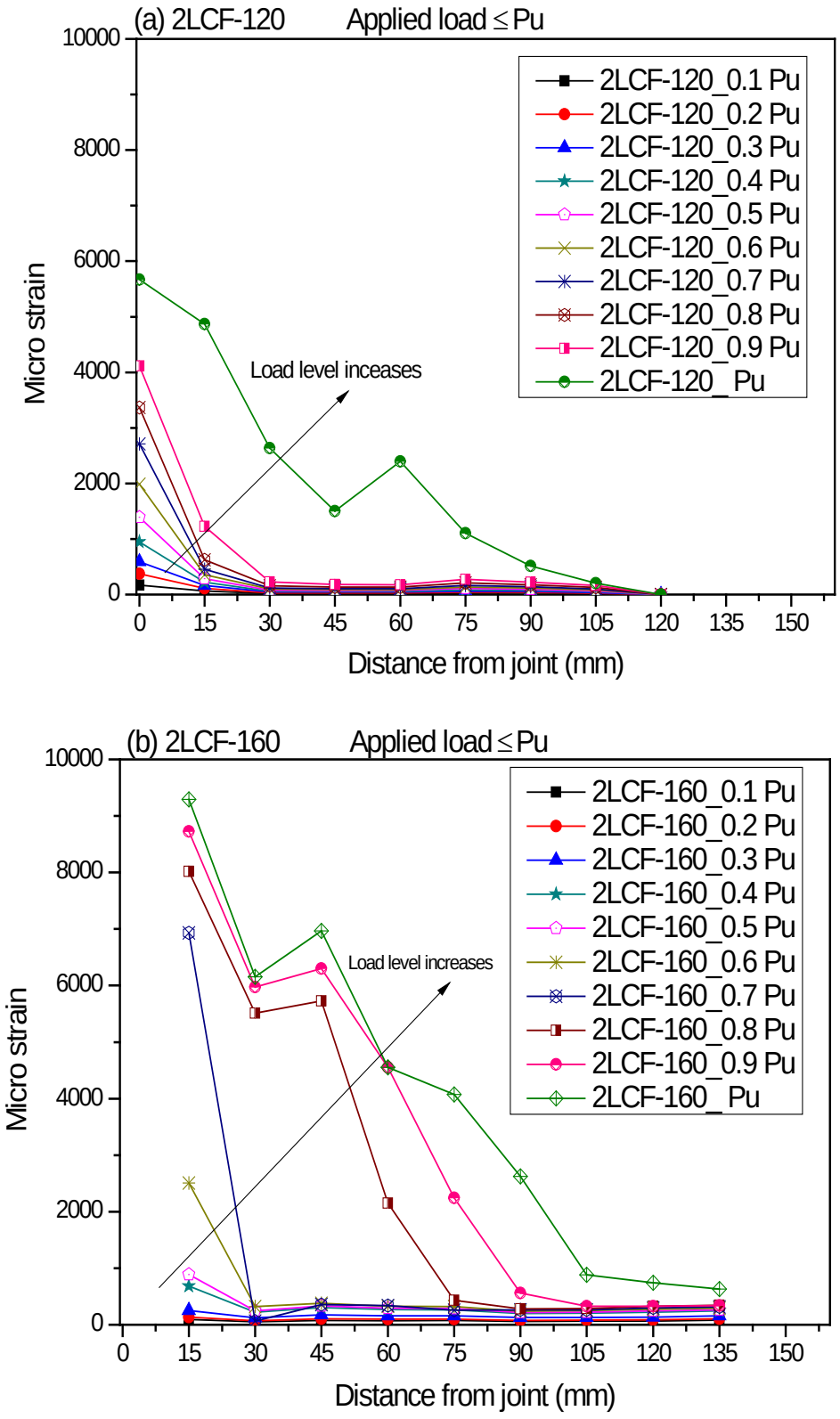

Figure 4.28: Axial strain distribution of 2LCF specimens at different load levels

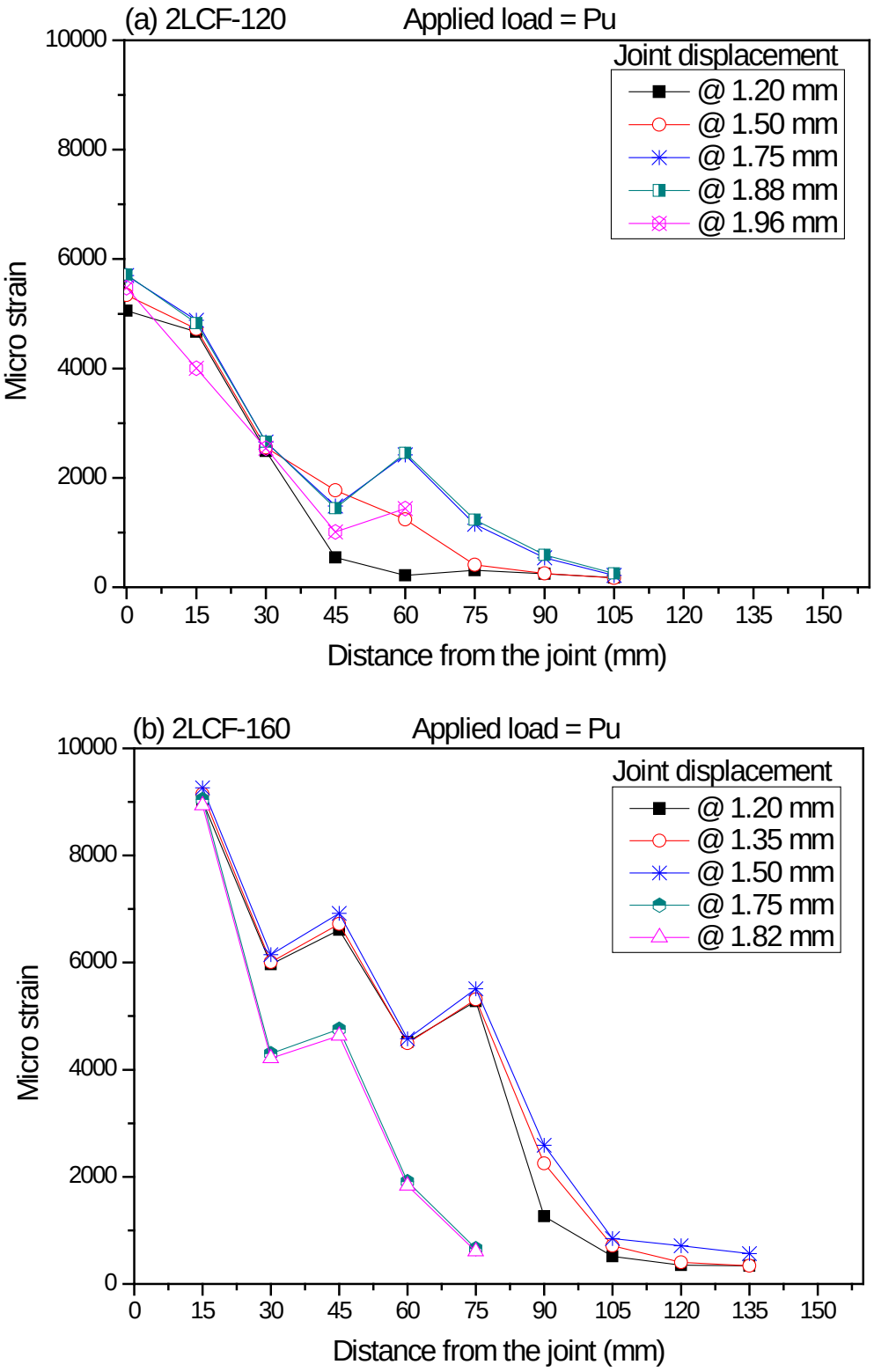

Figure 4.29: Axial strain distribution at ultimate load level

4.3.7 Bond slip behaviour

The interfacial shear behaviour of bonded joints is often studied based on the shear stress-slip curves which depict the response between the local interfacial shear and relative slip between two adherents. Shear stress-slip curves were developed using Equations 4.8 and 4.9 [36-38, 69],

$$\tau = \frac{E_f(\varepsilon_{f,i+1}-\varepsilon_{f,i})t_f}{\Delta L} \tag{4.8}$$

$$s_i = \frac{(\varepsilon_{f,i+1}+\varepsilon f_{,i})\Delta L}{2} + s_{i-1} \tag{4.9}$$

where, E_f and t_f are CFRP elastic modulus and thickness, $\varepsilon_{f,i+1}$ and $\varepsilon_{f,i}$ are CFRP strains, and ΔL is the distance between strain gauges. The average slip s_i is calculated as the incremental sum of the CFRP extension.

The equivalent longitudinal modulus of the fibre layer $E_{e,f}$ is determined by Equation 4.10:

$$E_{e,f} = \frac{E_a t_a + E_f t_f}{t_a + t_f} \tag{4.10}$$

where, E_a and E_f are the longitudinal tensile modulus of the adhesive and fibre, respectively and the terms t_a and t_f represent the adhesive and fibre thickness, respectively.

Under ambient conditions

Shear stress-slip curves for 2LCF specimens under ambient conditions are shown in Figure 4.30. The shear stress-slip curves have an approximately bilinear shape. It is observed that these curves gradually reach their maximum shear stress and then drop sharply to achieve their maximum slip. This type of behaviour in shear stress-slip accounts for debonding failure. In the debonding failure mode, steel-adhesive interface failure occurs suddenly, once the adhesive reaches its maximum shear capacity.

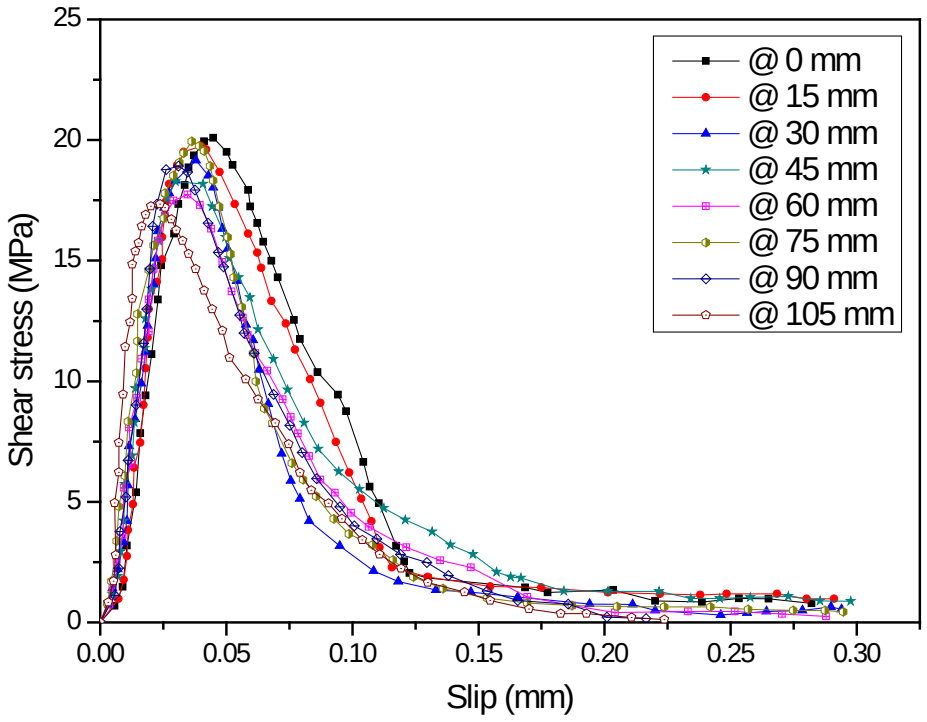

Figure 4.30: Shear stress-slip curves for two layers CFRP-steel double-strap joints under ambient conditions

After exposure to accelerated environmental conditioning

Figure 4.31 shows the shear stress-slip curves for specimens 2LCF-160, which failed due to steel-adhesive interface debonding. Several curves were developed for each specimen using the strain gauge readings recorded at different locations. The results show that the shear stress-slip behaviour is greatly affected by the environmental conditions imposed. Peak shear stress shows a significant drop due to the environmental conditions. It was noted that the shear stress-slip response became non-linear near the maximum shear stress region. However, the bond-slip relationships of degraded specimens can be approximated by a bilinear model. The recorded strain values represent only the outer CFRP fibre strain, which is directly exposed to the environmental conditions, and the innermost CFRP strain values may be differ from the recorded outer fibre strain. Some of the strain gauges became unusable during the tensile tests as a result of the rupture of CFRP attached to the gauges. These strain gauge readings were omitted when developing the shear stress-slip curves. Damage to the outer fibres could lead to the non-linearity of shear stress-slip relationships.

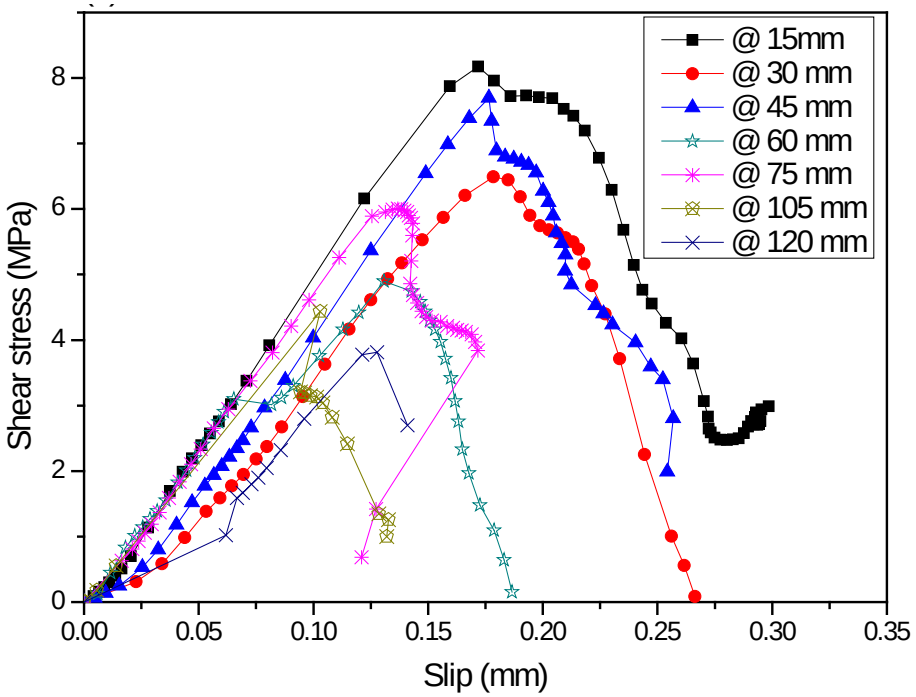

Figure 4.31: Shear stress-slip curves for two layer CFRP-steel double-strap joints after being exposed to accelerated environmental conditions

4.4 CFRP STRENGTHENED BEAM SPECIMENS (SERIES 3)

4.4.1 Failure loads and failure modes

The failure loads and failure modes of tested beam specimens are shown in Table 4.6. The failure modes of the beams were identified as lateral torsional buckling irrespective of the exposure conditions. This was the expected failure mode for the laterally unrestrained simply-supported 150 UB14 section.

Table 4.6: Failure loads and failure modes – Series 3

Beam identification	Failure load (kN)	Failure mode
B300-A1	148	Lateral torsional buckling
B300-A2	152	Lateral torsional buckling
B300-B1	175	Lateral torsional buckling
B300-C1	164	Lateral torsional buckling
B300-C2	162	Lateral torsional buckling
B300-D1	164	Lateral torsional buckling
B300-D2	162	Lateral torsional buckling

The failure modes of each specimen tested are shown in Figures 4.32 to 4.35. In each of the beams, the compression flange underwent buckling failure underneath the two loading points. A comparison of the deformation of the top and bottom flanges is shown in Figure 4.36.

The failure mode observed is the common failure mode for an unrestrained universal beam section under bending [108, 109]. This type of failure can result in lower load-carrying capacity. Out-of-plane bending was observed in all the specimens.

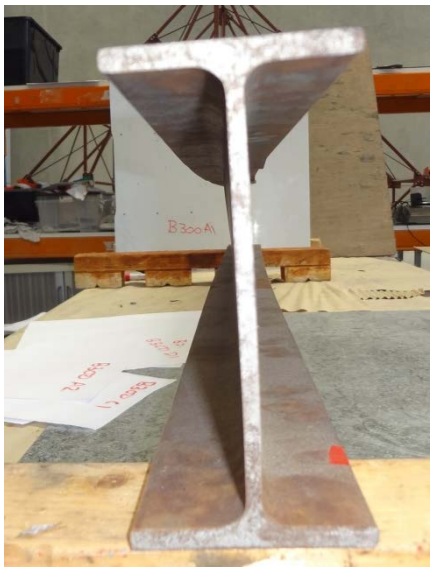

B300-A1

B300-A2

Figure 4.32: Failure mode of B300-A specimens

B300-B1

Figure 4.33: Failure mode of B300-B specimens

B300-C1

B300-C2

Figure 4.34: Failure mode of B300-C specimens

B300-D1

B300-D2

Figure 4.35: Failure modes of B300-D specimens

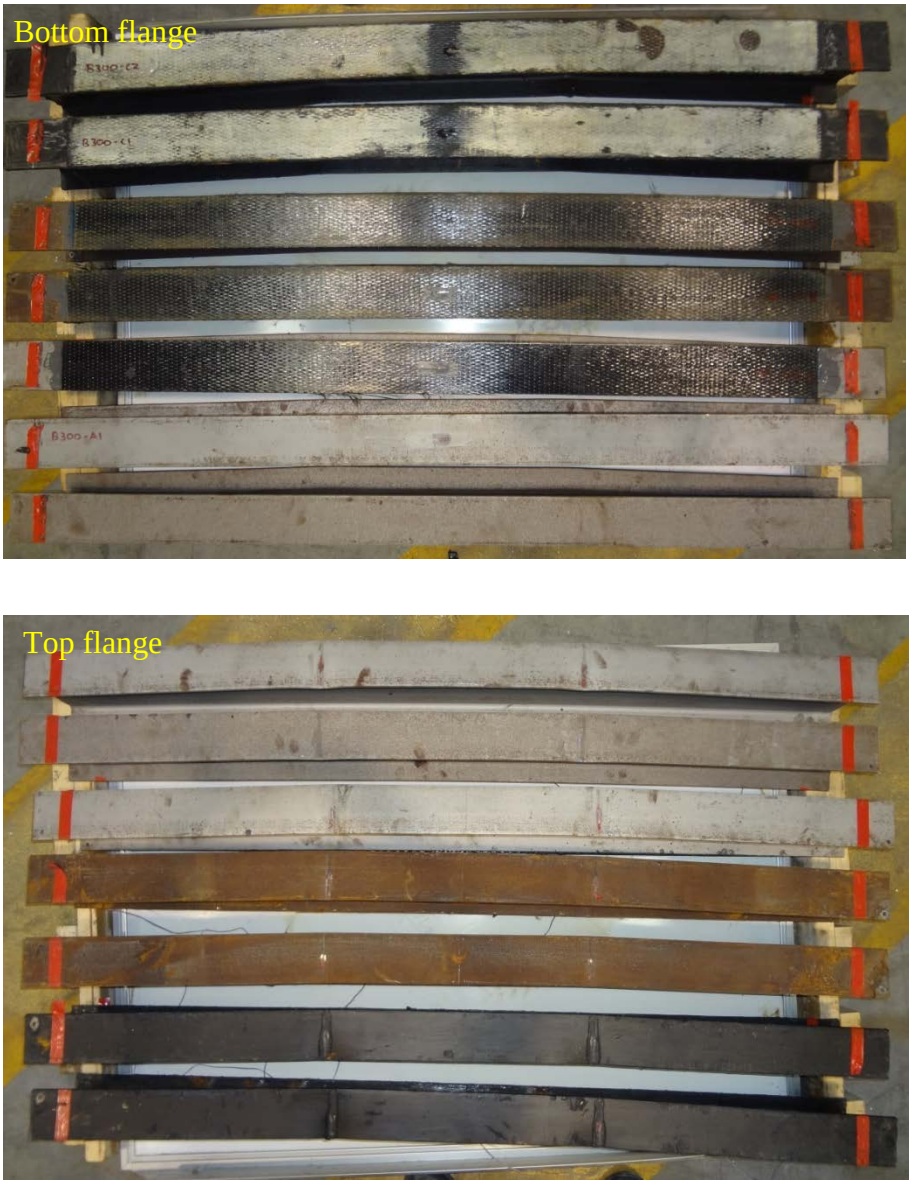

Figure 4.36: Comparison of failure modes of beam specimens

4.4.2 Effect of accelerated environmental exposure conditions

Figure 4.37 shows the load vs. deflection behaviour of the tested beam specimens. All the CFRP-strengthened beams showed an increment of load-carrying capacity compared to the unstrengthened beam, irrespective of the exposure conditions. The unexposed CFRP strengthened beam showed a 17% load-carrying capacity increment compared with the unstrengthened beam. Both the B300-C1 and B300-D1 specimens showed 6.3% capacity loss due to the environmental conditions applied. Load vs. deflection curves of these tested beams suggested that the elastic stiffnesses of conditioned beams are similar to the bare steel beams. Unconditioned CFRP-strengthened beam showed the highest load carrying capacity showing linear load-deflection behaviour up to 175 kN.

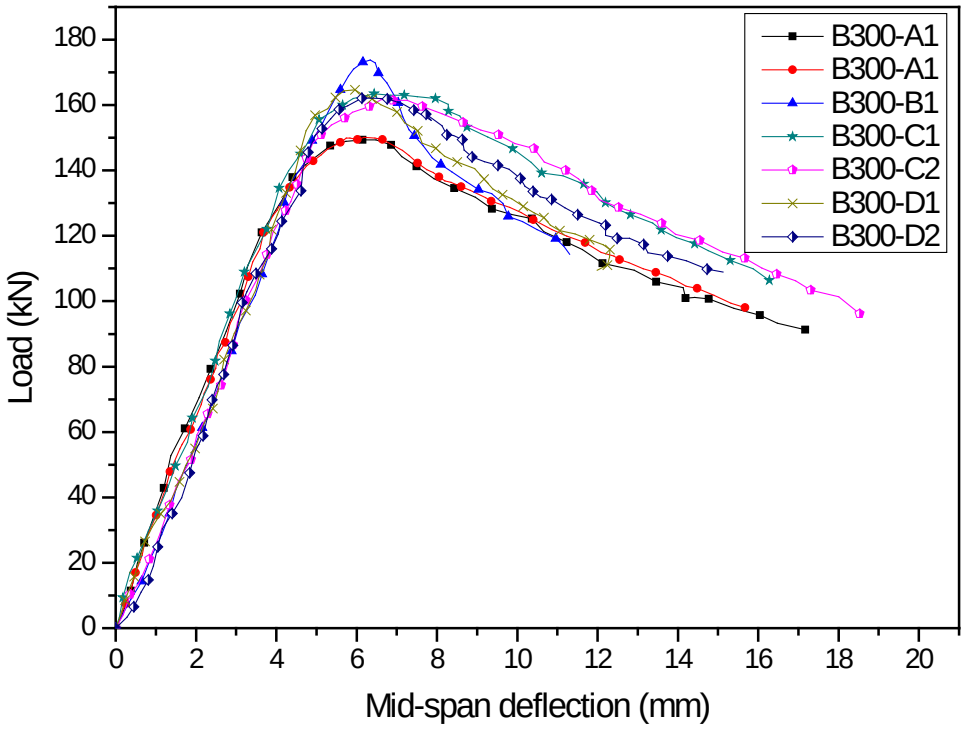

Figure 4.37: Load vs. mid-span deflection of beams

This similar load-carrying capacity loss can be attributed to the material degradation due to accelerated environmental conditions. B300-C specimens showed a significant colour difference in the outer fibre and the CFRP surface became soft after the environmental conditioning (Figure 4.38). B300-D specimens did not show significant colour change or softening of outer fibres. However, the B300-D specimen had significant steel deterioration because of the direct exposure of the steel surface to the accelerated environmental conditions. Although the capacity reduction was similar in these two groups of specimens, the cause of the reduction was different. The capacity loss of B300-C and B300-D specimens can be directly attributed to CFRP material degradation and steel deterioration respectively.

The mid-span deflections were similar for each specimen. This similarity of deflection is directly related to the failure mode of the beams. Lateral torsional buckling failure observed in the specimens resulted in the same deflection at the mid-span. This behaviour is somewhat similar to the results of an experimental study reported in the literature [66].

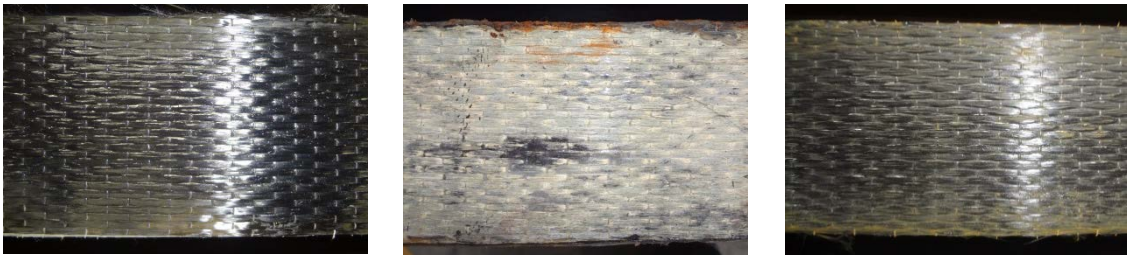

(a) B300-B (b) B300-C (c) B300-D

Figure 4.38: Colour change of CFRP due to exposure conditions

The load vs. strain relationships of tested beams are shown in Figure 4.39. All the beams that were exposed to the accelerated environmental conditioning showed

similar CFRP strain at failure. The strain values of exposed specimens are much lower compared to the CFRP strain of an unexposed CFRP-strengthened beam. This variation clearly shows that there may be material degradation due to the accelerated environmental conditions applied.

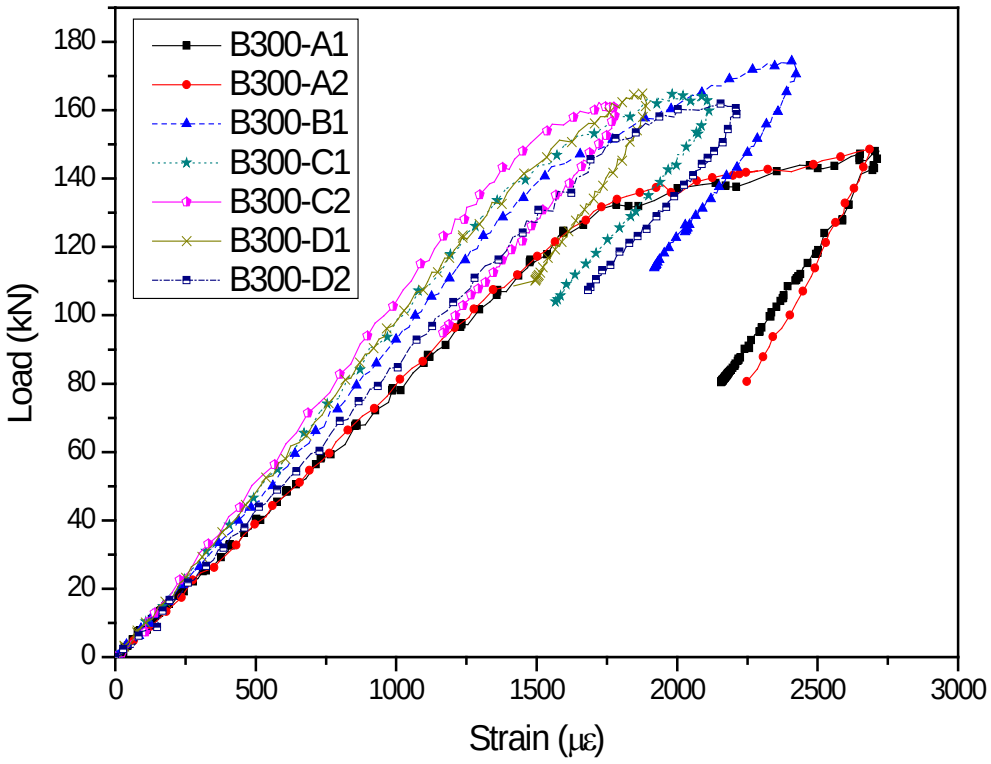

Figure 4.39: Load vs. bottom flange strain of beams

4.4.3 Environmental design durability factor

An environmental design factor can be proposed for a CFRP-steel strengthening system under bending based on the ultimate loads. The beam group B300-D was considered, in which only the CFRP layers were open to direct exposure. The ratios of ultimate loads of B300-D specimens to those of corresponding bare steel beams are listed in Table 4.7.

Table 4.7: Ultimate load ratios

Beam identification	Failure load (kN)	Load ratio
B300-B1	175	-
B300-D1	164	0.93
B300-D2	162	

The load ratio of the CFRP strengthened conditioned beams to the corresponding control beam is 0.93. Therefore, an environmental durability factor of 0.9 was selected. According to the Italian guidelines [1] and ACI guideline [90] an environmental safety factor of 0.85 is recommended for use in aggressive environmental conditions. Therefore, the proposed environmental design durability factor in this study is within the range of existing guidelines.

It should be noted that the environmental design durability factor proposed here is applicable only where beam failure is expected on the top flange undergoing lateral torsional buckling. The failure modes and corresponding ultimate load values may be different under bending about the major axis where the lateral movements are restrained.

4.5 CHAPTER SUMMARY

The experimental section of the present investigation was conducted in three series. The failure modes, failure loads, structural behaviour and material behaviour of CFRP-strengthened steel structures subjected to accelerated environmental conditions were studied, using double-strap joints and universal beam specimens. Load vs. displacement, load vs. strain, joint strength, joint stiffness and other relevant data were analysed and presented. A summary of the experimental results is presented below.

1. The consistent results obtained for each test group confirmed that the specimen preparation and test methods used were maintained at the same accuracy level throughout the experimental program.
2. The selection of the surface preparation method is crucial in CFRP-steel strengthening systems.
3. CFRP can undergo significant colour change when subjected to accelerated environmental conditions and significant swelling and softening of outer CFRP fibres were observed.
4. CFRP-steel double-strap joint degradation levels can be predicted using the proposed empirical expression.
5. The bond properties of steel and CFRP are highly dependent on the exposure conditions.
6. Application of a primer coat can enhance the bond properties and durability of a CFRP-steel composite system.
7. Multi-layer CFRP systems perform better under accelerated environmental conditions.
8. An embedded GFRP layer can enhance the durability of a composite system.
9. The shear stress-slip relationships of a CFRP-steel interface are significantly affected by the environmental conditioning.
10. Accelerated environmental conditions can result in the reduction of the load-carrying capacity of CFRP-strengthened beams.

11. The proposed environmental factor (0.90) can be used in CFRP-strengthened beams and is consistent with the Italian and ACI guidelines.
12. Severe corrosion damage can be expected on the steel surface when both CFRP and steel are subjected to marine environments.

Chapter 5: Finite Element Modelling

5.1 INTRODUCTION

This chapter presents the FE modelling of CFRP-steel composite systems. CFRP-steel double strap joints were modelled in ABAQUS 6.14-2 [110]. Full 3D models were developed with similar geometry, strengthening parameters and boundary conditions as those employed in the experiments, and ABAQUS/implicit was used to simulate the quasi-static tensile loading.

5.2 DEVELOPMENT OF FINITE ELEMENT MODELS

All the developed FE models consisted of two steel segments with identical steel cross sections (25 mm×6 mm) and adhesive layer followed by CFRP layers. One face was fixed by applying the required displacement and rotation boundary conditions. The joint was created by defining separate part instances and assembling them to simulate the double-strap joint. The adhesive layer was modelled on the steel segments followed by the CFRP layer. Surface-to-surface tie contacts were used to define the contact between the different parts. These tie constraints were capable of transferring the applied tensile load between the modelled layers without sliding. The tensile load was applied as a displacement to the free end of the steel part. Figures 5.1 and 5.2 show some key parts and features of the developed FE models.

A total of 14 models were developed to study the structural behaviour of CFRP-steel double strap joints. Model identification and CFRP layer arrangements in FE models are given in Table 5.1.

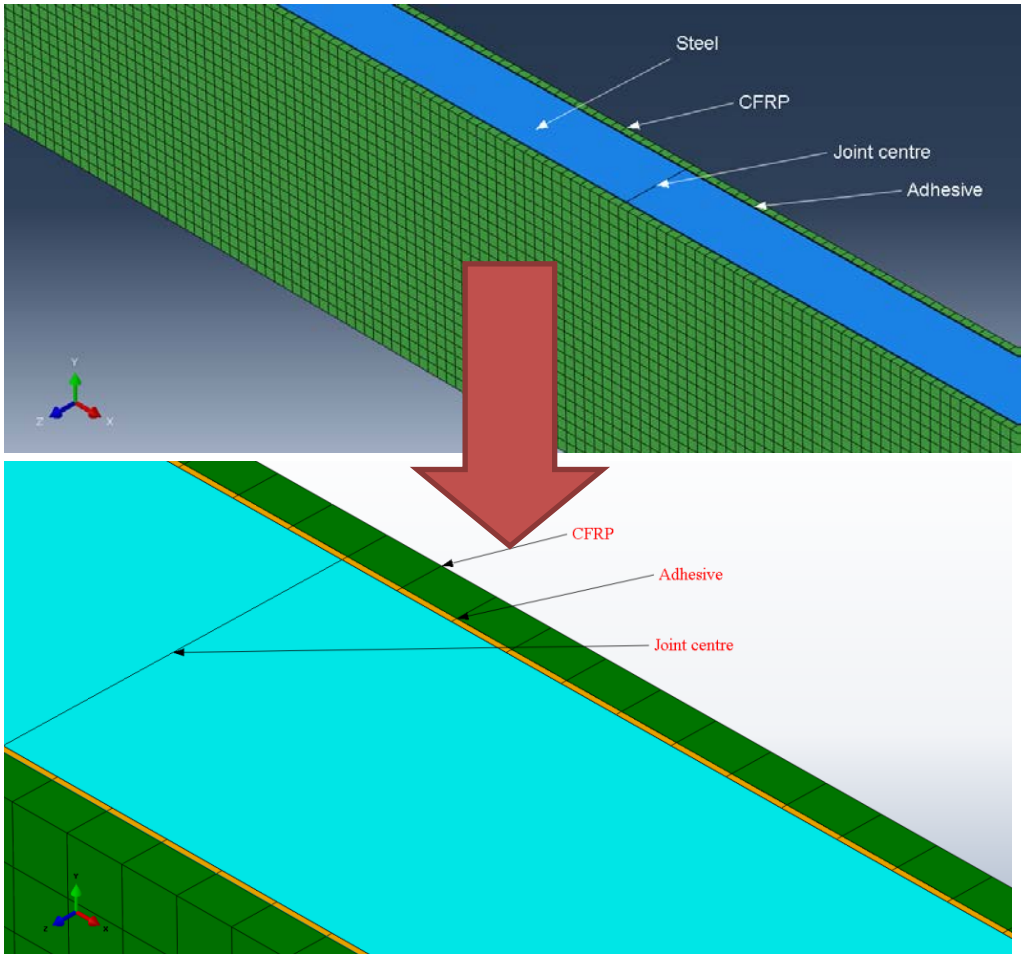

Figure 5.1: Parts of FE model

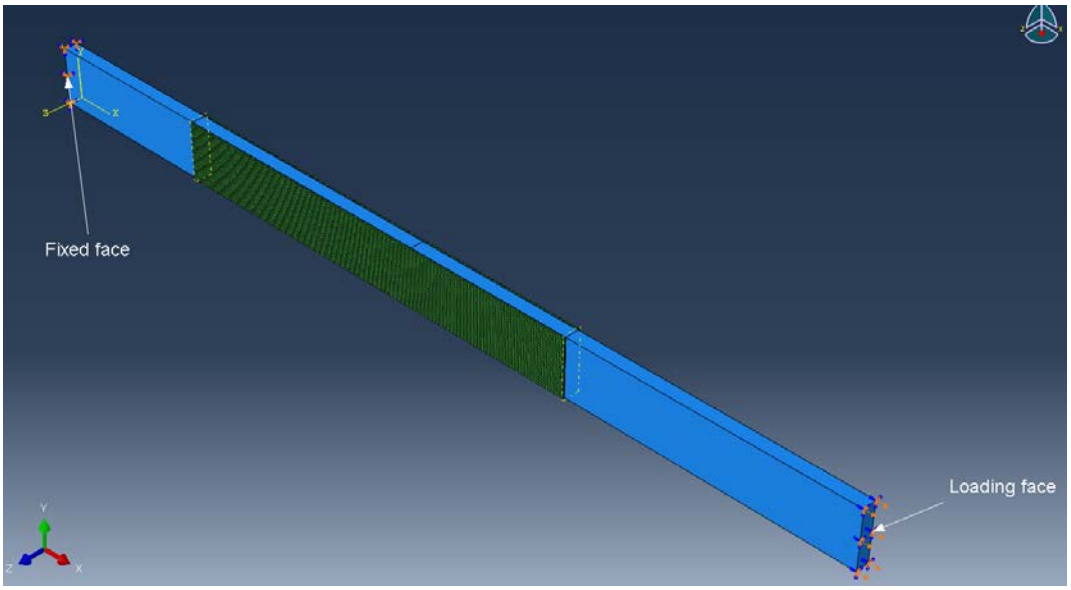

Figure 5.2: Boundary conditions

Table 5.1: FE model identification and CFRP layer arrangement

Model identification	CFRP arrangement
1LCF-CS	One longitudinal CFRP layer
2LCF-CS	Two longitudinal CFRP layers
3LCF-CS	Three longitudinal CFRP layers
4LCF-CS	Four longitudinal CFRP layers
5LCF-CS	Five longitudinal CFRP layers
1LCF-A	One longitudinal CFRP layer
1LCF-B	
1LCF-C	
2LCF-A	Two longitudinal CFRP layers
2LCF-B	
2LCF-C	
3LCF-A	Three longitudinal CFRP layers
3LCF-B	
3LCF-C	

5.2.1 Element types

The selection of the appropriate element type for each modelled part is critical in composite modelling. The results can have a significant effect depending on the element type used in the simulation. It is always a challenging task to simulate the behaviour of composite materials accurately because these composites involve various types of failure modes. Cohesive elements have been used successfully in numerical simulations to model adhesive layers [17, 18, 96, 98] to overcome most of the difficulties. In the present simulation, the adhesive layer was modelled using 8-node-3-D cohesive element (COH3D8) available in the ABAQUS element library. CFRP layers were modelled with 8-node quadrilateral continuum shell elements (SC8R). This type of element was used in previous research to successfully model CFRP composite damage failure [17]. Steel was modelled using 8-node linear brick elements with reduced integration and hourglass control (C3D8R).

5.2.2 Material models

Steel was modelled using an isotropic classic metal plasticity model to consider the elastic-plastic behaviour of steel. This material model has been successfully

employed in numerical simulations by various researchers. As reported in the literature [68, 102, 111, 112], most of the CFRP-steel composite systems show debonding failure mode. It was observed in the present research that CFRP composite material can also undergo rupture failure due to accelerated environmental conditions. To accurately simulate both types of failure modes, two approaches were taken as described below.

Cohesive zone modelling

Accurate modelling of the adhesive layer is a vital aspect in simulating the bonded joints. The results depend very much on the input properties of the adhesive for debonding failure. To accurately model the interface between CFRP and steel, the epoxy adhesive layer was modelled using particular types of elements known as cohesive elements with 0.1 mm thickness. The failure of the modelled cohesive elements was defined based on traction-separation law available in ABAQUS [113]. Traction-separation law defines the stress failure criteria of the cohesive zone using the following equation [113],

$$\left(\frac{t_n}{N}\right)^2 + \left(\frac{t_s}{S}\right)^2 + \left(\frac{t_t}{T}\right)^2 = 1 \tag{5.1}$$

where, t_n, t_s and t_t are traction stresses in normal, first and second directions of the adhesive layer respectively, and N, S and T are the maximum nominal stresses of the adhesive layer in normal and two shear directions respectively. The traction stresses are calculated using Equation 5.2, in which, δ_n, δ_s and δ_t are corresponding separations and k_{ij} are the stiffness in corresponding directions.

$$\begin{Bmatrix} t_n \\ t_s \\ t_t \end{Bmatrix} = \begin{bmatrix} k_{nn} & k_{ns} & k_{nt} \\ k_{ns} & k_{ss} & k_{st} \\ k_{nt} & k_{st} & k_{tt} \end{bmatrix} \begin{Bmatrix} \delta_n \\ \delta_s \\ \delta_t \end{Bmatrix} \tag{5.2}$$

Once the degradation process of the adhesive material begins, the material stiffness is subjected to degradation using the damage variable d given in Equation 5.3. Exponential softening damage evolution was used in this FE modelling.

$$d = 1 - \left\{\frac{\delta_m^0}{\delta_m^{max}}\right\}\left\{1 - \frac{1-\exp\left(-\alpha\left(\frac{\delta_m^{max}-\delta_m^0}{\delta_m^f-\delta_m^0}\right)\right)}{1-\exp(-\alpha)}\right\} \quad (5.3)$$

In the above equation, δ_m^0 = effective displacement at damage initiation, δ_m^{max} = maximum effective displacement attained during loading history, δ_m^f = effective displacement at complete failure, α = non dimensional damage evolution parameter and $\exp(x)$ is the exponential function. Displacement type damage evolution was used having exponential softening coefficient of 8. Displacements at failure were ranged from 0.0001 mm to 0.0015 mm.

CFRP damage modelling

As observed during the tensile tests, there were two main types of failure modes; (i) adhesive-steel interface debonding and (ii) CFRP fibre rupture. It is crucial to take this into account in numerical modelling to predict failure behaviour accurately. The linear-elastic brittle behaviour of normal modulus CFRP material can be accurately modelled using the material models available in ABAQUS. Most of the FE models developed have used the facility of damage initiation propagation criteria to simulate CFRP failure behaviour. To account for the CFRP composite failure modes in the current simulation, Hashin damage criteria [114, 115] were used with energy-type damage evolution and linear softening. By adopting this material model, the plasticity of the CFRP composite is neglected, and material damage is detected and characterised based on the material stiffness reductions. This damage model in ABAQUS is capable of modelling the damage and the failure modes of composite materials. Four different CFRP failure modes can be modelled using the input

parameters. These failure modes are (i) fibre rupture in tension (ii) fibre buckling and kinking under compression (iii) matrix cracking under transverse tension and shearing and (iv) matrix crushing under transverse tension and shearing. These approaches resulted in a more accurate validation of the numerical models with the experimental data.

5.3 MATERIAL PROPERTIES IN FE ANALYSIS

The values used for steel, adhesive and CFRP are listed in Table 5.2.

Table 5.2: Material properties used in FE models

Material	Parameter	Value
Steel	ρ_{st} (kgm^{-3})	7850
	E_{st} (GPa)	200
	F_y (MPa)	352
	ν	0.3
CFRP	ρ_{CFRP} (kgm^{-3})	1807
	E_{CFRP} (GPa)	150
	$\sigma_{t,xx,CFRP}$ (MPa)	970
	$\sigma_{t,yy,CFRP}$ (MPa)	271
	$\sigma_{c,xx,CFRP}$ (MPa)	292
	$\sigma_{c,yy,CFRP}$ (MPa)	292
	$\tau_{xx,CFRP}$ (MPa)	166
	$\tau_{yy,CFRP}$ (MPa)	133
Adhesive	P_{AD} (kgm^{-3})	1100
	E_{AD} (GPa)	2.25
	X_{AD} (MPa)	3.8-7.0
	k_{nn} (GPa/mm)	1.3
	k_{ss}=k_{tt} (GPa/mm)	0.65

5.4 VALIDATION OF FINITE ELEMENT MODELS

5.4.1 Ultimate loads

The developed FE models were validated using the experimental results. The experimentally-measured ultimate loads were compared with the ultimate loads obtained from the FE simulation. Table 5.3 compares the FE results with the

experimental results and it is evident that both sets of results compare well. The ratios of ($P_{U,FE}/P_{U,exp}$) are very close to unity with the coefficient of variation 0.01. The results show that the joint capacities are greatly dependent on the exposure conditions.

Table 5.3: Comparison of failure loads

Model identification	Experimental failure load ($P_{U,exp}$)	FE failure load ($P_{U,FE}$)	($P_{U,FE}/P_{U,exp}$)
1LCF-CS	12.2	11.9	1.03
2LCF-CS	18.1	18.9	0.96
3LCF-CS	21.9	22.0	1.00
1LCF-A	9.9	9.8	1.01
1LCF-B	6.0	6.0	1.00
1LCF-C	4.1	4.1	1.00
2LCF-A	18.6	18.6	1.00
2LCF-B	14.5	14.5	1.00
2LCF-C	13.2	13.2	1.00
3LCF-A	22.6	22.5	1.00
3LCF-B	20.5	20.3	1.01
3LCF-C	18.2	18.1	1.01
		Mean	1.00
		COV	0.01

5.4.2 Load vs. axial displacement response

The load vs. axial displacement obtained from the developed FE models were compared with those from the experimental results. The validation of 2LCF-A and 3LCF-B were not considered since these specimens behaved similarly to their control specimens.

Validation of models: control specimens

Comparisons between numerically and experimentally-obtained load vs. axial displacement behaviours of the control specimens are shown in Figures 5.3 to 5.5. It is evident from these figures that there is a good agreement between the simulated and experimental results for the load vs. axial displacement responses.

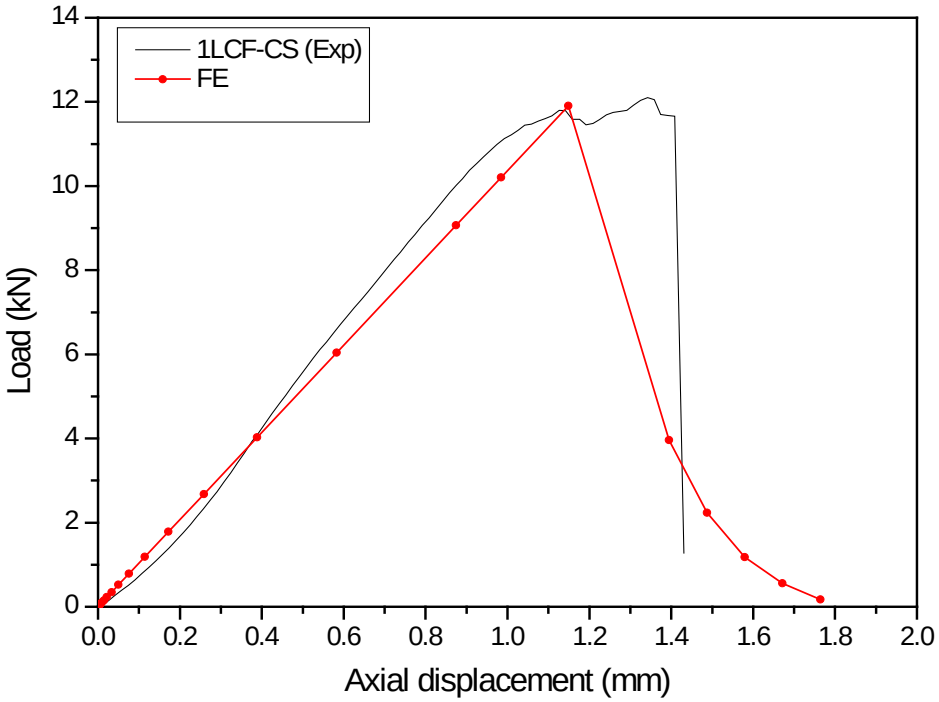

Figure 5.3: Validation of 1LCF-CS models

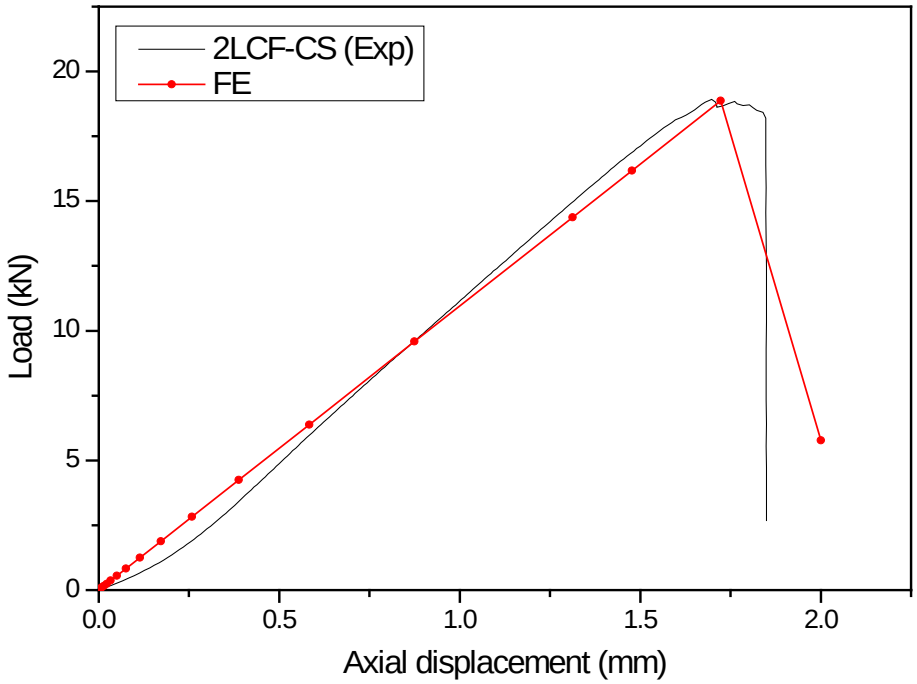

Figure 5.4: Validation of 2LCF-CS models

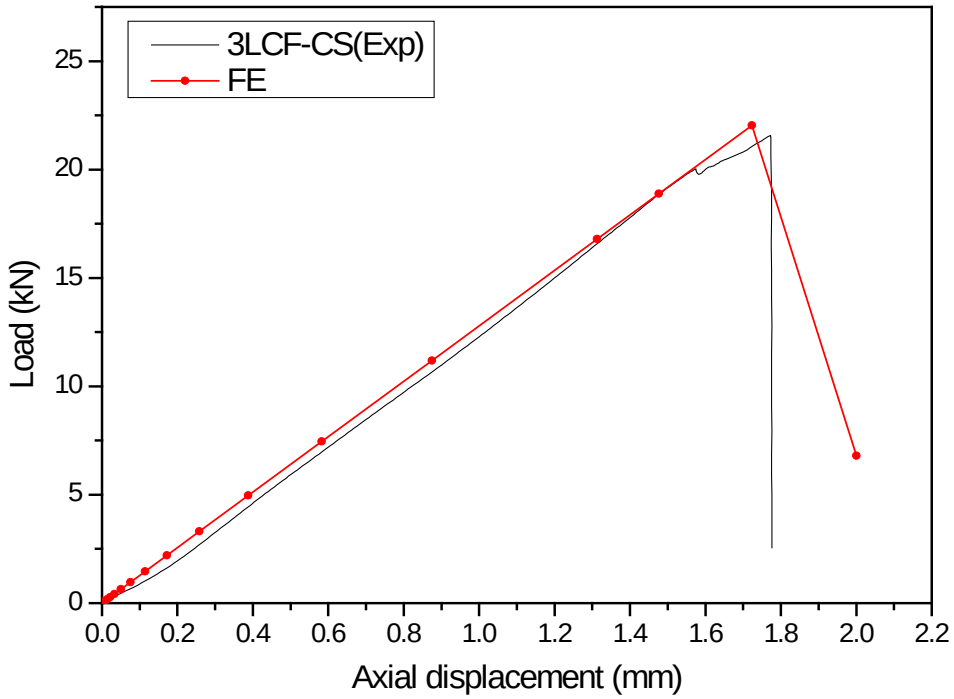

Figure 5.5: Validation of 3LCF-CS models

Validation of models: 1LCF after exposure

Comparisons between the numerically- and experimentally-obtained load vs. axial displacement behaviour of the 1LCF specimens after exposure are shown in Figures 5.6 to 5.8. The models are capable of successfully simulating CFRP damage at failure. It is evident from these figures that there is good agreement between the simulated and experimental results for the load vs. axial displacement responses.

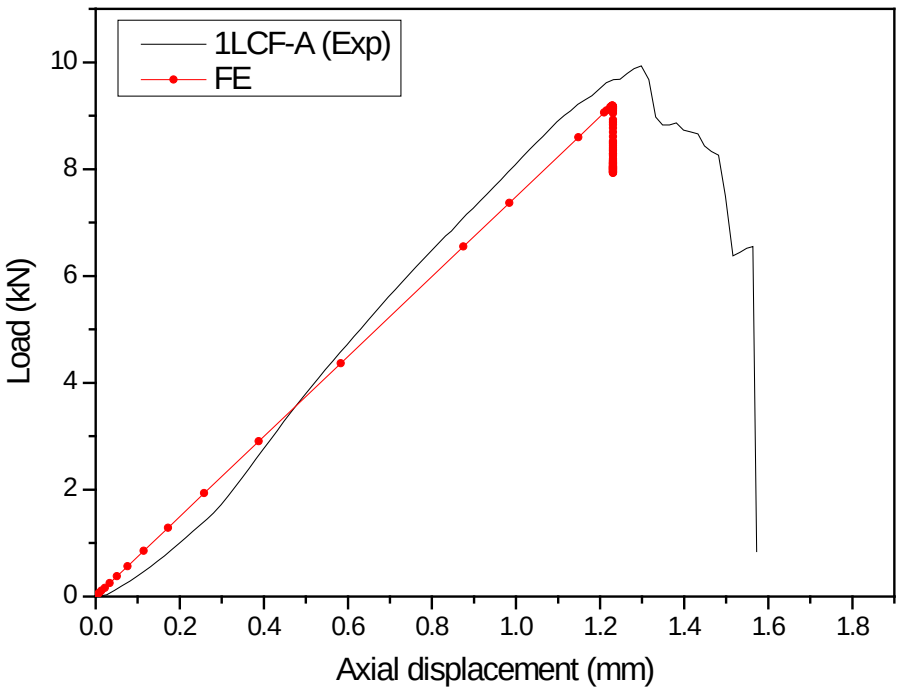

Figure 5.6: Validation of 1LCF-A models

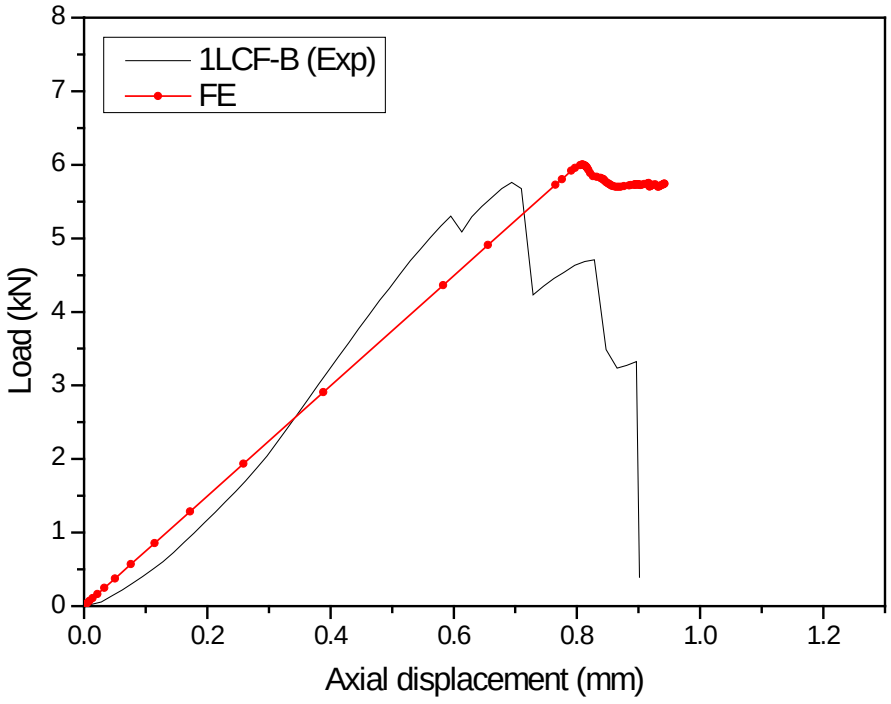

Figure 5.7: Validation of 1LCF-B models

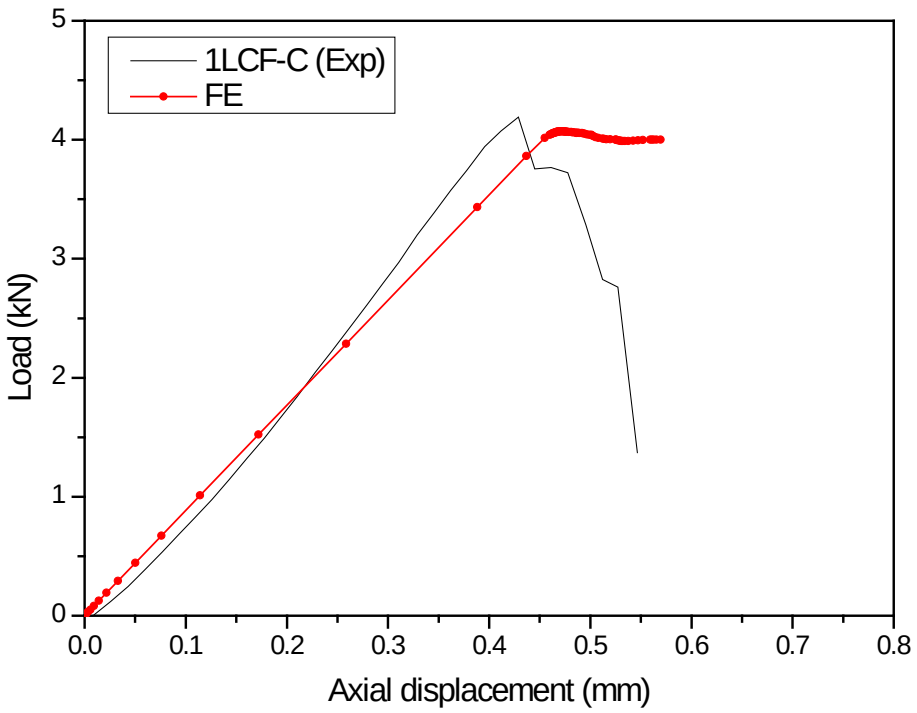

Figure 5.8: Validation of 1LCF-C models

Validation of models: 2LCF after exposure

Comparisons between numerically and experimentally-obtained load vs. axial displacement behaviour of 2LCF specimens after exposure are shown in Figures 5.9 and 5.10. The models are capable of successfully simulating CFRP damage at failure. It is evident from these figures that there is good agreement between the simulated and experimental results for the load vs. axial displacement responses.

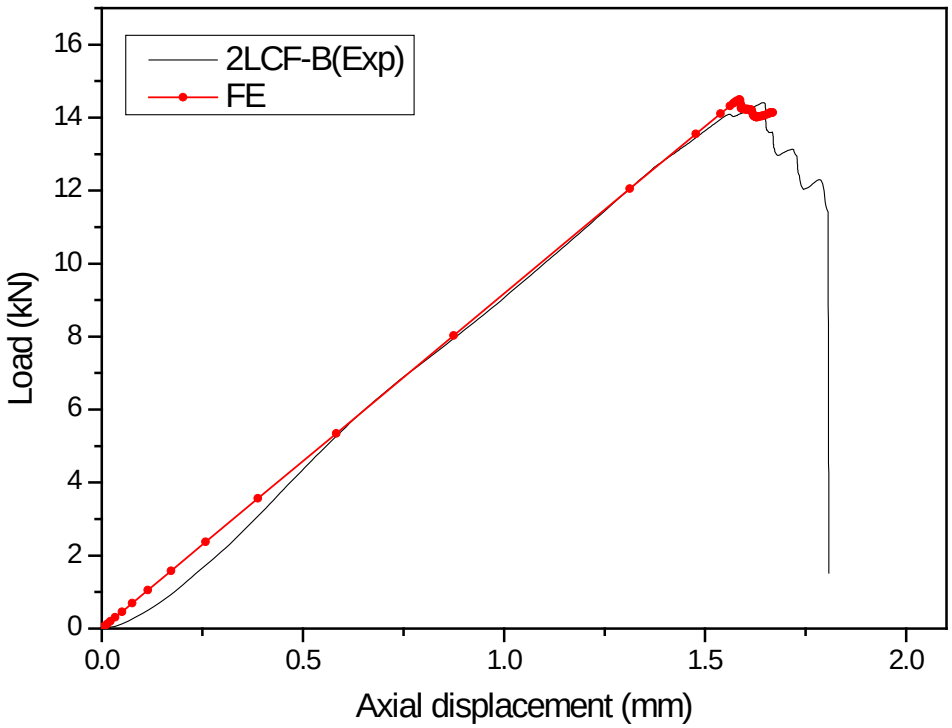

Figure 5.9: Validation of 2LCF-B models

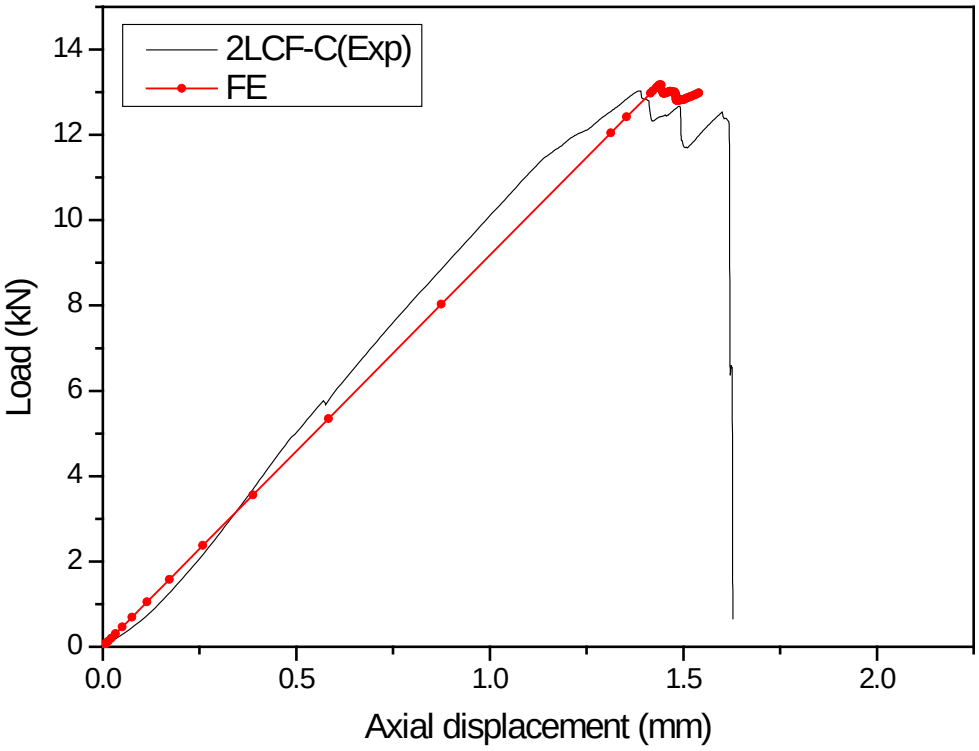

Figure 5.10: Validation of 2LCF-C models

Validation of models: 3LCF specimens after exposure

Comparisons between numerically- and experimentally-obtained load vs. axial displacement behaviour of 3LCF specimens after exposure are shown in Figures 5.11 and 5.12. The models are capable of successfully simulating CFRP damage at failure. It is evident from these figures that there is good agreement between the simulated and experimental results for the load vs. axial displacement responses.

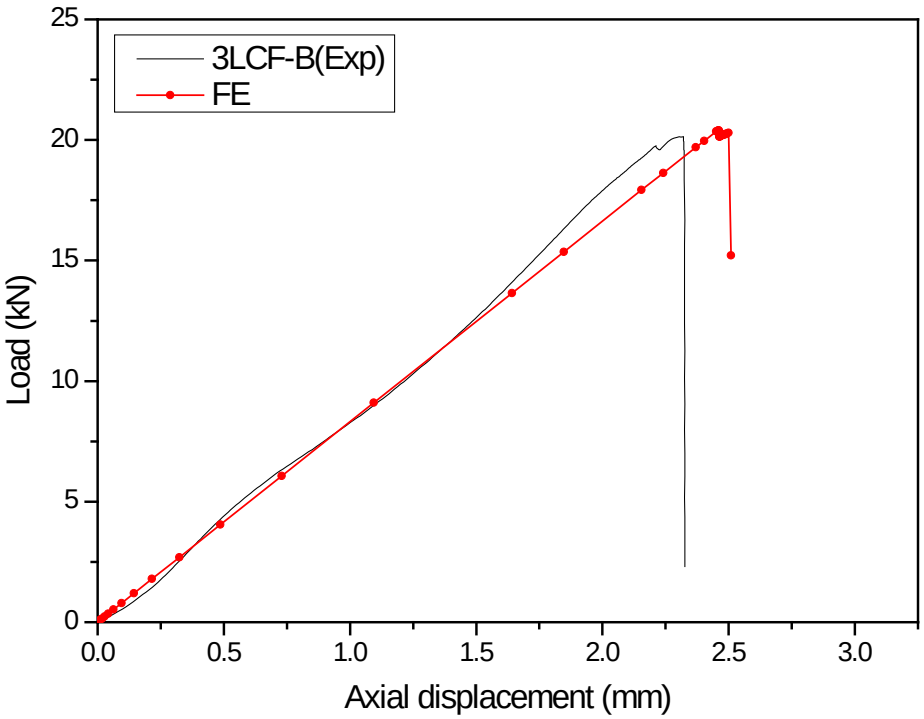

Figure 5.11: Validation of 3LCF-B models

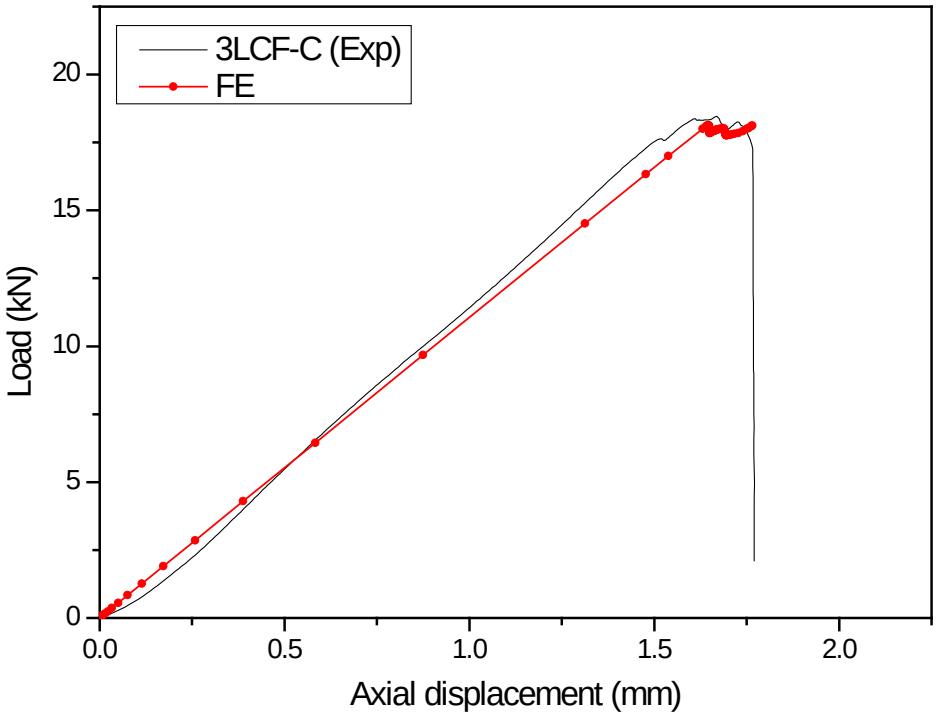

Figure 5.12: Validation of 3LCF-C models

5.4.3 Failure modes

Figure 5.13 shows a comparison of the numerically-simulated and experimental failure modes. Observations made in the experiments during the failure of control specimens revealed that the opening of a gap at the joint location, and the FE models are capable of successfully capturing that effect. The tested specimens showed complete debonding of CFRP from the steel surface after failure. Figure 5.14 shows the simulated adhesive failure in FE models. Numerically obtained failure modes are in good agreement with the corresponding failure modes observed in the experiments.

(a) Debonding failure - experimental

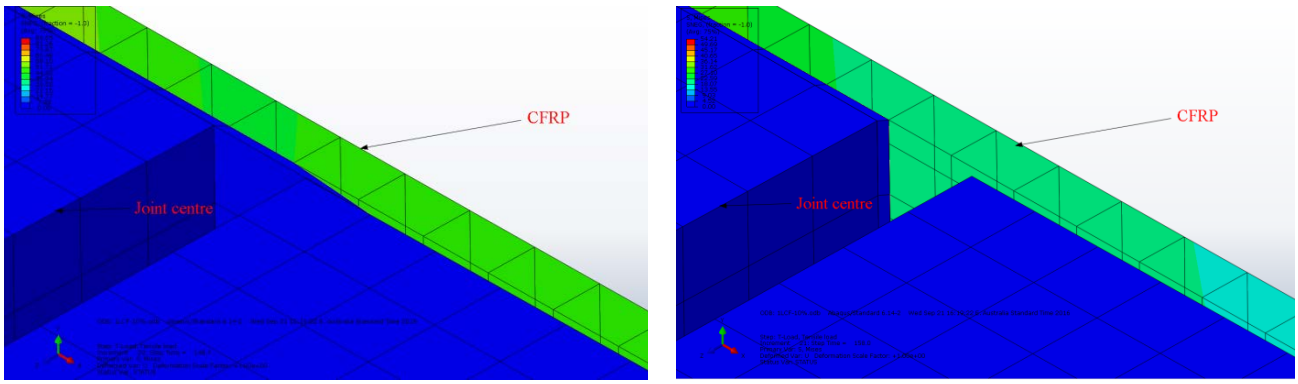

Before failure After failure

(b) Debonding failure - numerical

Figure 5.13: Comparison of failure modes

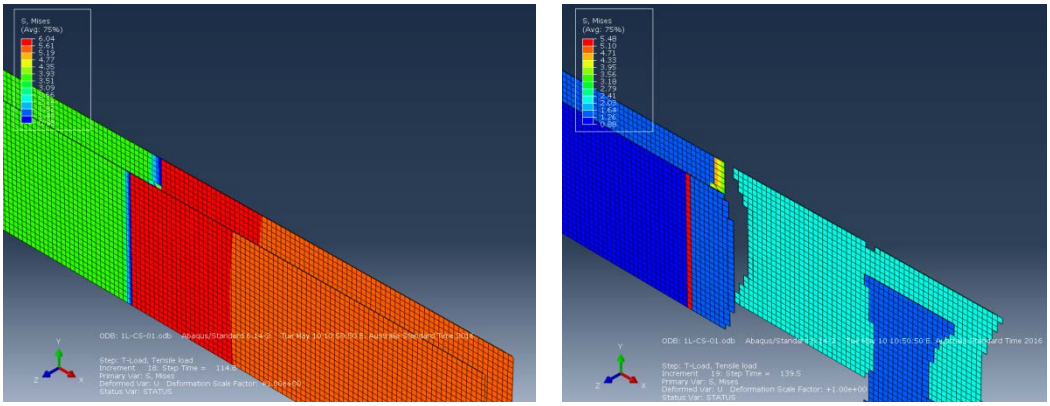

(a) Before failure (b) After failure

Figure 5.14: Adhesive failure

5.4.4 CFRP stress at failure

Table 5.4 compares calculated and numerically-simulated CFRP composite stresses at failure. CFRP composite stresses were calculated based on the experimental failure loads. CFRP stress levels at failure were evaluated using a cross-sectional analysis of failed joint specimens. The CFRP composite average thicknesses were 0.7 mm, 1.4 mm and 2.1 mm for 1L, 2L and 3L respectively. The width of CFRP was 25 mm in this experiment. The comparison shows that the numerically-obtained CFRP stress levels are in good agreement with the experimental results. The ratios of ($\sigma_{CFRP,FE}/\sigma_{CFRP,calculated}$) are very close to unity with the coefficient of variation 0.04.

Table 5.4: Comparison of CFRP composite stress at failure

Model	Calculated CFRP stress at failure (MPa) ($\sigma_{CFRP,calculated}$)	CFRP stress from FE model (MPa) ($\sigma_{CFRP,FE}$)	($\sigma_{CFRP,FE}/\sigma_{CFRP,calculated}$)
1LCF-CS	349	372	1.07
2LCF-CS	259	279	1.08
3LCF-CS	209	234	1.12
1LCF-A	264	263	1.00
1LCF-B	171	174	1.02
1LCF-C	119	118	0.99
2LCF-A	266	279	1.05
2LCF-B	208	213	1.02
2LCF-C	189	198	1.05
3LCF-A	215	234	1.09
3LCF-B	196	219	1.12
3LCF-C	173	185	1.07
		Mean	1.06
		COV	0.04

5.5 PARAMETRIC STUDY

Validated FE models were used to evaluate the effect of different parameters on the structural behaviour of double-strap joints. The effects of exposure conditions, the number of CFRP layers, effective bond length, CFRP degradation level and adhesive degradation level were evaluated using joint capacity, adhesive stress at failure and CFRP stress at failure as response parameters.

5.5.1 Effect of exposure condition

1LCF specimens showed a lower joint capacity under ambient conditions compared with two- and three-layered CFRP double strap joints. The joint capacities of 2LCF and 3LCF specimens showed 58% and 83% joint capacity increments with the use of two and three layers of CFRP, respectively. Joint capacities decreased with increased exposure conditions, and the joint capacity reduction was greater with the single-layer CFRP specimens. ILCF specimens were highly vulnerable to the exposure conditions, and the joint capacity reduction was 66% after 72 h exposure. 2LCF and 3LCF specimens showed 27% and 17% joint capacity reductions after the same exposure conditions.

Results obtained from the specimens after exposure to environmental conditioning indicated that the durability of the joints had increased with the usage of multilayer CFRP systems. Further analysis has been carried out to obtain the adhesive and CFRP stresses at failure using developed FE models. Figure 5.15 shows the variation of adhesive stress after different exposure levels. 1LCF models started to show a decrement of the adhesive stress with the increment of exposure conditions. 1LCF models showed that the adhesive stresses at failure are reduced with the increased exposure duration. This implies that longer exposure durations could result in significant composite degradation resulting in a lower joint capacity.

Failure adhesive stress levels remained same in 2LCF-CS and 2LCF-A models. 2LCF-B and 2LCF-C models showed a gradual decrement in adhesive stresses at failure. No significant difference in the adhesive stresses at failure was observed in 3LCF models. Overall, the analysis of the adhesive stresses implies that the joint capacities are greatly affected by the exposure duration. Longer exposure duration could lead to lower joint capacities. The effect is significant with single layer CFRP systems. Using multi-layer CFRP system can effectively delay the damage initialisation.

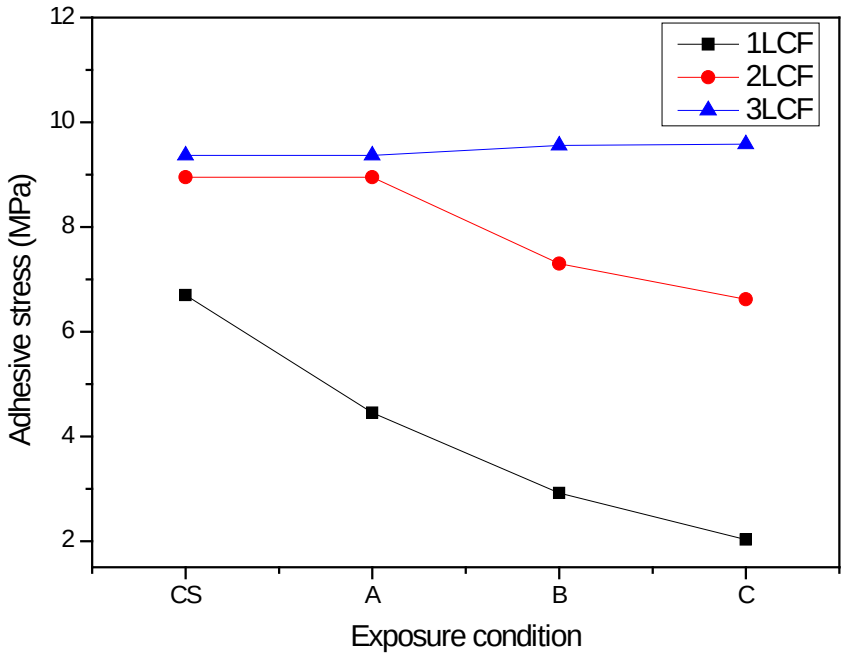

Figure 5.15: Adhesive stresses under different exposure conditions

Figures 5.16 to 5.18 show the numerically obtained CFRP composite stress levels at failure. The composite stresses at the failure of 1LCF models are highly sensitive to the exposure conditions. Visual inspections of the test specimens showed a significant deterioration of the composite in the experiment [116]. CFRP stresses obtained from 2LCF and 3LCF models showed that the reductions in failure stress

become smaller with increased exposure conditions. This analysis clearly suggests that CFRP composite damage can be minimised by using multi-layer CFRP systems.

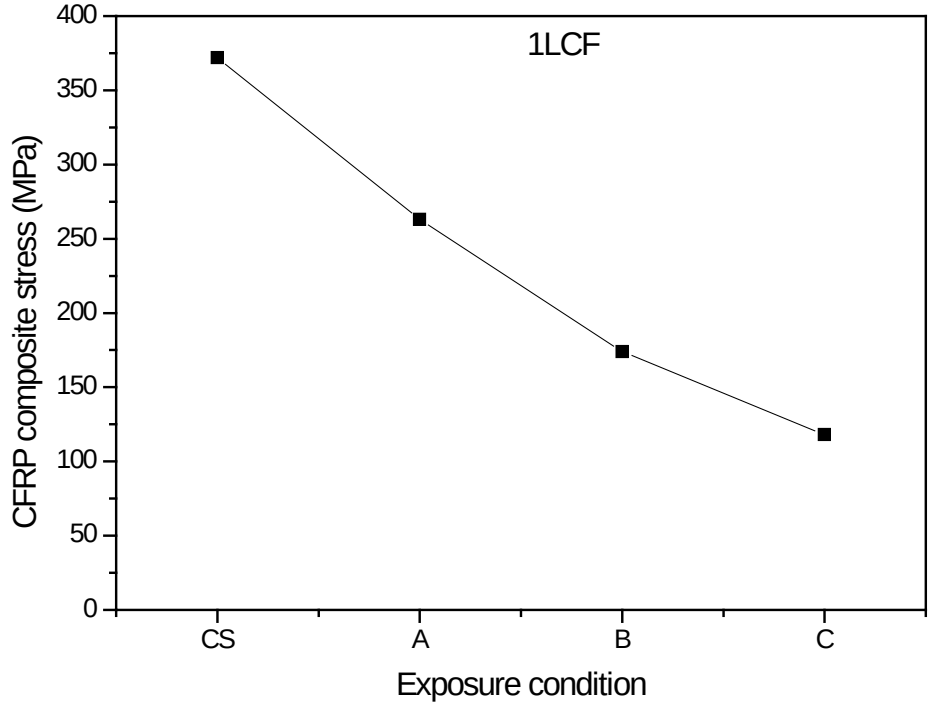

Figure 5.16: CFRP composite stresses under different exposure conditions-1LCF models

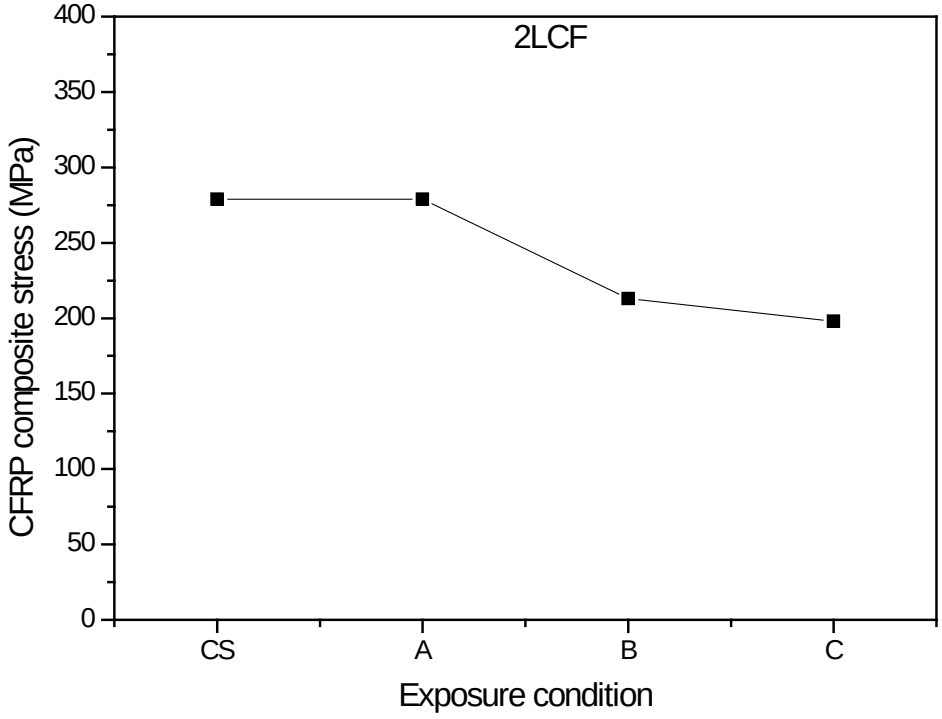

Figure 5.17: CFRP composite stresses under different exposure conditions-2LCF models

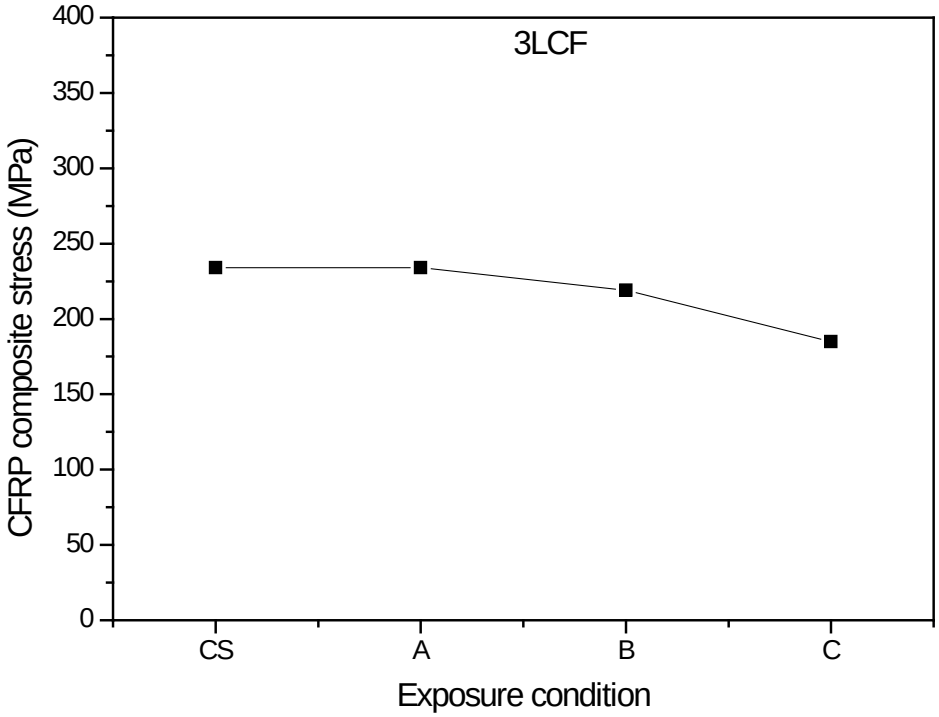

Figure 5.18: CFRP composite stress at failure under different exposure conditions-3LCF models

5.5.2 Effect of number of CFRP layers

The effect of using multi-layer CFRP systems was investigated using developed FE models. The experiments consisted of double-strap joint specimens which had a maximum of three CFRP layers. FE models were developed and extended to investigate the effect of multi-layer CFRP systems which ranges from 1-5 layers. Figure 5.19 shows the effect of the number of CFRP layers on the joint capacity. Joint capacity is increased with the increment in the number of CFRP layers. Maximum joint capacity is reached with three CFRP layers bonded to each side of the joint and the same joint capacity is observed in the double-strap joint models with four and five CFRP layers. The failure mode of the tested control specimens showed adhesive-steel interface debonding failure. This failure mode suggest that the joint capacity is mainly attributed to the interface properties of the bonded substances. The adhesive shear stress vs. number of CFRP layers was plotted to study the interface behaviour of the bonded joints and the results are shown in Figure 5.20. 1LCF specimens show a lower adhesive stress compared to the multi-layer CFRP specimens. Adhesive stress increases with the increment of the number of CFRP layers and reaches a plateau with 4LCF specimens. This behaviour explains the reason for the optimum joint capacity of the 3LCF specimens.

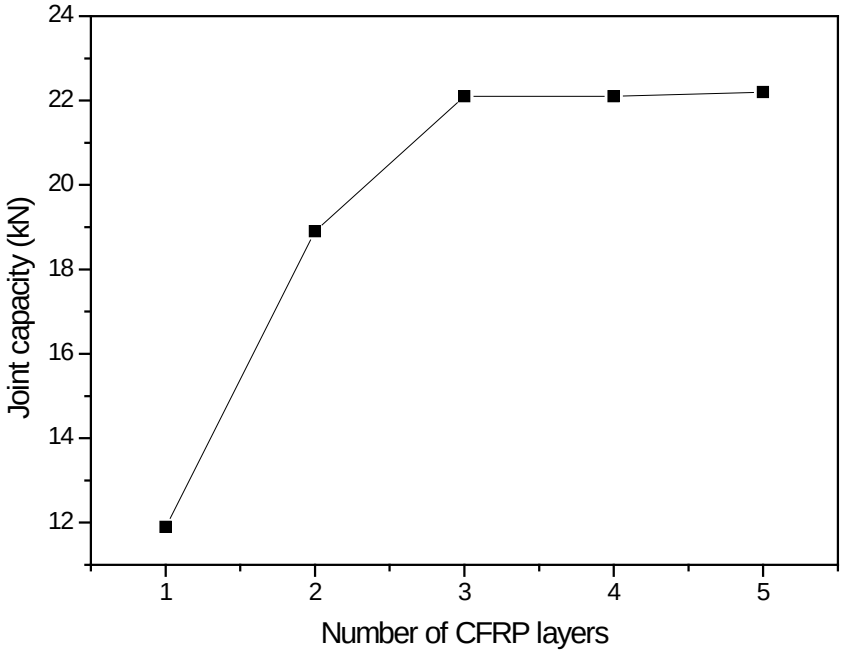

Figure 5.19: Effect of number of CFRP layers on joint capacity

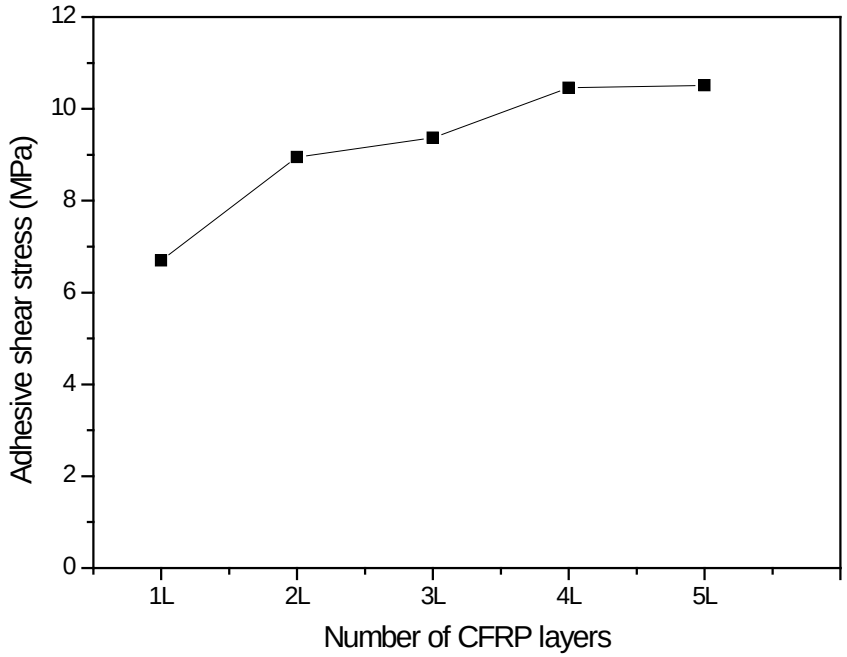

Figure 5.20: Effect of number of CFRP layers on adhesive stress

FE models were used to obtain CFRP stresses at failure. Figure 5.21 shows the CFRP composite stress variation with the number of CFRP layers. 1LCF model

shows the highest stress of 358 MPa at failure, and a decrement of the composite stress was observed when using multi-layer CFRP systems. Composite stresses decreased to 279 MPa when using two layers of CFRP. It further decreased to 219 MPa with three layers of CFRP. No further significant stress reduction was observed in the FE models 4LCF and 5LCF which were developed with four and five CFRP layers respectively. This result suggests that maximum joint capacity can be achieved using three CFRP layers. Further installation of CFRP layers will not help to increase the load carrying capacity of double-strap joints.

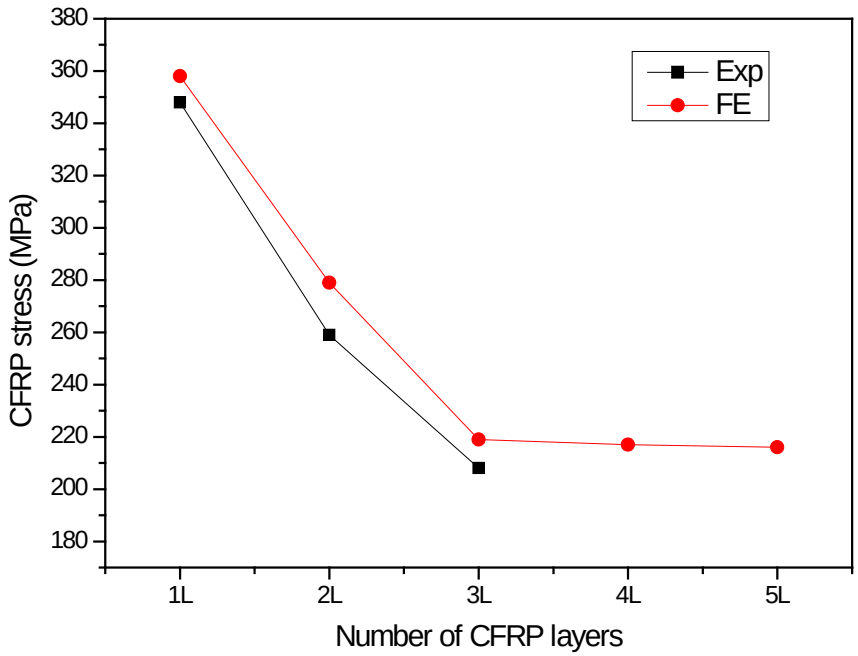

Figure 5.21: Variation of CFRP composite stress at failure with number of CFRP layers

5.5.3 Effect of CFRP degradation

Validated FE models were used to investigate the effect of CFRP degradation levels on the structural behaviour of CFRP-steel double-strap joints. Figure 5.22 shows the variation of CFRP stress with CFRP degradation level. It can be seen that the CFRP stress remains constant up to 50% degradation level. Once it exceeds 50%

of degradation, CFRP stress at failure decreases significantly with increased CFRP degradation level. The results show that this behaviour is common for one-layer CFRP-steel double-strap joints as well as multi-layer CFRP-steel double-strap joints.

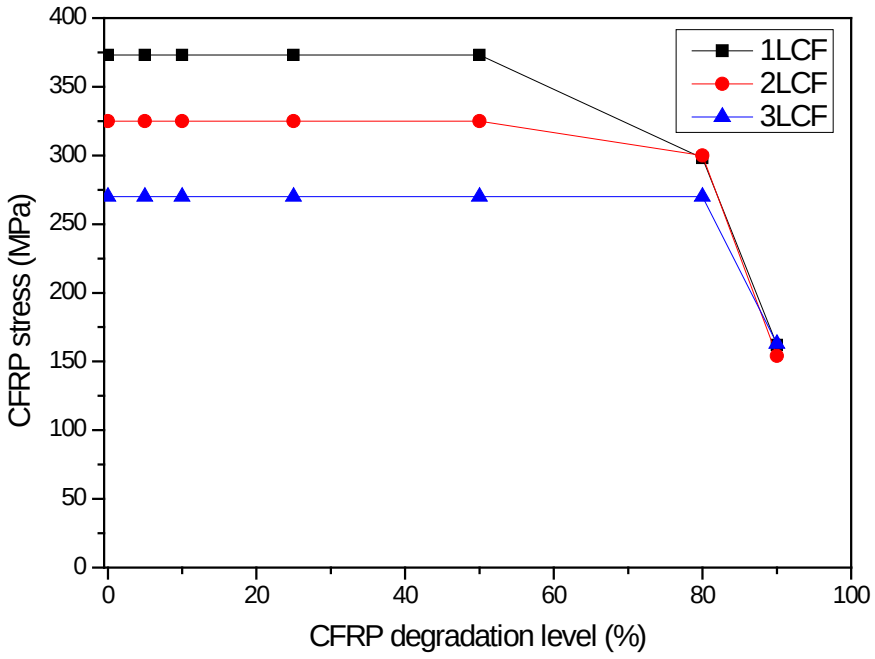

Figure 5.22: CFRP composite stress at failure for different CFRP degradation levels

Figure 5.23 shows the effect of adhesive stress at failure for different CFRP degradation levels. Adhesive stress at failure remains constant with the increase of CFRP degradation level up to 50% CFRP material degradation. After that, a slight increment of adhesive failure stress is observed. This type of stress increment is attributed to the CFRP failure at that particular degradation level. Once the CFRP material fails, the resultant stresses transfer to the adjacent adhesive layer, resulting in a slight increment in the adhesive stress. However, the adhesive stresses remain very close to the failure stress at 80% CFRP degradation. Beyond 80% CFRP material degradation, the adhesive layer shows a lower stress value. This reduction of adhesive stress occurs because of the CFRP fibre failure at a lower stress due to the

high level of CFRP degradation. The adhesive stresses at failure are directly attributed to the reduction in the joint capacities.

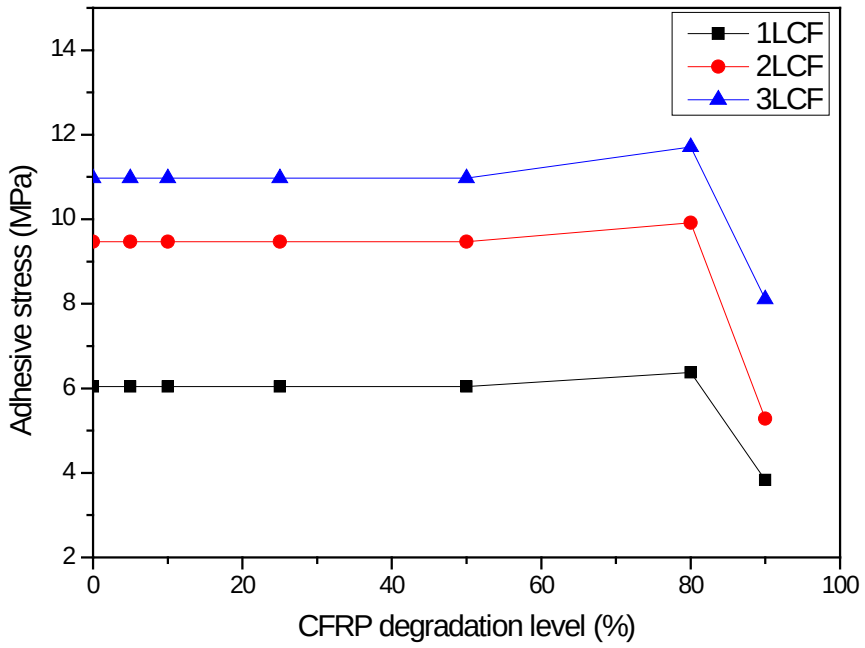

Figure 5.23: Adhesive stress at failure for different CFRP degradation levels

5.5.4 Bond lengths for different CFRP degradation levels

The variation of joint capacity with various bond lengths is shown in Figures 5.24 to 5.26. Results show that the effective bond length is 80 mm for single layer CFRP-steel double-strap joints under ambient conditions. A constant joint capacity was achieved with increased bond lengths beyond 80 mm. Double-strap joint models showed a reduction in the joint capacity beyond 50% CFRP degradation level. However, the effective bond lengths were not affected by the amount of CFRP degradation. The effective bond length was found to be around 100 mm for both two- and three-layers CFRP-steel double-strap joints.

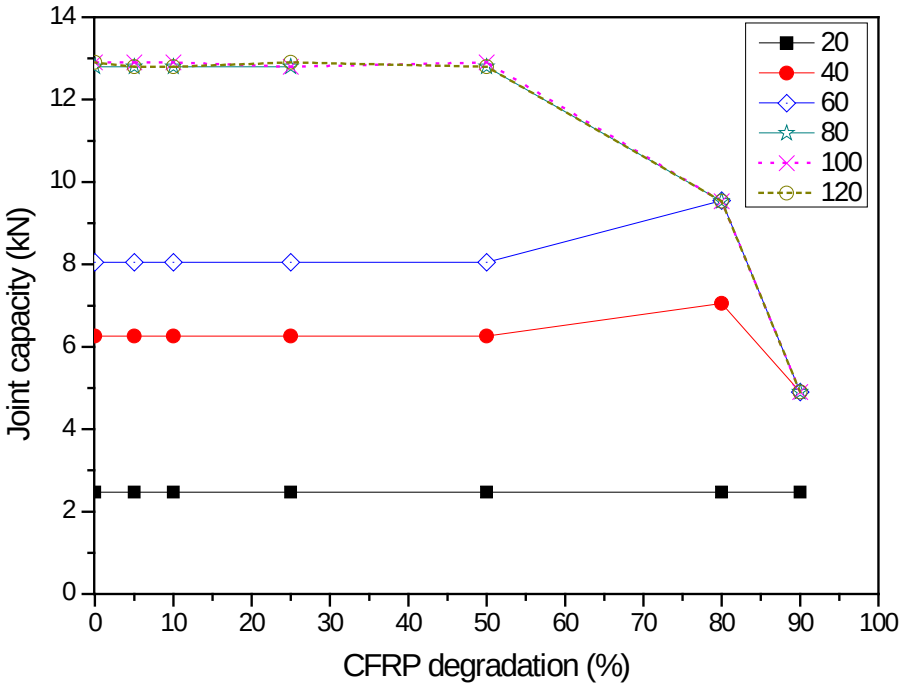

Figure 5.24: Effect of CFRP degradation level on joint capacity – 1LCF

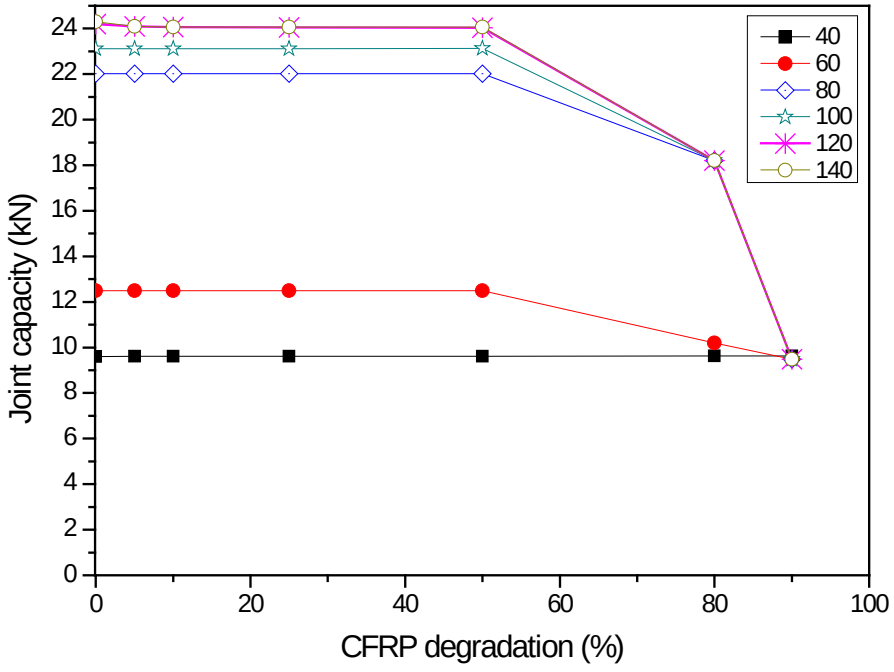

Figure 5.25: Effect of CFRP degradation level on joint capacity – 2LCF

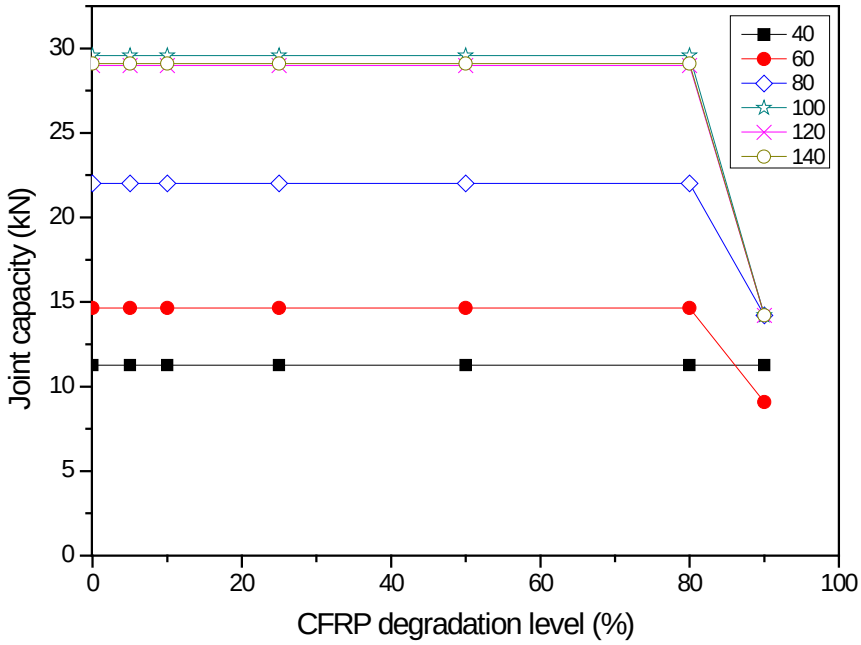

Figure 5.26: Effect of CFRP degradation level on joint capacity – 3LCF

5.5.5 Effect of adhesive degradation

Various adhesive degradation levels were simulated using the established models to investigate the effects of adhesive degradation levels on CFRP-steel double-strap joints. Figure 5.27 shows the variation of joint capacity with adhesive degradation. It can be observed that the joint capacity is greatly highly dependent on the adhesive strength. Greater adhesive strength can result in higher joint capacities. The 1LCF, 2LCF and 3LCF models show that the joint capacity reduces gradually with increased adhesive degradation level. Figure 5.28 shows the adhesive stress at failure with different adhesive degradation levels. Adhesive stress at joint failure shows a reduction with increased adhesive degradation level. This result explains the cause of the joint capacity reduction illustrated in Figure 5.27.

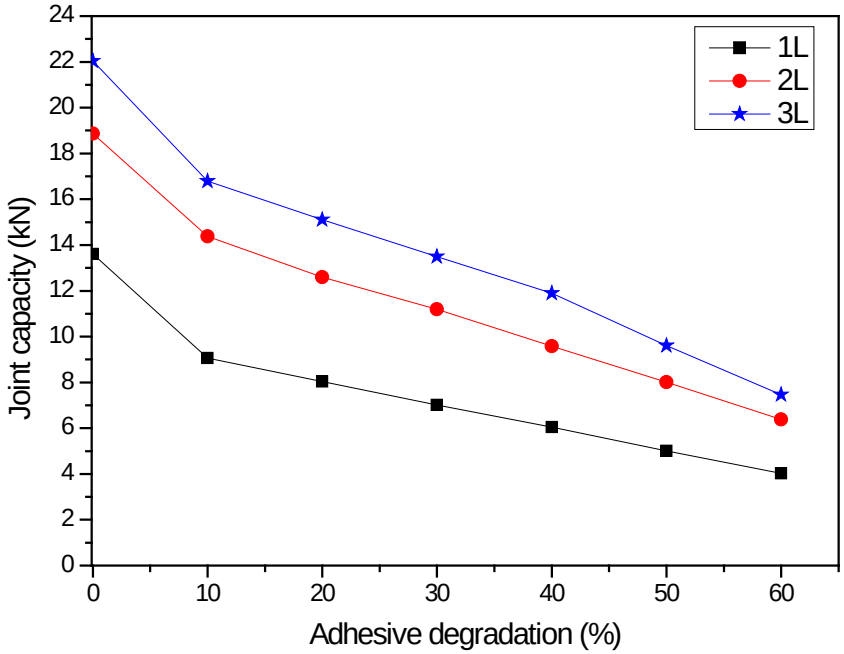

Figure 5.27: Effect of adhesive degradation level on joint capacity

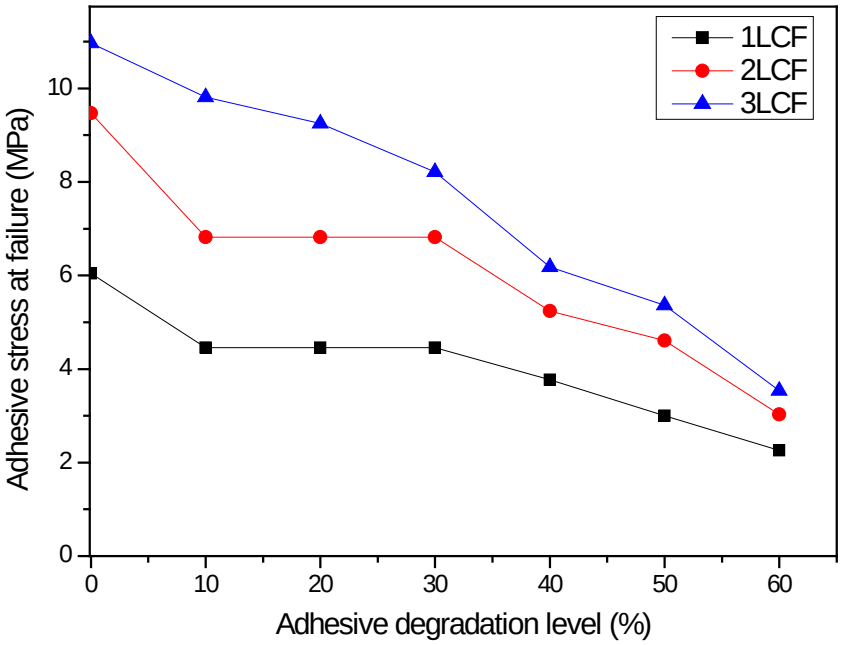

Figure 5.28: Variation of adhesive stress at failure for different adhesive degradation levels

5.6 CHAPTER SUMMARY

This chapter has presented the details of the developed finite element models and their validation, followed by a comprehensive parametric study. FE results were compared with the experimental data and found to be in good agreement. Adhesive-CFRP interface failure and CFRP failure modes were successfully modelled.

The validated models were used to evaluate the effect of relevant parameters on the structural behaviour of CFRP-steel double-strap joints. The key response parameters were (i) joint capacity, (ii) CFRP composite stress at failure and (iii) adhesive stress at failure. The structural behaviour of CFRP-steel double-strap joints subjected to accelerated environmental conditions was studied by varying the relevant input parameters. The effects of (i) number of CFRP layers, (ii) bond length for different degradation levels, (iii) CFRP degradation level and (iv) adhesive degradation level were evaluated.

Chapter 6: Conclusions and Recommendations for Future Research

6.1 SUMMARY OF RESEARCH

This thesis has reported the results of a durability study of CFRP-strengthened steel structures under accelerated environmental conditions. The experimental program consisted of three test series. The first and the second series studied the bond properties and associated failure modes of CFRP-steel double-strap joints under accelerated environmental conditions. Based on the results of the first two test series, finite element models were developed and validated. The validated models were then used to carry out a comprehensive parametric study to evaluate the effects of bond-related properties which affect the long-term durability of CFRP-steel bonded joints. The third test series evaluated the effectiveness of CFRP-strengthened beams under accelerated environmental conditions and the associated failure modes.

The main contribution of this thesis is the addition of new knowledge to the field of strengthening systems related to durability of CFRP-steel systems. Investigated bond properties and associated failure modes of degraded composite systems using CFRP-steel double strap joints/universal beam specimens showed that there can be significant difference in the bond properties and failure modes compared with those at ambient environmental conditions. Identified failure modes and bond properties can be used to asses and predict the structural behaviour of degraded CFRP-steel strengthening systems. Developed shear stress-slip models will help in the understanding of the structural behaviour of degraded CFRP-steel composite systems. Developed FE models can be effectively used to study the structural

behaviour of degraded CFRP-steel strengthening systems. Carried out parametric study using FE models evaluated the effects of critical parameters on the structural behaviour of degraded CFRP-steel composite systems.

6.2 CONCLUSIONS

Based on the results of the experimental program and FE modelling, the following conclusions are drawn:

1. Sandblasting is the most efficient and economical surface preparation method for an adhesively-bonded CFRP-steel surface considering the load-carrying capacity under tensile loading. Aluminium grit-blasting slightly enhances the performance of the CFRP-steel interface compared to sandblasting. Optimum bond performance cannot be achieved using mechanical grinding as a surface preparation method.

2. The application of a primer coat prior to installation of CFRP systems improves the bond properties of adhesively-bonded CFRP-steel joints leading to enhancement of the load-carrying capacity. Inspection of the failure surface showed no corrosion activity within the steel surface. In the long term, a primer layer is capable of delaying the damage initiation of CFRP-bonded joints under marine environmental conditions by acting as a barrier to protect the bonded steel surface from moisture ingress.

3. The stiffness and strength of adhesively-bonded CFRP-steel double-strap joints are significantly affected by the simulated marine environmental conditions. Reduction in the stiffness does not depend on the exposure duration. On the contrary, the joint strength is significantly

dependent on the exposure duration. The reduction in stiffness of one- and two-layered CFRP-steel double-strap joints was 32% after three days of exposure to the accelerated environmental conditions and 20% for joints fabricated with three CFRP layers. The reductions in stiffness and strength were primarily due to deterioration of the CFRP composite layer as a result of moisture ingress and CFRP material deterioration.

4. Three types of failure mode were observed in the tested CFRP-steel double strap specimens: (i) steel-adhesive interface debonding, (ii) CFRP fibre rupture and (iii) mixed mode failure (a combination of (i) and (ii)). The failure modes and failure loads are significantly dependent on the CFRP deterioration level. A large amount of CFRP deterioration can lead to a lower load carrying capacity of CFRP-steel double-strap joints undergoing CFRP rupture failure.

5. Embedded GFRP layers enhance the durability of a composite system. However, the comparison of joint strengths showed that optimum structural performance cannot be achieved using embedded GFRP layers in CFRP-steel composite systems. Analysis of the GFRP-steel bonded interface showed lower bond strength compared to the CFRP-steel bonded interface under ambient conditions and this lower bond strength leads to the lower load-carrying capacity of double-strap joints with an embedded GFRP layer.

6. Multi-layer CFRP systems effectively improve structural performance as well as the durability of CFRP-steel strengthened double strap-joints. The bond properties are governed by the innermost CFRP layer. In a multi-layer system, the inner fibres are protected by the outer CFRP

layers. Therefore, additional CFRP layers are effective in a multi-layer composite CFRP-steel strengthening system. Three-layer CFRP double-strap joints show the optimum load-carrying capacity, and the installation of further CFRP layers does not increase the load carrying capacity of CFRP-steel double-strap joints. Analysis of adhesive stress levels showed that they reached the maximum limit with this CFRP configuration. As a result, the joint capacities were not significantly affected by additional CFRP layers beyond the first three layers.

7. Effective bond lengths were found to be 80 mm and 100 mm for single-layer and multi-layer degraded CFRP-steel double-strap joints respectively. Single-layer CFRP-steel double-strap joints showed CFRP rupture failure beyond 80 mm bond lengths, indicating that CFRP material degradation can be significant in single-layer CFRP-steel systems. Two-layer CFRP-steel double-strap joints showed steel-adhesive interface debonding beyond 100 mm bond lengths, confirming that multi-layer CFRP systems can delay damage initiation under accelerated environmental conditions.

8. The effect of CFRP material degradation on joint capacities was not prominent up to 50% CFRP material degradation. Significant reductions of joint capacities were observed beyond 50% CFRP material degradation, resulting in CFRP rupture failure. Joint capacities significantly depended on the adhesive degradation levels. Lower adhesive strengths resulted in lower joint capacities of CFRP-steel double-strap joints undergoing debonding failure.

9. CFRP-steel double-strap joints showed a reduction in load-carrying capacity after exposure to simulated marine environmental conditions. Analysis of the shear stress-slip relationships of degraded CFRP-steel double-strap joints showed a reduction in peak shear stress compared to that under ambient conditions. CFRP composite material degradation significantly affected the shear stress-slip behaviour of CFRP-steel double-strap joints. The shear stress-slip response was approximated by a bi-linear bond-slip model.

10. The failure load of CFRP-strengthened beams after exposure to accelerated environmental conditions showed a reduction in load-carrying capacity. Inspection of the exposed CFRP surface showed significant colour change and softening of outer fibres, indicating CFRP deterioration. The observed CFRP deterioration level did not have a significant effect on the failure modes of the beams, which was lateral torsional buckling.

6.3 FUTURE RESEARCH

Although the work presented in this thesis has addressed a wide range of parameters related to the durability of CFRP-steel composite systems, further research is needed to quantify the effects of environmental conditions on the durability of CFRP-steel strengthening systems. Accelerated environmental tests are widely used to evaluate the long-term durability of CFRP-steel composite strengthening systems. This research has shown that CFRP composite material may undergo severe deterioration under accelerated environmental conditions. The bond properties are significantly affected by the accelerated environmental conditions, leading to lower load-carrying capacity and change in the failure modes. Future

research should focus on the durability of CFRP-steel composite systems to quantify the deterioration of CFRP material during the design life of strengthening systems. The following topics are recommended for future research:

- Durability performance and structural behaviour of CFRP-strengthened steel beams and investigation of the associated failure modes.
- Durability performance and structural behaviour of CFRP-strengthened axially-loaded steel columns and investigation of the associated failure modes.
- Effect of localised material degradation on the structural behaviour of CFRP-steel composite systems and evaluation of associated failure modes.
- Development and validation of theoretical models to predict the deterioration of CFRP-steel strengthening systems under different environmental conditions.
- Structural behaviour of degraded CFRP-steel composite systems and failure modes under dynamic loading conditions.
- Effects of sustained load levels on the structural behaviour of degraded CFRP-steel composite systems.

Bibliography

[1] Guidelines for the Design and Construction of Externally Bonded FRP Systems for Strengthening Existing Structures - Metallic structures. CNR-DT 202/2005. Rome: National Research Council; 2005.
[2] Seica MV, Packer JA. FRP materials for the rehabilitation of tubular steel structures, for underwater applications. Composite Structures. 2007;80:440-50.
[3] Schnerch D, Dawood M, Rizkalla S, Sumner E, Stanford K. Bond Behavior of CFRP Strengthened Steel Structures. Advances in Structural Engineering. 2006;9:805-17.
[4] Schnerch D, Dawood M, Rizkalla S, Sumner E. Proposed design guidelines for strengthening of steel bridges with FRP materials. Construction and Building Materials. 2007;21:1001-10.
[5] Fawzia S, Al-Mahaidi R, Zhao XL, Rizkalla S. Strengthening of circular hollow steel tubular sections using high modulus CFRP sheets. Construction and Building Materials. 2007;21:839-45.
[6] Kabir MH, Fawzia S, Chan THT, Gamage JCPH, Bai JB. Experimental and numerical investigation of the behaviour of CFRP strengthened CHS beams subjected to bending. Engineering Structures. 2016;113:160-73.
[7] Shamsuddoha M, Islam MM, Aravinthan T, Manalo A, Lau K-t. Effectiveness of using fibre-reinforced polymer composites for underwater steel pipeline repairs. Composite Structures. 2013;100:40-54.
[8] Mandel M, Krüger L. Electrochemical corrosion studies and pitting corrosion sensitivity of a self-pierce rivet joint of carbon fibre reinforced polymer (CFRP) - laminate and EN AW-6060-T6. Materialwissenschaft und Werkstofftechnik. 2012;43:302-9.
[9] Kim YJ, Bumadian I, Park J-S. Galvanic Current Influencing Interface Deterioration of CFRP Bonded to a Steel Substrate. Journal of Materials in Civil Engineering. 2016;28:04015129.
[10] Gholami M, Sam ARM, Yatim JM, Tahir MM. A review on steel/CFRP strengthening systems focusing environmental performance. Construction and Building Materials. 2013;47:301-10.
[11] Kabir MH, Fawzia S, Chan THT, Badawi M. Durability of CFRP strengthened steel circular hollow section member exposed to sea water. Construction and Building Materials. 2016;118:216-25.
[12] Kabir MH, Fawzia S, Chan TH, Gamage J. Durability performance of carbon fibre-reinforced polymer strengthened circular hollow steel members under cold weather. Australian Journal of Structural Engineering. 2014;15:377-92.
[13] Borrie D, Liu HB, Zhao XL, Raman RKS, Bai Y. Bond durability of fatigued CFRP-steel double-lap joints pre-exposed to marine environment. Composite Structures. 2015;131:799-809.
[14] Zhu J-H, Wei L, Wang Z, Liang CK, Fang Y, Xing F. Application of carbon-fiber-reinforced polymer anode in electrochemical chloride extraction of steel-reinforced concrete. Construction and Building Materials. 2016;120:275-83.
[15] Lambert P, Van Nguyen C, Mangat PS, O'Flaherty FJ, Jones G. Dual function carbon fibre fabric strengthening and impressed current cathodic protection (ICCP) anode for reinforced concrete structures. Materials and Structures. 2014;48:2157-67.

[16] Marouani S, Curtil L, Hamelin P. Ageing of carbon/epoxy and carbon/vinylester composites used in the reinforcement and/or the repair of civil engineering structures. Composites Part B: Engineering. 2012;43:2020-30.
[17] Alam MI, Fawzia S, Liu X. Effect of bond length on the behaviour of CFRP strengthened concrete-filled steel tubes under transverse impact. Composite Structures. 2015;132:898-914.
[18] Alam MI, Fawzia S. Numerical studies on CFRP strengthened steel columns under transverse impact. Composite Structures. 2015;120:428-41.
[19] Nguyen T-C, Bai Y, Zhao X-L, Al-Mahaidi R. Durability of steel/CFRP double strap joints exposed to sea water, cyclic temperature and humidity. Composite Structures. 2012;94:1834-45.
[20] Sugiman S, Crocombe AD, Aschroft IA. Experimental and numerical investigation of the static response of environmentally aged adhesively bonded joints. International Journal of Adhesion and Adhesives. 2013;40:224-37.
[21] Kabir MH, Fawzia S, Chan THT, Gamage JCPH. Comparative durability study of CFRP strengthened tubular steel members under cold weather. Materials and Structures. 2016;49:1761-74.
[22] Dawood M. Durability of steel components strengthened with fiber-reinforced polymer (FRP) composites. In: Karbhari VM, editor. Rehabilitation of Metallic Civil Infrastructure using Fiber-reinforced Polymer (FRP) Composites: Woodhead Publishing Limited; 2014. p. 96-114.
[23] Nguyen T-C, Bai Y, Zhao X-L, Al-Mahaidi R. Mechanical characterization of steel/CFRP double strap joints at elevated temperatures. Composite Structures. 2011;93:1604-12.
[24] Karbhari VM, Ghosh K. Comparative durability evaluation of ambient temperature cured externally bonded CFRP and GFRP composite systems for repair of bridges. Composites Part A: Applied Science and Manufacturing. 2009;40:1353-63.
[25] Silva MAG, Biscaia HC, Marreiros R. Bond–slip on CFRP/GFRP-to-concrete joints subjected to moisture, salt fog and temperature cycles. Composites Part B: Engineering. 2013;55:374-85.
[26] Böer P, Holliday L, Kang THK. Independent environmental effects on durability of fiber-reinforced polymer wraps in civil applications: A review. Construction and Building Materials. 2013;48:360-70.
[27] Dawood M, Rizkalla S. Environmental durability of a CFRP system for strengthening steel structures. Construction and Building Materials. 2010;24:1682-9.
[28] Lai WL, Kou SC, Poon CS, Tsang WF, Lee KK. A durability study of externally bonded FRP-concrete beams via full-field infrared thermography (IRT) and quasi-static shear test. Construction and Building Materials. 2013;40:481-91.
[29] Sen R. Developments in the durability of FRP-concrete bond. Construction and Building Materials. 2015;78:112-25.
[30] Karagah H, Shi C, Dawood M, Belarbi A. Experimental investigation of short steel columns with localized corrosion. Thin-Walled Structures. 2015;87:191-9.
[31] Chung L, Jay Kim J-H, Yi S-T. Bond strength prediction for reinforced concrete members with highly corroded reinforcing bars. Cement and Concrete Composites. 2008;30:603-11.
[32] Fang C, Lundgren K, Chen L, Zhu C. Corrosion influence on bond in reinforced concrete. Cement and Concrete Research. 2004;34:2159-67.

[33] Arronche L, Gordon K, Ryu D, La Saponara V, Cheng L. Investigation of galvanic corrosion between AISI 1018 carbon steel and CFRPs modified with multi-walled carbon nanotubes. Journal of Materials Science. 2012;48:1315-23.
[34] Kabir MH, Fawzia S, Chan THT, Badawi M. Numerical studies on CFRP strengthened steel circular members under marine environment. Materials and Structures. 2016;49:4201-16.
[35] Kabir MH, Fawzia S, Chan THT. Durability of CFRP strengthened circular hollow steel members under cold weather: Experimental and numerical investigation. Construction and Building Materials. 2016;123:372-83.
[36] Yu T, Fernando D, Teng JG, Zhao XL. Experimental study on CFRP-to-steel bonded interfaces. Composites Part B: Engineering. 2012;43:2279-89.
[37] Wu C, Zhao X, Hui Duan W, Al-Mahaidi R. Bond characteristics between ultra high modulus CFRP laminates and steel. Thin-Walled Structures. 2012;51:147-57.
[38] Fawzia S, Zhao X-L, Al-Mahaidi R. Bond–slip models for double strap joints strengthened by CFRP. Composite Structures. 2010;92:2137-45.
[39] Fawzia S, Al-Mahaidi R, Zhao X-L. Experimental and finite element analysis of a double strap joint between steel plates and normal modulus CFRP. Composite Structures. 2006;75:156-62.
[40] Fawzia S. Evaluation of shear stress and slip relationship of composite lap joints. Composite Structures. 2013;100:548-53.
[41] Mojarrad P. Composites australia and CRC-ACS conference. 2015.
[42] Mojarrad P. Bridge rehabilitation using frp- case studies. 2015.
[43] Al-Zubaidy H, Zhao X-L, Al-Mahaidi R. Mechanical characterisation of the dynamic tensile properties of CFRP sheet and adhesive at medium strain rates. Composite Structures. 2013;96:153-64.
[44] FRP reinforcement in RC structures, Technical report on the Design and use of fiber reniforced polymer rinforcement (FRP) in rinforced concrete structures Task group-9.3. Lausanne, Switzerland2006.
[45] Nozaka K, Shield CK, Hajjar JF. Effective bond length of carbon-fiber-reinforced polymer strips bonded to fatigued steel bridge I-girders. Journal of Bridge Engineering. 2005;10:11.
[46] Fawzia S, Zhao XL, Al-Mahaidi R, Rizkalla S. Bond characteristics between CFRP and steel plates in double strap joints. The International Journal of Advanced Steel Construction. 2005;1:17-27.
[47] Kim YJ, Bumadian I. Electrochemical reactions for steel beams strengthened with CFRP sheets. Engineering Structures. 2016;125:471-80.
[48] Fernando D, Teng JG, Yu T, Zhao XL. Preparation and Characterization of Steel Surfaces for Adhesive Bonding. Journal of Composites for Construction. 2013;17.
[49] Amada S, Satoh A. Fractal analysis of surfaces roughened by grit blasting. Journal of Adhesion Science and Technology. 2000;14:27-41.
[50] Harris AF, Beevers A. The effects of grit-blasting on surface properties for adhesion. International Journal of Adhesion and Adhesives. 1999;19:445-52.
[51] Photiou NK, Hollaway LC, Chryssanthopoulos MK. Selection of carbon-fiber-reinforced polymer systems for steelwork upgrading. Journal of Materials in Civil Engineering. 2006;18:641-9.
[52] ASTM D5573-99(2012), Standard Practice for Classifying Failure Modes in Fiber-Reinforced-Plastic (FRP) Joints. D5573. West Conshohocken, PA: ASTM International; 2012.

[53] Han Q, Wang L, Xu J. Experimental research on fracture behaviors of damaged CFRP tendons: Fracture mode and failure analysis. Construction and Building Materials. 2016;112:1013-24.
[54] Bremont M, Brockmann W, Guimon MF, Pfisterguillouzo G. Improvement of the Durability of Zinc-Coated Steel Epoxy Bonded Joints. Journal of Adhesion. 1993;41:147-68.
[55] Dillingham G. Chapter 10 - Priming to improve adhesion A2 - Chaudhury, M. In: Pocius AV, editor. Adhesion Science and Engineering. Amsterdam: Elsevier Science B.V.; 2002. p. 433-64.
[56] da Silva LFM, Banea MD. Adhesively bonded joints in composite materials: an overview. Proceedings of the Institution of Mechanical Engineers, Part L: Journal of Materials: Design and Applications. 2009;223:1-18.
[57] Molitor P, Barron V, Young T. Surface treatment of titanium for adhesive bonding to polymer composites: a review. International Journal of Adhesion and Adhesives. 2001;21:129-36.
[58] Marsh J, Scantlebury JD, Lyon SB. The effect of surface/primer treatments on the performance of alkyd coated steel. Corrosion Science. 2001;43:829-52.
[59] Miller TC, Chajes MJ, Mertz DR, Hastings JN. Strengthening of a steel bridge girder using cfrp plates. Journal of Bridge Engineering. 2001;6:514-22.
[60] Buyukozturk O, Gunes O, Karaca E. Progress on understanding debonding problems in reinforced concrete and steel members strengthened using FRP composites. Construction and Building Materials. 2004;18:9-19.
[61] Xia SH, Teng JG. Behaviour of frp-to-steel bonded joints. Proceedings of the International Symposium on Bond Behaviour of FRP in Structures (BBFS 2005). Hong Kong, China2005. p. 419-26.
[62] Peng FM, Zhang N, Yang YX, Yue QR. Experimental and finite element studies on deteriorated steel members repaired with CFRP sheets. FRP Composites in Civil Engineering - CICE 2004: Taylor & Francis; 2004. p. 121-6.
[63] Colombi P, Panzeri N, Poggi C. EXPERIMENTAL CHARACTERIZATION OF STEEL ELEMENTS REINFORCED BY ADHESIVELY BONDED CFRP PLATES. Advanced Polymer Composites for Structural Applications in Construction: Woodhead Publishing; 2004. p. 245-57.
[64] Colombi P, Poggi C. An experimental, analytical and numerical study of the static behavior of steel beams reinforced by pultruded CFRP strips. Composites Part B: Engineering. 2006;37:64-73.
[65] Hollaway LC, Zhang L, Photiou NK, Teng JG, Zhang SS. Advances in adhesive joining of carbon fibre/polymer composites to steel members for repair and rehabilitation of bridge structures. Advances in Structural Engineering. 2006;9:791-803.
[66] Deng J, Lee MMK. Behaviour under static loading of metallic beams reinforced with a bonded CFRP plate. Composite Structures. 2007;78:232-42.
[67] Linghoff D, Haghani R, Al-Emrani M. Carbon-fibre composites for strengthening steel structures. Thin-Walled Structures. 2009;47:1048-58.
[68] Al-Mosawe A, Al-Mahaidi R, Zhao X-L. Effect of CFRP properties, on the bond characteristics between steel and CFRP laminate under quasi-static loading. Construction and Building Materials. 2015;98:489-501.
[69] Pham HB, Al-Mahaidi R. Modelling of CFRP-concrete shear-lap tests. Construction and Building Materials. 2007;21:727-35.
[70] Tavakkolizadeh M, Saadatmanesh H. Environmental effects on tensile properties of frp laminates made using wet-lay-up method. Advanced Polymer

Composites for Structural Applications in Construction: Woodhead Publishing; 2004. p. 619-32.
[71] Pizzi A, Mittal KL. Handbook of adhesive technology. New York: Marcel Dekker, 2003.
[72] Bowditch MR. The durability of adhesive joints in the presence of water. International Journal of Adhesion and Adhesives. 1996;16:73-9.
[73] Kafodya I, Xian G, Li H. Durability study of pultruded CFRP plates immersed in water and seawater under sustained bending: Water uptake and effects on the mechanical properties. Composites Part B: Engineering. 2015;70:138-48.
[74] Karbhari VM, Chin JW, Hunston D, Benmokrane B, Juska T, Morgan R, et al. Durability Gap Analysis for Fiber-Reinforced Polymer Composites in Civil Infrastructure. Journal of Composites for Construction. 2003;7:238-47.
[75] Agarwal A, Foster SJ, Hamed E. Testing of new adhesive and CFRP laminate for steel-CFRP joints under sustained loading and temperature cycles. Composites Part B: Engineering. 2016;99:235-47.
[76] Al-Shawaf A, Al-Mahaidi R, Zhao XL. Effect of Elevated Temperature on Bond Behaviour of High Modulus CFRP/Steel Double-Strap Joints. Australian Journal of Structural Engineering. 2009;10:63-74.
[77] Al-Shawaf A. Influence of fibres' stiffness on wet lay-up CFRP/steel joints' behaviour under subzero exposures. Composites Part B: Engineering. 2015;73:61-71.
[78] Chin JW, Nguyen T, Aouadi K. Effects of environmental exposure on fibre-reinforced plastic (FRP) materials used in construction. Journal of Composites Technology and Research. 1997;19:205-13.
[79] Feldman D. Polymer Weathering: Photo-Oxidation. Journal of Polymers and the Environment. 2002;10:163-73.
[80] Pang S-S, Li G, Helms JE, Ibekwe SI. Influence of ultraviolet radiation on the low velocity impact response of laminated beams. Composites Part B: Engineering. 2001;32:521-8.
[81] Hollaway LC. A review of the present and future utilisation of FRP composites in the civil infrastructure with reference to their important in-service properties. Construction and Building Materials. 2010;24:2419-45.
[82] Lopez JL, Sain M, Cooper P. Performance of natural-fiber–plastic composites under stress for outdoor applications: Effect of moisture, temperature, and ultraviolet light exposure. Journal of Applied Polymer Science. 2006;99:2570-7.
[83] Liau WB, Tseng FP. The effect of long-term ultraviolet light irradiation on polymer matrix composites. Polymer Composites. 1998;19:440-5.
[84] Nguyen T-C, Bai Y, Zhao X-L, Al-Mahaidi R. Effects of ultraviolet radiation and associated elevated temperature on mechanical performance of steel/CFRP double strap joints. Composite Structures. 2012;94:3563-73.
[85] Tavakkolizadeh M, Saadatmanesh H. Galvanic Corrosion of Carbon and Steel in Aggressive Environments. Journal of Composites for Construction. 2001;5:11.
[86] Santos TFA, Vasconcelos GC, de Souza WA, Costa ML, Botelho EC. Suitability of carbon fiber-reinforced polymers as power cable cores: Galvanic corrosion and thermal stability evaluation. Materials & Design. 2015;65:780-8.
[87] Sun H, Wei L, Zhu M, Han N, Zhu J-H, Xing F. Corrosion behavior of carbon fiber reinforced polymer anode in simulated impressed current cathodic protection system with 3% NaCl solution. Construction and Building Materials. 2016;112:538-46.

[88] Bai Y, Keller T. Effects of thermal loading history on structural adhesive modulus across glass transition. Construction and Building Materials. 2011;25:2162-8.
[89] Hart-Smith LJ. Adhesive-Bonded Double-Lap Joints, Technical Report NASA CR-112235. Douglas Aircraft Company, Long Beach, California, USA1973.
[90] Guide for the Design and Construction of Externally Bonded FRP Systems for Strengthening Concrete Structures. ACI 4402R-08. Farmington Hills, MI 48331: American Concrete Institute; 2008.
[91] TR55 Design guidance for strengthening concrete structures using fibre composite materials. Crowthorne, UK: The Concrete Society; 2000.
[92] Hollaway LC, Teng JG. Strengthening and rehabilitation of civil infrastructures using fibre-reinforced polymer (FRP) composites. Cambridge, UK: Woodhead Publishing/CRC Press, 2008.
[93] da Silva LFM, Campilho RDSG. Advances in Numerical Modelling of Adhesive Joints. 2012:1-93.
[94] Al-Zubaidy H, Al-Mahaidi R, Zhao X-L. Finite element modelling of CFRP/steel double strap joints subjected to dynamic tensile loadings. Composite Structures. 2013;99:48-61.
[95] Campilho RDSG, Banea MD, Neto JABP, da Silva LFM. Modelling adhesive joints with cohesive zone models: effect of the cohesive law shape of the adhesive layer. International Journal of Adhesion and Adhesives. 2013;44:48-56.
[96] Fernando D. Finite element analysis of debonding failures in CFRP-strengthene: University of Wollongong, 2012.
[97] Sugiman S, Crocombe AD, Aschroft IA. Modelling the static response of unaged adhesively bonded structures. Engineering Fracture Mechanics. 2013;98:296-314.
[98] Teng JG, Fernando D, Yu T. Finite element modelling of debonding failures in steel beams flexurally strengthened with CFRP laminates. Engineering Structures. 2015;86:213-24.
[99] ASTM E8 / E8M-16a. Standard Test Methods for Tension Testing of Metallic Materials. ASTM International: West Conshohocken; 2016.
[100] ASTM D3039 / D3039M-14. Standard Test Method for Tensile Properties of Polymer Matrix Composite Materials. ASTM International: West Conshohocken; 2014.
[101] Tamer A. El Maaddawy, Soudki KA. Effectiveness of Impressed Current Technique to Simulate Corrosion of Steel Reinforcement in Concrete. Journal of Materials in Civil Engineering. 2003;15:41-7.
[102] Nguyen T-C, Bai Y, Zhao X-L, Al-Mahaidi R. Curing effects on steel/CFRP double strap joints under combined mechanical load, temperature and humidity. Construction and Building Materials. 2013;40:899-907.
[103] Lee HK, Pyo SH, Kim BR. On joint strengths, peel stresses and failure modes in adhesively bonded double-strap and supported single-lap GFRP joints. Composite Structures. 2009;87:44-54.
[104] da Costa Mattos HS, Monteiro AH, Palazzetti R. Failure analysis of adhesively bonded joints in composite materials. Materials & Design. 2012;33:242-7.
[105] He J, Xian G. Debonding of CFRP-to-steel joints with CFRP delamination. Composite Structures. 2016;153:12-20.
[106] Zou GP, Shahin K, Taheri F. An analytical solution for the analysis of symmetric composite adhesively bonded joints. Composite Structures. 2004;65:499-510.

[107] Bocciarelli M, Colombi P. Elasto-plastic debonding strength of tensile steel/CFRP joints. Engineering Fracture Mechanics. 2012;85:59-72.
[108] Ghafoori E, Motavalli M. Lateral-torsional buckling of steel I-beams retrofitted by bonded and un-bonded CFRP laminates with different pre-stress levels: Experimental and numerical study. Construction and Building Materials. 2015;76:194-206.
[109] Dahmani L, Boudjemia A. Lateral Torsional Buckling Response of Steel Beam with Different Boundary Conditions and Loading. Strength of Materials. 2014;46:429-32.
[110] Abaqus/CAE. 6.14-2 ed. Dassault Systemes Simulia Corp., Providence, RI, USA2014.
[111] K. Galal. Flexural Performance of Steel Girders Retrofitted Using CFRP Materials. 2012.
[112] Penagos-Sanchéz DM, Légeron F, Demers M, Langlois S. Strengthening of the Net Section of Steel Elements under Tensile Loads with Bonded CFRP Strips. Journal of Composites for Construction. 2015:04015007.
[113] ABAQUS. Abaqus user's manuals. Dassault Systèmes Simulia Corp., Providence, RI, USA2011.
[114] Hashin Z, Rotem A. A fatigue failure criterian for fiber reinforced materials. Journal of composite Materials. 1973;7:448-64.
[115] Hashin Z. Failure Criteria for Unidirectional Fiber Composites. Journal of Applied Mechanics. 1980;47:329-34.
[116] Batuwitage C, Fawzia S, Thambiratnam D, Al-Mahaidi R. Durability of CFRP strengthened steel plate double-strap joints in accelerated corrosion environments. Composite Structures. 2017;160:1287-98.

Appendices

Appendix A

CFRP strengthening procedure

Figure A1: Sandblasted specimens cleaned with acetone

Figure A2: Application of primer coat

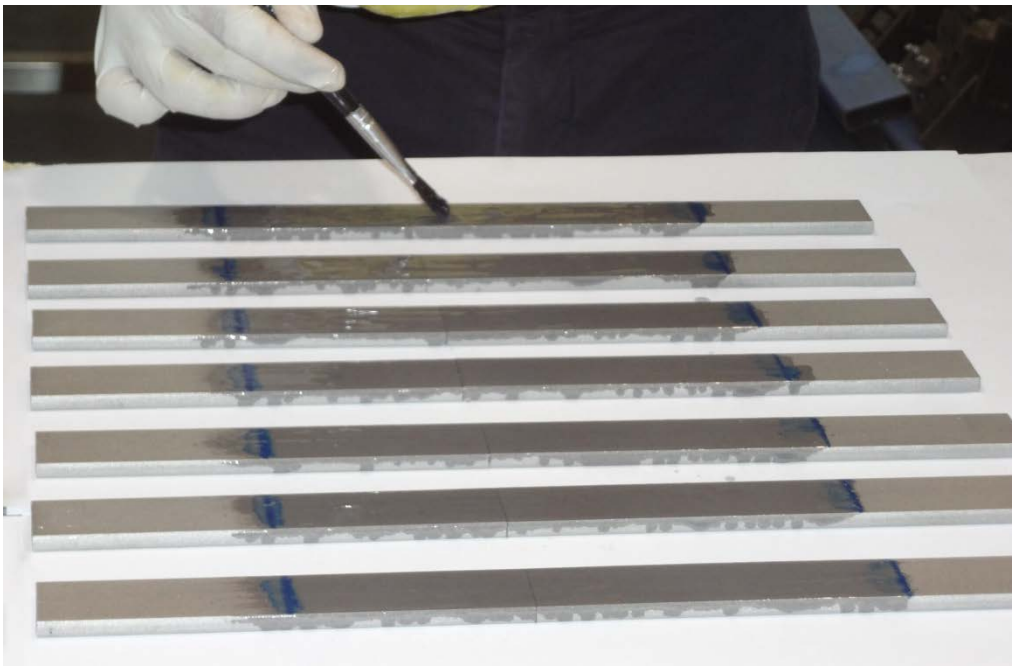

Figure A3: Application of epoxy-adhesive

Figure A4: CFRP installation

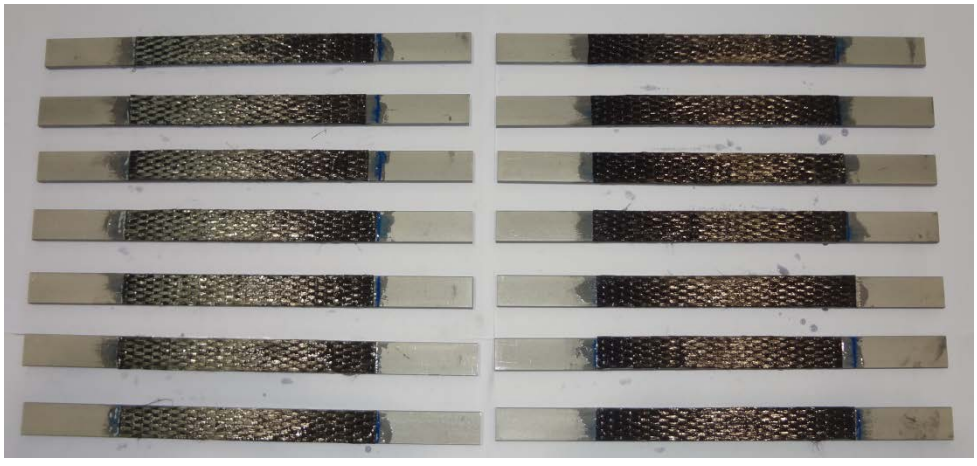

Figure A5: Completed CFRP-steel double strap joint specimens

Appendix B

Manufacturer provided Material properties

Table B1: MBrace P3500

Bonding to concrete, pr EN 1542 (direct)	> 3.5 MPa (concrete failure)
Ultimate elongation, ASTM D638	3%
Tensile strength:	
direct, ASTM D638	>12 MPa
by flexing, ASTM D790	>24 MPa
Modulus of elasticity:	
tensile, ASTM D638	>700 MPa
flexural, ASTM D790	>580 MPa
Composition	Two-part Epoxy resin
Solids by volume	100%
Mixing ratio by volume:	3 ; 1 (A:B)
Specific gravity (mixed)	1.08 ± 0.024 kg/L
Colour	Transparent
Overall thickness	150 micron
coverage approximately-	6m²/L
Recommended layers	1
Pot life	
7°C;	1 hour
23°C;	35 min
32°C;	25 min
Tack-free	
7°C;	9 hours
23°C;	5 hours
32°C;	3 hours

Table B2: MBrace P4500

Supply form	Translucent blue liquid
Volume solids	100 %
Mixed density (kg/litre)	1.13 ± 0.03
Mixing ratio, by weight (A:B)	100:50
Mixed viscosity (cps, at 25°C)	4000 ± 500
Pot life (in minutes)	30 min at 40°C
Setting time	< 3 hrs. at 25°C < 2 hrs. at 40°C
Full cure	7 Days
Compressive strength (ASTM C579)	> 40 MPa at 1 Day > 60 MPa at 7 Days
Tensile strength (BS:6319, pt 7)	> 17 MPa
Flexural strength (BS:6319, pt 3)	> 35 MPa
Coverage: 200 ~ 350 gsm fibre sheet : 0.8 to 1.0 kg/m^2 350 ~ 450 gsm fibre sheet : 0.9 to 1.2 kg/m^2 750 ~ 900 gsm fibre sheet : 1.5 to 1.8 kg/m^2	

Table B3: CFRP material properties

MasterBrace FIB 300/50 CFS

Fiber Areal Weight	300g/m^2
Fabric Design Thickness	0.166mm
Fibre Tensile Strength	4900 MPa
Fibre Tensile E-modulus	230 GPa
Elongation at break	2.1%
Fabric length/roll	100m
Fabric width	50cm

Table B4: GFRP material properties

STYLE:	**MU 4500G**
MULTIAXIAL FABRIC TYPE:	Unidirectional 0°
DESCRIPTION:	100% E-Glass
CONSTRUCTION:	Angle° — Weight (g/m²) 0° (Top layer) — 424.0 90° (Bottom layer) — 38.0
INPUT YARN:	Angle° — Yarn Count (tex) 0° (Top layer) — 1200 90° (Bottom layer) — 300
TOTAL WEIGHT: (nominal)	470 g/m² (including stitching yarn 8 g/m^2)
WIDTH: (nominal)	1270 mm
THICKNESS: (nominal):	0.5 mm
ROLL LENGTH: (nominal):	83 linear metres (105.41 m²)
ROLL WEIGHT: (nominal):	49.6 kgs
MOISTURE CONTENT:	0.5% (max.)
LOSS ON IGNITION:	4.5% (max.)

Appendix C

Material test data

Table C1: CFRP coupons test data

Coupon number	Dimensions (mm) (Thickness×Width×Length)	Ultimate load (kN)	Ultimate axial extension (mm)
1	15.76×1.01×138	16.1	6.2
2	15.36×1.13×138	15.7	5.6
3	15.22×1.02×138	14.9	6.1
4	15.25×1.05×138	15.5	5.3
5	15.32×1.04×138	16.4	5.8

Figure C1: Failure modes of CFRP coupons

Table C2: Steel coupons test data

Coupon number	Young's Modulus (GPa)	Yield Strength (0.2 %) (MPa)	Ultimate Tensile Strength (MPa)
1	208	353.34	380.38
2	211	354.65	387.54
3	227	348.34	376.21